DISSERTATION

CAVITATION DAMAGE SCALE EFFECTS: SUDDEN ENLARGEMENTS

Submitted by

Travis Earl Stripling

In partial fulfillment of the requirements

for the Degree of Doctor of Philosophy

Colorado State University

Fort Collins, Colorado

Summer, 1975

COLORADO STATE UNIVERSITY

Summer 1975

WE HEREBY RECOMMEND THAT THE THESIS PREPARED UNDER OUR SUPERVISION

BY Travis Earl Stripling

ENTITLED CAVITATION DAMAGE SCALE EFFECTS: SUDDEN ENLARGEMENTS

BE ACCEPTED AS FULFILLING IN PART REQUIREMENTS FOR THE DEGREE OF

Doctor of Philosophy

Committee on Graduate Work

H. G. Olson

Robert M. Murray

James E. Ball

J. Paul Tullis
Adviser

Head of Department

ABSTRACT OF DISSERTATION

CAVITATION DAMAGE SCALE EFFECTS:
SUDDEN ENLARGEMENTS

The present study was aimed at investigating the cavitation damage downstream from sudden enlargement energy dissipators. Tests were conducted on geometrically similar circular orifices of five different orifice to pipe diameter ratios in three different pipe sizes of 3-, 6-, and 12-inches. Highly polished 1100-O aluminum specimens were mounted in the downstream pipe wall to detect the cavitation damage. Two different stages or levels of cavitation damage were defined for study: (1) "incipient damage" level based upon maintaining a maximum pitting rate of 1 pit/in.^{2}/min on 1100-O aluminum, (2) cavitation damage regime where the maximum pitting rate was greater than 1 pit/in.^{2}/min.

Previously defined incipient damage scaling equations based upon damage data taken in the 3-in. pipe accurately predicted the incipient damage condition in the 6- and 12-in. pipes. Pressure scale effects on the incipient damage condition were constant for all pipe sizes tested. There were no size scale effects found for the incipient damage condition based upon maintaining a maximum pitting rate of 1 pit/in.^{2}/min.

The incipient damage condition was investigated in greater detail by studying the variation in the volume of the damage pits in the soft aluminum. The volume of the damage pit was related to the energy expended in formation of the pit which was assumed to be a measure of the intensity of the cavitation impact blow forming the pit. It was

found that at the incipient damage condition the intensity of cavitation impact blows varied with pipe size and orifice to pipe diameter ratio.

The damage in the cavitation damage regime was found to be a function of both cavitation pitting rate and intensity of cavitation impact blows (energy of pit formation). A cavitation intensity parameter, defined as the product of cavitation pitting rate and energy of pit formation, was used to measure cavitation damage. Data was presented to show the general variation of cavitation intensity under conditions of varying cavitation index, varying upstream pressure, and varying pipe size. In addition, the cavitation damage scaling equations introduced by Thiruvengadam were used along with experimentally measured flow field data to predict variations in cavitation pitting rate and intensity of impact blows.

The experimental results indicate that it is impossible to simulate total prototype cavitation loading conditions in terms of both cavitation pitting rate and intensity of impact blows in a hydraulic model of reduced size. An example is introduced demonstrating this fact. An alternative method using the cavitation intensity parameter is proposed for modeling prototype cavitation loading conditions in a model of reduced size.

Travis Earl Stripling
Civil Engineering Department
Colorado State University
Fort Collins, Colorado 80523
Summer, 1975

ACKNOWLEDGMENTS

The author wishes to express gratitude to his major professor, Dr. J. Paul Tullis, and to Mr. J. W. Ball for their advice and criticism during the course of this investigation and the preparation of this dissertation.

Gratitude is also expressed to Dr. R. N. Meroney and Dr. H. G. Olson for their participation as members of the graduate committee.

Mr. C. E. Sweeney and Mr. W. J. Rahmeyer greatly encouraged and helped the present author during the investigation.

Mr. Ralph V. Asmus and shop personnel materially assisted with the construction and development of experimental equipment.

Mr. Dick Vesely of Woodward Governor Company helped the author obtain the microscopic measurements made in this study.

Also, the author wishes to thank Mrs. Joella Matthews for helping to organize and for typing this dissertation.

This study was supported by Grant No. GK-35862 from the National Science Foundation.

TABLE OF CONTENTS

TABLE OF CONTENTS - Continued

LIST OF TABLES

LIST OF TABLES - Continued

LIST OF FIGURES

LIST OF SYMBOLS

Symbol	Description
C	Speed of sound in the liquid
CD	Cavitation degree at cavitation index σ, Eq. (5-1)
C_d	Coefficient of discharge = $\dfrac{V}{\sqrt{V^2 + 2(P_u - P_d)/\rho}}$
$C_{p,min}$	Minimum pressure coefficient for unseparated flow condition, Eq. (8-30), Appendix I
$\overline{C}_{p,min}$	Minimum pressure coefficient for separated flow condition, Eq. (2-7)
c	Subscript denoting critical cavitation condition
ch	Subscript denoting choking cavitation condition
D	Inside pipe diameter
d	Diameter of cavitation nuclei
$\overline{d}$	Mean diameter of cavitation nuclei
d^*	Critical diameter of cavitation nuclei, Eq. (8-35), Appendix I
d_N	Diameter of nozzle
d_o	Diameter of orifice
E_p	Energy of pit formation, Eq. (5-14)
$\overline{E}_p$	Average energy of pit formation
$\overline{E}_p$-X%	Average energy of pit formation for the X% of pits with the largest volume
$\lvert Err \rvert_{max}$	Largest absolute error when scaling equation is used to predict experimental results
$\overline{\lvert Err \rvert}$	Average absolute error when scaling equation is used to predict experimental results
f	Frequency of indentations on a solid surface due to cavitation
f_2, f_3, f_4	Functional relationships for incipient damage scaling equations

Symbol	Description
I_e	Cavitation intensity or intensity of erosion defined by Eq. (2-6)
I_{exp}	Cavitation intensity found by multiplying cavitation pitting rate by the average energy of pit formation
I_{exp}-X%	Cavitation intensity considering largest X% of pits in cavitation damage region, Eq. (5-15)
i	Subscript denoting incipient cavitation condition
id	Subscript denoting the incipient damage condition
K	A constant for a given d_o/D ratio and P_u, Eq. (AII-2), Appendix II
K_1	Constant relating Q_o to Vol_o given by Q_{ini} Vol_i
L	Exponent defining relation between I_{exp}-X% and $\frac{V-V_{id}}{V_{ch}-V_{id}}$ under conditions of varying sigma
ln	Natural logarithm
ℓ	Characteristic length used in cavitation damage scaling equations, Appendix I
M	Mach number given by V_o/C
m	Exponent defining relation between MPR and V for varying sigma, Eq. (4-1)
N	Exponent defining relation between MPR and V for varying upstream pressure (velocity), Eq. (4-2)
n	Cumulative number of cavitation nuclei passing a given point corresponding to the diameter d in a given time interval
n_o	Cumulative number of cavitation nuclei that pass a given point in a given time interval
n*	Cumulative number of cavitation nuclei passing a given point corresponding to diameter d* in a given time interval
O_t	Orifice plate thickness

Symbol	Description
P	Characteristic system pressure for cavitation index
P_c	Collapse pressure due to spherical collapse of a cavitation cavity
P_d	Mean pressure at the pipe wall measured ten pipe diameters downstream of the orifice or nozzle and projected back to the orifice or nozzle by adding equivalent frictional loss
P_i	Impact pressure on solid surface due to cavitation attack
P_{min}	Minimum mean pressure at the pipe wall before pressure recovery, approximately 1/2 pipe diameter downstream from the orifice
P_o, p_o	Free stream pressure
P_u	Mean pressure at the pipe wall measured one pipe diameter upstream of the orifice or nozzle and projected forward to the orifice or nozzle by subtracting equivalent frictional loss
P_v, p_v	Vapor pressure of water
$p(R)$	Pressure at cavitation bubble boundary
$p(t)$	Ambient pressure field acting on cavitation cavity, assumed to be a function of time during the life history of the cavity
p_{min}	Minimum pressure in flow field assuming unseparated flow
$\bar{p}_{min}$	Minimum pressure in flow field assuming separated flow
Q	Volume flow rate of liquid past a cross section, volume/time
Q_{ini}	Partial pressure of gas within cavitation cavity at beginning of growth cycle
Q_o	Partial pressure of gas within cavitation cavity at beginning of collapse
R	Radius of cavitation cavity
R_1	Distance downstream of orifice to reattachment location

Symbol	Description
R_a	Average cavitation pitting rate over cavitation damage region (three pipe diameters downstream of orifice) given in pits/in.^{2}/min
R_a-X%	Average cavitation pitting rate for largest X% of pits over cavitation damage region given in pits/in.^{2}/min
R_c	Radius of cavitation cavity at collapse
R_j	Radius of liquid jet for jet type cavitation damage
R_o	Radius of cavitation cavity at beginning of collapse
r	Rate of cavitation erosion for a solid, weight loss/time
S	Standard deviation of absolute error
S_e	Strain energy of a solid material up to fracture
T	Orifice lip thickness
t	Time variable
V	Average velocity of flow through the pipe
V_{jet}	Average velocity of flow through pipe orifice
V_o	Free stream velocity
Vol_i	Volume of cavitation cavity at beginning of growth cycle
Vol_o	Maximum volume of cavity at beginning of collapse
Vol_p	Volume of cavitation damage pit
W	Weber number, Eq. (8-42), Appendix I
X	Percentage of pits with largest volume, depth, or diameter
x	Distance downstream from orifice or nozzle
α	Weibull shape parameter, Eq. (8-34), Appendix I
β	Expansion ratio = $\frac{\text{Pipe Area}}{\text{Orifice Area}}$

Chapter I

INTRODUCTION

The use of modern high-head pressure systems has generated a need for a simple economical high-head energy dissipator. The sudden enlargement when designed correctly can function very efficiently as this needed energy dissipator. However, the phenomenon of cavitation may introduce serious problems and must be carefully considered in design. These problems include vibration, pressure fluctuations, objectionable noise, and erosion of solid surfaces. The extent of these problems depends directly upon the conditions of flow through the sudden enlargement.

The fluid flow through sudden enlargements is characterized by an abrupt increase in the cross-sectional area and a localized section of non-uniform flow. Orifices and nozzles, commonly used as sudden enlargements, produce high velocity jets and a definite surface of separation in the enlarged downstream section. The surface of separation is one of high velocity gradients and intense shear. Also there is an adverse pressure gradient in the separation region. These factors lead to instability and turbulence production which leads to a mixing process causing the fluid along the plane of separation to be entrained. Because of continuity, a return flow is established from downstream, causing a quasi-stable zone of backflow, a standing eddy. The process of turbulence production, convection, diffusion, and decay is the basic reason for the energy loss in the sudden enlargement. The intense turbulence and local pressure reductions along the plane of separation can produce cavitation under certain flow conditions.

Cavitation is a dynamic phenomenon and is concerned with the growth and collapse of cavities. During the operation of a sudden enlargement there is a constant flux of cavitation nuclei (undissolved air pockets) and liquid flowing through the enlargement. In order for cavitation to exist, the nuclei must be subjected to low pressures, equal approximately to the vapor pressure of the liquid, and grow into a cavity as a result of vaporization. The cavity is formed and subjected to a higher pressure where collapse occurs "implosively". Under certain flow conditions in the sudden enlargement, the local pressure reductions in the vortices along the plane of separation may reach vapor pressure and provide areas for growth of the cavitation nuclei. This action is known as "vortex cavitation" and is the principle process for cavitation in sudden enlargements.

Various degrees or levels of cavitation may exist in the sudden enlargement depending on flow conditions. The sudden enlargement may pass from a state of no cavitation to the incipient level as the discharge is increased. The *incipient cavitation level* represents onset of cavitation where the noise consists of light intermittent popping sounds. This level is often used in design of sudden enlargement energy dissipators where noise, damage, and vibration cannot be tolerated. Increasing the discharge further will produce a light steady cavitation noise similar to frying bacon, critical cavitation. The *critical cavitation level* produces negligible vibrations, minor noise, and the prospect of damage to adjacent boundaries for many conditions is remote.

The next cavitation level is known as *incipient damage* and is characterized by minor damage of adjacent solid boundaries caused by

implosion of vapor cavities on or near the boundary. This level of cavitation may produce objectionable noise and some vibration but damage is minor. Increasing the flow above the incipient damage level will produce more severe damage to conduit walls. Finally, further increases in discharge will eventually produce a condition where the mean pressure just downstream of the enlargement reaches the vapor pressure of the liquid and there is no further increase in discharge with decreasing downstream pressure assuming constant upstream pressure. The onset or beginning of this *choking cavitation level* produces cavitation of maximum intensity. Noise and vibration are excessive and heavy damage to solid boundaries is likely. Such a stage of cavitation intensity should be avoided in design.

The effective hydraulic design of sudden enlargement energy dissipators depends on available information to predict the flow conditions for the four levels of cavitation mentioned above. Scaled models and laws of hydraulic similitude have most often been used to predict cavitation levels in prototype structures. However, cavitation scale effects exist that complicate the application of model data. The term scale effects is given to the deviations from the elementary similarity relations linking the cavitation index to geometric and kinematic conditions.

It is possible to use scaled models and laws of hydraulic similitude to estimate cavitation damage on prototype structures. The present research was conducted to increase knowledge concerning cavitation damage modeling in sudden enlargements. This will specifically include:

(1) Determining the geometrical location and distribution of cavitation damage on the conduit walls downstream of sudden enlargements.

(2) Estimating the magnitude of pressure (velocity) and size scale effects for cavitation damage in sudden enlargements.

(3) Further study of the empirical equations developed by Sweeney [55] for defining flow conditions at "incipient damage" for submerged orifice and nozzle flows.

(4) A comparison of Thiruvengadam's analytical equations [60], Appendix I, for scaling cavitation intensity with the experimental data obtained in this research.

Chapter II

REVIEW OF LITERATURE

This chapter presents relevant background material concerning the cavitation process in sudden enlargements. Special emphasis is placed on the topic of damage to solid surfaces by cavitation. This involves a discussion concerning the influence of imploding cavitation cavities on or near solid surfaces and the reaction of these surfaces to the cavitation attack.

The cavitation parameter, sigma, will be introduced. This parameter is often used for extrapolation of cavitation behavior from one set of conditions to another. Past studies are noted that show extrapolation of cavitation results by maintaining sigma constant can lead to serious errors due to scale effects. These scale effects are further explained and possible reasons for their existence are discussed.

Finally, background material is mentioned concerning the interrelation of cavitation and the fluid flow through a sudden enlargement Past studies are noted that define cavitation scale effects for certain stages of cavitation in a sudden enlargement.

Fundamentals of Cavitation

Inception of Cavitation

In order for cavitation to exist in a liquid flow system several actions must be present. First, cavitation nuclei, small gas bubbles, must be entrained in the liquid to provide potential growth areas for cavitation cavities. Secondly, there must be low pressure areas available to provide a means for growth of the nuclei; vortices

with low pressure cores can provide such growth areas. Finally, once formed the cavitation cavity must collapse violently.

Role of cavitation nuclei - Natural waters generally contain small free gas bubbles within the liquid or in crevices on the surface of a solid [13]. The solid may be the boundary containing the flow or small particles entrained in the flow. The gas trapped in the small bubbles may be in stable balance with local pressure conditions, surface tension forces, and dissolved gas in the surrounding water. However, if the local pressure is reduced, the bubble may grow in volume at a nominal rate by diffusion of dissolved gases into the bubble. These small gas bubbles are also known as cavitation nuclei because they provide a source for the formation of larger vapor cavities necessary in the cavitation process.

Daily and Johnson [6] assumed that the growth of small gas bubbles or cavitation nuclei by vaporization into the bubble depends on the balance between surface tension forces, external pressure, vapor pressure of water, and gas pressure in the bubble. Assuming pure radial motion of the bubble wall, they found that rapid bubble growth did not occur unless the local pressure dropped to a certain critical value. This rapid growth of gas bubbles produced larger vapor cavities.

Normally aerated water will by diffusion gaseously grow bubbles to diameters of the order of 5×10^{-3} inches [43]. Using the above ideas of Daily and Johnson, gas bubbles of this diameter will expand vaporously when subjected to only a few inches of head below the vapor pressure of water.

Once created the vapor cavities are eventually subjected to higher surrounding pressure and become unstable. The higher local pressure

causes the walls of the vapor cavity to implode; the entire collapsing mass is directed toward the center of the vapor cavity. This action causes the collapsing liquid to rapidly decelerate to rest generating a waterhammer-type pressure rise and outgoing acoustic pressure waves, or noise. This total process of formation of vapor cavities from small gas bubbles and their subsequent collapse is known as cavitation.

Role of liquid flow field, vortex cavitation - In order for cavitation to exist in a flow field, the cavitation nuclei must be subjected to low pressure regions and grow to larger vapor cavities. The low pressures generated along shear layers are especially relevant to the study of cavitation in sudden enlargements. Submerged jets and fluid flow past bodies having continuous but bluff profiles are specific examples of shear layer flows that may produce low pressure regions and associated cavitation. Actually, low pressure regions occur at the centers of vortices generated along such shear layers; the vortex cores provide regions for cavitation nuclei to grow into cavitation cavities. However, due to eddy dissipation the core eddy pressure increases with time causing the cavities to finally become unstable and collapse. This particular type of cavitation is found in the sudden enlargement and is known as vortex cavitation.

Kermeen and Parkin [20] investigated cavitation inception behind sharp-edged disks. Dye studies showed a distinct shear layer which was turbulent up to the edge of the disk. The layer was composed of a succession of vortex filaments shed from the disk. Cavitation inception occurred in the shear layer when relatively large cavitation nuclei (about 0.002 inch in diameter) grew explosively into large cavities. The authors used a model of cavitation occurring at the low pressure

centers of vortex cores and attempted to formulate a relation for inception of cavitation.

Hooper [17] photographed inception of cavitation behind accelerated circular disks. He found cavitation was initiated in the high intensity vortex behind the disk. Also Young and Holl [70] have photographed cavitation within Kármán street type of trailing vortices. These tests were conducted using symmetrical wedges.

Rouse and colleagues [44,45,48] have studied cavitation in submerged jets. Their experiments show that cavitation occurs in the low pressure cores of turbulent eddies generated in the shear zone.

Sanford and Appel [53] studied flow through abrupt two-dimensional expansions by photographic methods. Both cavitating and noncavitating conditions were investigated. They found, under noncavitation conditions, the vortices shed from the expansion broke into loops extending in the direction of flow. This action destroyed the two-dimensionality of the vortices. They concluded that vortices which formed along the surface of separation at high Reynolds numbers were unstable. When cavitation was induced in the expansion, regular two-dimensional vortices were clearly evident. Sanford and Appel theorized that the cavitation vapor core stabilizes the vortices and suppresses their tendency to break up soon after they are formed.

Vigander [68] also conducted a visual study of cavitation in a two-dimensional expansion. At incipient conditions, cavitation was found to occur within irregular three-dimensional vortex filaments along the surface of separation. At more advanced stages of cavitation the vapor cavities appeared in the core of regular two-dimensional vortices. A comparison was made between cavitating and noncavitating conditions.

Similar to the findings of Sanford and Appel [53], Vigander noted that the vapor core, present in cavitating conditions, seemed to stabilize the two-dimensional vortices.

Mechanics of Transient Cavities

As seen from the last section, the fundamental cavitation process includes the transient growth and collapse of individual cavities or bubbles. It is therefore important to study the behavior of a single bubble throughout growth and collapse. The following material discusses various single bubble growth equations and comments on such factors as wall interferences, bubble rebound, and collapse pressures.

Bubble growth equations - In 1917, Lord Rayleigh [42] treated the problem of collapse of an empty cavity in a constant density liquid with constant pressure at infinity. He assumed spherical symmetry and radial, irrotational flow. Performing an energy balance, he derived an expression for cavity wall velocity as a function of cavity radius. Combining this equation with another equation obtained from momentum considerations, he was able to predict the pressure rise in the surrounding fluid as the cavity collapsed. Rayleigh's solutions did not include the effects of cavity contents or variable pressure field and the only liquid property considered was density. In addition, at complete collapse the equations predicted infinite cavity wall velocities and infinite pressure.

Plesset [37] took a somewhat different approach to the same problem by deriving the dynamic equation of motion for the cavity wall. The formulation was more general since a variable pressure field could be present, the cavity could contain gas and vapor, and surface tension

forces were allowed during the process of inception and in the final collapse stages of bubbles that contained little gas. Surface tension forces tended to reduce the maximum size of cavities and increase the rate of collapse of the cavities.

Poritsky [41] continued the analysis by including viscous effects and produced a second-order differential equation for bubble wall motion. The viscous forces tended to decrease both the growth and collapse rate.

In order to describe the phenomena of cavity collapse in greater detail, the effect of liquid compressibility and gas filled cavities must be considered. Trilling [65] considered the collapse of a gas-filled cavity in a compressible liquid, but neglected viscosity and surface tension. He used the equations of motion to derive an equation for the liquid motion at the bubble wall. He considered a weak shock-wave impulse from the bubble surface giving a compression wave radiating into the liquid. Trilling was able to predict shock waves and maximum pressures during cavity collapse.

Gilmore [9] extended Trilling's analysis by using the Kirkwood-Bethe hypothesis [21] that pressure disturbances are propagated with a velocity equal to the sum of the acoustical velocity and the local fluid velocity. Gilmore was able to approximate the velocity and pressure fields throughout the liquid at cavity collapse. The detailed solutions were for cavities collapsing with constant internal pressure, constant pressure at infinity, and without viscous or surface tension effects.

Hickling and Plesset [15] used Gilmore's approach along with high-speed computer solutions to predict collapse of a gas-filled cavity in a compressible fluid without viscosity or surface tension. They presented

the most complete set of results for both cavity-wall and liquid motions.

Ivany [18] treated the same problem as Gilmore, Hickling, and Plesset; however, viscous and surface tension effects were included. The results showed that viscosity and surface tension do not influence the general behavior during collapse.

Bubble growth equations: vortex cavitation - The bubble growth and collapse equations just mentioned treat idealized cases but add considerable knowledge to the cavitation process. Application of the above results to vortex cavitation presents several complicated problems. First, all the above methods assume the flow surrounding the cavity moves only in a radial direction. This greatly simplifies the equations of motion for the surrounding liquid. However, in vortex type cavitation there are certainly tangential velocities in the liquid surrounding the cavity. Secondly, there is a pressure drop, that is very difficult to measure or estimate, between the liquid outside the vortex and the vortex core. If a cavitation cavity is positioned at the vortex core, it would be difficult to predict just what pressure is acting on the cavity and how this pressure would vary.

The author could not find bubble growth equations in the literature, similar to the ones mentioned in the previous section, especially derived for vortex type cavitation. However, there does exist related material that will now be discussed.

Rouse [46,47] derived expressions concerning the growth and decay of a vortex filament. The equations describe the time variation in core diameter, minimum pressure, and kinetic energy for a Rankine vortex.

Kermeen and Parkin [20], as previously mentioned, used a model of cavitation occurring at low-pressure centers of Rankine vortex cores. These authors used experimental data to obtain a specific equation for the core vortex pressure in the wakes behind disks.

In a more general approach, Müller and Gyr [33] again used a Rankine vortex model to predict the pressure drop across vortices. This pressure drop was related to the velocity fluctuation in the direction of flow.

Wall interference, bubble rebound, collapse pressures - The assumption of a spherical bubble collapse is questionable especially near a solid wall. Numerous studies [7,28,31,34,39,64] show cavities tend to flatten as they approach a wall. Often this flattening continues to dimpling and penetration of the liquid as a jet into and through the cavity.

Another interesting phenomena noted in vapor cavity collapse is the action of bubble rebound. Analyses of gas-filled spherical bubbles in compressible fluids [9,15,18,65] predict a nonzero minimum radius at initial collapse followed by reopening and oscillations.

The maximum pressure generated by a cavity at collapse is a very important factor. Trilling [65] arrived at a maximum pressure of 2200 atmospheres. Also, Hickling and Plesset [15] demonstrated that the attenuation of the maximum-pressure intensity was proportional to $1/r$, r = distance from collapse center. Both analyses assumed spherical bubble collapse. Actual experimental measurement of cavity collapse pressures has not been possible due to the micro-size of the mechanism. However, theoretical work estimates pressures transmitted to solid boundaries from collapsing cavities are of the order of 1000 atmospheres.

Cavitation Index

Dimensional analysis is often used to obtain dimensionless parameters, π-terms, for modeling flow problems. In case of the cavitation phenomenon, dimensional analysis may produce seven or more π-terms when all variables are considered [55]. If a scaled model is used to simulate a prototype structure, it would be impossible to equate all these π-terms in model and prototype. Therefore, in practice, only the most important π-terms are maintained constant in model and prototype; the other π-terms are allowed to vary. The most revelant π-term in the cavitation process is known as the cavitation index, sigma -σ, and has the form:

$$\sigma = \frac{P-P_v}{1/2\ \rho V^2} \qquad (2\text{-}1)$$

in which P = characteristic pressure; P_v = vapor pressure of liquid; ρ = fluid mass density; and V = characteristic velocity. Another form of this index, often used in submerged orifice, nozzle, and valve flow [10,55,67], is given by:

$$\sigma = \frac{P-P_v}{P_u-P_d} \qquad (2\text{-}2)$$

in which P_u = pressure measured one pipe diameter upstream of the orifice, nozzle or valve and corrected to the device by subtracting the equivalent line loss, and P_d = pressure measured 10 pipe diameters downstream of the orifice, nozzle or valve and corrected to the device by adding the equivalent line loss.

The numerator of the cavitation index, in Eq. (2-1) or (2-2), is related to the net pressure or head which tends to collapse a cavitation

cavity. The denominator may be considered a measure of the pressure reductions that may occur to cause a cavity to form or expand. Therefore, the cavitation index is the ratio of pressure available for collapsing the cavity to pressure available for formation or growth of a cavity.

Scale effects - As mentioned previously, often only the cavitation index is maintained constant in the hydraulic model and prototype. Since other π-terms may vary, the cavitation behavior of the prototype may not be the same as the model. The term scale effects is given to the deviations from the elementary similarity relations linking the cavitation index to geometric and kinematic conditions. Viscosity, gravity, surface tension, thermodynamic, and cavitation nuclei properties can give rise to scale effects.

Hydraulic tests of cavitation in prototype structures are often made in model tests with reduced size and pressure. Several investigators [10,55,67] have therefore defined two types of scale effects for submerged orifice and nozzle flow. Size scale effects cause deviation in cavitation performance between model and prototype when the model is reduced in size, but the cavitation index and system pressure are maintained constant in model and prototype. Pressure (velocity) scale effects cause deviation in cavitation performance between model and prototype when model pressure and velocity are reduced, but the cavitation index and system size are maintained constant.

A number of experimental studies have been conducted to determine pressure and size scale effects for cavitation in submerged orifice flow. Tullis and Govindarajan [67] found no pressure scale effects for the incipient, critical or choking cavitation level; however,

size scale effects were found to exist for both incipient and critical levels. Sweeney [55] has found pressure scale effects to exist for the incipient damage level.

Cavitation Damage to Solid Surfaces

The interactions between a cavitating flow and a solid surface are quite complicated. Depending on the flow field and the surface material properties, various degrees of damage may be inflicted on the solid surface. Many numerical and experimental studies demonstrate that collapsing cavities can develop pressures sufficiently high to mechanically produce damage. Therefore, it can be concluded that one of the major factors that causes cavitation damage is purely mechanical and that this factor is always present. However, it is true that other factors such as chemical and corrosive effects are also important in some cases.

The intensity of cavitation attack on a solid boundary may be measured in various ways. For example, a standardized material may be placed at the boundary and the cavitation pitting rate (pits/area/time) calculated as a measure of intensity of cavitation attack [24,25]. Possibly a better measurement of the intensity would be a calculation of weight loss/area/time for the standardized material. Probably the most general measurement of intensity of cavitation attack would be to calculate the energy/area/time or power/area directed by the cavitation attack on the boundary surface [60].

Hydraulic model studies can be conducted to predict cavitation damage in prototype structures. These studies may be classified into two categories. First, the model results could possibly be used to

predict the flow conditions in the prototype at incipient (threshold) damage conditions [51]. Sweeney [55] conducted such a study for sudden enlargements based on the measurement of cavitation intensity in terms of cavitation pitting rate. Secondly, some investigators believe that hydraulic models could be used to predict the material removal in prototype structures operating in the damaging cavitation range. A method for conducting such tests has been outlined by Thiruvengadam [60]; however, the method has not been tested in actual model tests.

Mechanical aspects of cavitation damage - The mechanical nature of cavitation damage is most often characterized in terms of impact "blows" that are hydrodynamically produced. The actual process by which such blows are produced can be explained as follows. Some researchers maintain that damage is due to impacts from pressure shock waves that radiate from the collapse center of a cavitation cavity. These shock waves are of much larger magnitude if the cavity collapse is symmetrical [60]. As previously mentioned, wall interference often causes nonsymmetrical collapse with the formation of liquid jets. Many investigators have studied this phenomenon [4,31,39,66] and attribute cavitation damage to the high velocity jet impinging on the solid surface.

Kling and Hammitt [12,22,23] noted that nonsymmetrical collapses with rebound occur almost exclusively in real flow systems. Hammitt [12] discussed numerical calculations showing that if rebound occurs such that the cavity grows again after collapsing, the event is similar to a micro-explosion. This action generated shock waves

that were much stronger than corresponding waves found during cavity collapse. The author theorized that actual damage is usually a result of microjet impact and shock-wave pressures generated by bubble rebounds.

Knapp, Daily, and Hammitt [26] discussed cavitation damage to annealed aluminum in a magnetostriction type apparatus. They noted that once a relatively large pit was formed it sometimes acted as a wave guide to concentrate further damage within the same pit. This process is known as the "wave-guide" effect and indicates that cavitation damage may increase at a more rapid rate as the solid surface becomes pitted.

Related factors in cavitation attack - Although the mechanical aspects of cavitation damage usually are predominant, there are secondary factors that should be mentioned. For example, it was found that cavitation and corrosion are mutually reinforcing with the resulting damage often much greater than the sum of the two, if each acted alone [38,60,69]. Also some investigators believe that cavitation erosion could be caused by the melting of the metal due to localized high temperatures [8,36].

Resistance of materials to cavitation attack - If a given cavitation intensity acts on a solid surface, the eventual surface damage depends on the characteristics of the solid. Peterson [35] explained that a solid could be considered to fail in shear (ductile material) or in tension (brittle material). For ductile materials there is some impact pressure such that rapid plastic flow will occur. In brittle materials, the impact pressure is insufficient to produce

hydrodynamic deformation; however, stresses are produced in the material that may lead to material failure.

Hackworth and Adler [11] also studied cavitation damage to ductile and brittle materials in an ultrasonic testing facility. They theorized that since the cavitation type pressure pulse was applied over an area microscopic in size, the microscopic properties and microstructure of the material should dictate the damage mechanisms. Three metals were tested: 1100 aluminum, 316 stainless steel, and Titanium-6Al-4V; the damage process on the aluminum and stainless steel were described as follows [11]:

> "Bubble collapse pressure pulses readily deform the low-strength 1100 aluminum forming pits which became preferential sites for subsequent bubble collapse. The walls between these preferential pits grow thinner and are extruded outward forming lips as the pits enlarge and deepen during this incubation period. Shearing of the pit lips by subsequent pressure pulses appears to be the erosion mechanism for pure aluminum.
>
> "The magnitude of most of the pressure pulses is insufficient to indent the surface of the 316 stainless steel and impact pits, per se, do not contribute to the erosion of the stainless steel. However, the magnitude is sufficient to induce shearing in favorably oriented grains. The incubation period consists of the relative displacement of grains across grain boundaries and the formation of slip bands within the grains. These grain boundary steps and slip bands concentrate the stresses produced by the pressure pulses so that localized fracture of the material occurs with subsequent removal of small particles which serve as nucleation sites for the development of larger pits. The radial growth of these pits by fracture of small particles at the outer periphery appears to be the erosion mechanism for annealed 316 stainless steel."

Mousson [32] and other experimenters have shown that resistance to cavitation erosion depends upon the ability of a metal to be work hardened under repeated impact. Mousson measured the change in hardness of various metals after exposure to cavitation damage and found large increases in hardness.

Many experimental tests have been conducted to actually determine a measure of the resistance of various materials to cavitation attack. Most often the cavitation damage resistance is considered to be a function of some easily measured mechanical property such as strain energy, ultimate strength, yield strength, Brinell hardness, etc. of the test material. Thiruvengadam and Waring [63] have summarized the results and found that strain energy appeared to be the most significant parameter.

Most cavitation damage experiments are conducted by creating a cavitation environment of given intensity (I_e = power/area) and subjecting a test specimen to the cavitating field. The amount of damage suffered by the specimen is usually measured by the rate of erosion (r = weight loss/time). It is now well established that I_e and the rate of erosion as a function of exposure time can be divided into four periods: incubation, acceleration, deceleration, and steady. The periods and the time variance of erosion have important implications in hydraulic modeling of cavitation damage [60].

Past studies - Thiruvengadam [60] noted that there are two types of problems concerning cavitation damage prediction:

> "The first one is the understanding of the threshold conditions wherein the impact stresses reach a limiting value just sufficient to initiate erosion either at the first blow or after repetitive blows. The second problem is the prediction of the amount of erosion if the erosive forces are above the threshold for the material."

The author first studied the threshold or incipient cavitation damage problem by performing studies in a rotating disk apparatus [61]. The ratio between the yield strength and the hydrodynamic pressure was

found to be linearly proportional to the cavitation inception parameter.

Thiruvengadam [62] continued the study for incipient cavitation damage by using a vibratory testing device. The experiments showed that there was a minimum displacement amplitude for each metal below which there was no cavitation erosion. Using this data, a threshold intensity for cavitation damage was established for six metals as a function of high frequency fatigue strength at one billion cycles.

Knapp [24,25] studied the cavitation and cavitation damage potential of fixed type cavities around a 2-in. diameter cylindrical section with a hemispherical nose. Soft (1100-0 aluminum) specimens were attached flush with the cylinder surface to register the location and intensity of the hydrodynamic blows. Photomicrographs were taken of the specimens in order to calculate cavitation intensity, in terms of pitting rate, and size distribution of the pits. The cavitation pitting rate was found to be independent of exposure time for a given flow field. Analysis of the data showed that cavitation pitting rate varied with about the sixth power of velocity for a constant cavitation index. Also, increasing velocity at a constant cavitation index increased the percentage of large pits on the test specimens. Knapp then concluded that cavitation pitting rate (pits/area/time) was a rough measurement of cavitation intensity; however, a better estimate could be made if pitting size distributions were also taken into consideration.

The analysis was extended by using photographic methods to predict the number of cavitation cavities swept into the damaging area per unit

time. This number was compared to the number of damage pits; the results indicated that only one in 30,000 traveling cavities produced a damaging blow on the soft metal. Knapp concluded that only the very large cavities could approach the surface closely enough to cause a pit. The great majority of cavities collapsed at too great a distance from the boundary to produce damaging blows. Finally, the author demonstrated a method using measured values of pit depth and diameter to estimate intensity of the individual cavitation blows.

Shal'nev [54] conducted a systematic study to define the effect of the cavitation index on the erosion process. The tests were conducted in a two-dimensional venturi using a circular cylinder with its axis normal to the flow direction. Shal'nev found that the rate of erosion on lead greatly depended on the cavitation index.

Thiruvengadam and Kohl [27,59,60] conducted cavitation damage studies in a rotating foil apparatus using NACA 16-021 hydrofoils of two sizes (3 inches and 1 1/2 inches in chord length). These investigations again confirmed that the rate of erosion was greatly dependent on the exposure time and cavitation index. The authors also concluded that the cavitation intensity was a function of hydrofoil size:

> "For example, the three-inch foil at 175 fps has a peak intensity of 1.2 w/m^2 which occurs at a cavitation number of 0.30; whereas the peak intensity is only 0.6 w/m^2 at a cavitation number of 0.36, for the 1 1/2-inch foil at the same velocity."

Thiruvengadam [60] has suggested some mathematical expressions for scaling the cavitation intensity. These equations are based upon the assumption that cavitation intensity is proportional to the intensity of bubble collapse. Although these equations can be used to predict

the general trends of past experimental results; the equations have not been thoroughly tested against results of cavitation damage tests. These equations will be investigated in greater detail in a later section of this chapter.

Cavitation and the Sudden Enlargement

The immediate concern of the present study is to describe cavitation damage to pipe walls downstream of sudden enlargements. Material thus far presented in Chapter II will serve as a basis for further analysis of the sudden enlargement.

For example, the fact that a shear layer exists along the separation streamline downstream of the sudden enlargement indicates that vortex type cavitation may be present for certain flow conditions. As mentioned in Chapter I, there are several degrees or levels of cavitation that may exist in a sudden enlargement: incipient, critical, incipient damage, and choking. One advantage of the sudden enlargement, with respect to cavitation design, is the fact that a considerable intensity or level of cavitation may exist without damage being inflicted on downstream conduit walls. This fact is due to the shear layer being geometrically situated within the fluid flow and removed from conduit walls. This geometry requires that for wall damage to occur, not only must cavitation be initiated in the shear layer; but once formed the cavitation cavities must be transferred to, and collapse in close proximity of, the pipe wall.

Another important consideration is the fact that as cavitation proceeds from inception to choking condition there is a change from practically single phase to a two-phase flow regime. Often the non-cavitating flow field can be assumed to describe the flow at incipient

cavitation conditions. However, released gas and two-phase flow effects are considerable at advanced levels of cavitation. Vigander [68] described his visual studies of advanced stages of cavitation in sudden enlargements:

> "3. Quasi-Steady Cavitation. In this regime, cavitation bubbles occupy most of the mixing zone. Individual vortices cannot be seen clearly except as waviness on the boundary of the cavitation region. The cavitation appears as a steady pocket which occupies the region of maximum shear-stress and minimum mean pressure. A large amount of released gas and vapor bubbles accumulates in the zone of separation. Released gas is also convected downstream intermittently."

Flow Field Downstream of Sudden Enlargement

Chaturvedi [5] conducted an experimental study into the flow field downstream of a nozzle using hot wire anemometry. Air was used as the fluid, the expansion ratio was 2:1, and a Reynolds number of 2×10^5 was maintained during the tests. Chaturvedi determined mean velocities and pressures at certain downstream cross-sections. Turbulent intensities, production, and shearing stresses were also calculated.

Sami [52] studied an air jet issuing with an efflux velocity of about 35 feet per second from a 1.0-ft diameter nozzle into still air. This study is of particular interest since pressure fluctuations were measured and described.

Teyssandier [57] used an integral numerical method to solve for turbulent flow downstream of expansions, nozzles, and orifices. The method was used to solve for the discharge coefficient as a function of axial position beyond the vena contracta.

Ball and Simmons [3] conducted a study concerning pipeline orifices and sudden enlargements used for energy dissipators. The authors measured

velocity distributions and mean pressures at certain cross-sections for both cavitating and noncavitating flow. There was little change in the velocity distribution when the cavitation conditions varied from light to heavy.

Wall Pressure Studies in Sudden Enlargements

Mean and fluctuating pressures have been studied at the conduit walls downstream of sudden enlargements. Rouse and Jezdinsky [50] conducted a study concerning mean and fluctuating wall pressures downstream of nozzles under noncavitating conditions.

Vigander [68] measured wall pressure fluctuations in both cavitating and noncavitating flows. He calculated the points of maximum pressure fluctuation for the case of incipient cavitation. The author stated that maximum wall-pressure fluctuations increased at advanced stages of cavitation [68]:

> "Maximum wall-pressure fluctuations of six times those in noncavitating flow occurred near the end of the separation zone, at cavitation numbers between 0.3 and 0.4. At still lower cavitation numbers, wall-pressure fluctuations and vortex frequencies decrease as released gas accumulates in the zone of separation."

Rouse and Jezdinsky [49] continued their work on submerged jets by studying cavitation and energy dissipation in sudden enlargements. Measurements of the distribution of piezometric head along the wall of each expansion showed almost no variation in form between incipient and heavy cavitation. The change in head was essentially completed within four or five diameters from the section of abrupt enlargement.

Govindarajan [10] studied wall pressure fluctuations downstream of pipeline orifices. He first defined the locations on the pipe wall where the negative peaks of pressure were closest to vapor pressure at

incipient cavitation conditions. Experimental tests were then conducted in 3-, 6-, 12-, and 24-in. diameter pipelines using geometrically similar orifices. An equation was developed to predict wall pressure fluctuation at locations where negative peaks were closest to vapor pressure under incipient cavitation conditions. The pressure fluctuations were shown to increase with increasing pipe size; however, under cavitating conditions this trend was reversed. Also for a given system size, orifice, and upstream pressure, the pressure fluctuations rapidly increased in value as the cavitation intensity increased from incipient to heavy. Wall pressure fluctuations were measured longitudinally downstream of the test orifices under incipient cavitation conditions. The fluctuations were found to be functions of orifice to pipe diameter ratio and distance downstream of the orifice for a given system size.

Cavitation Scale Effects: Incipient, Critical, Choking Levels

Considerable research work has been conducted at Colorado State University concerning the cavitation performance of pipeline orifices. Tullis and Govindarajan [67] largely summarized the cavitation studies including scale effects for incipient, critical, and choking cavitation. The authors found no pressure (velocity) scale effects for incipient, critical or choking cavitation conditions. Or, equivalently, the value of the cavitation index, sigma, at incipient, critical or choking conditions is a constant, independent of upstream pressure (velocity) for a given system size and orifice to pipe diameter ratio. The choking level of cavitation had no pressure or size scale effects; sigma has a constant value at choking conditions, independent of system size, for a given orifice to pipe diameter ratio.

The authors did find a size scale effect for the incipient and critical cavitation levels; an equation was developed by Govindarajan [10] for these size scale effects. He attributed the scale effects to increasing pressure fluctuations downstream of the orifice plates with increasing system size for a given orifice to pipe diameter ratio and constant upstream pressure.

Lienhard and Goss [30] also studied the problem of cavitation inception during the flow of water through a submerged orifice. In their study, incipience was defined at the point where cavitation became a steady roar. They assumed, and later experimentally verified, that the cavitation index was not a function of Reynolds number. Their initial assumption was based on the fact that when a scale factor which compares two kinds of forces becomes large, such as Reynolds number in these studies, it ceases to exert influence on a system. The final results show a definite size scale effect for incipient cavitation.

Cavitation Damage Studies

Cavitation damage on downstream conduit walls of sudden enlargements has been investigated in a few isolated cases. However, no one unified comprehensive program of study had existed until the present studies began.

Ball [1] first studied cavitation damage downstream of pipeline valves used for flow regulation in 1957. A 6-in. gate valve at 20 percent opening discharged into an 8-in. diameter pipe lined with 1 in. of concrete. The location of cavitation damage on the concrete surface was then determined for various flow conditions. It was then postulated

that a change in shape of the flow passage immediately downstream of the valve would alter the flow conditions and thus the cavitation characteristics. Therefore a sand-cement-mortar-lined, 14-in. tee section was placed immediately downstream of an 8-in. standard gate valve. This configuration was tested for 9 hrs under heads of 150 and 118 ft with the valve 6 1/4 and 12 1/2 percent open. These tests showed no cavitation damage. On the basis of the tests Ball concluded, "One of the most effective means of eliminating cavitation damage below gate valves is the placing of sudden enlargements in the pipe sections immediately downstream."

Ball [3] continued the same type studies using a 3-in. gate valve at heads up to 500 ft. It was determined that as the downstream chamber was enlarged from 3 to 4.5 inches in diameter, the value of the cavitation index at incipient wall damage changed from 1 to 0.15. Considering orifice flow, Ball suggested an orifice to pipe diameter ratio of 0.5 would be optimum for good energy dissipation without damage to the conduit.

Rouse and Jezdinsky [49] used Ball's incipient damage data for gate valves to estimate incipient cavitation damage downstream of pipeline nozzles.

Russell and Ball [51] conducted a hydraulic model study to determine the cavitation characteristics of a low-level outlet expansion chamber used for energy dissipation. A section of 12-in. diameter steel pipe with a 1 1/4-in. thick concrete lining was used as the enlarged downstream section. Tests were conducted at various cavitation index values and demonstrated that it is possible to have quite

severe cavitation at a sudden enlargement without damaging the walls of the expansion chamber.

The first extensive research program to determine cavitation damage downstream of sudden enlargements is described by Sweeney [55]. The tests were conducted using five different concentric, sharp-edged, circular orifice plates in 3-in. inside diameter steel tubing to form sudden enlargements of varying expansion ratios. The tests covered cavitation levels from light damage to choking and upstream pressure levels were varied from 30-200 psig. Soft aluminum (1100-O) specimens placed in the walls of the enlargement were used to detect cavitation damage.

An "incipient cavitation damage level" was evaluated at several pressures for each orifice. The location of the cavitation damage area was located on the downstream pipe wall for more severe damage levels. In this study cavitation damage was defined as the number of cavitation damage pits per area per time on the aluminum test specimens. The major contribution of the study was identification of pressure (velocity) scale effects for the incipient cavitation damage level in sudden enlargements of varying geometry.

Analytical Considerations

A pure analytical solution for determining cavitation damage downstream from sudden enlargements is a very difficult problem. Some of the major factors causing these difficulties will now be discussed.

The cavitation erosion of a given component, usually measured in terms of weight loss/area/time, is dependent upon the impact stresses exerted on the surface by the cavitating flow. In a preliminary

analysis to determine the relation between the cavitation phenomenon and material damage, Thiruvengadam (see Appendix I) has suggested that cavitation intensity be used as a measure of these impact stresses. The cavitation intensity is defined as the power per unit area that a surface absorbs due to a cavitating flow. This impact stress or cavitation intensity is a direct result of the growth and collapse of vapor cavities within the fluid medium. Finally, the growth and collapse of vapor cavities is governed by the characteristics of the fluid flow.

With certain modifications the method presented in Appendix I can be used to predict the cavitation intensity directed upon conduit walls downstream from sudden enlargements. These modifications will be presented.

Problems associated with pure analytical solution - The actual cavitation damage to a solid surface is directly dependent upon the detailed growth and collapse characteristics of individual cavitation cavities. Various equations describing the growth and collapse of cavities were previously discussed in this chapter. One such equation derived by Lamb [29] will now be discussed for the case of irrotational motion:

$$R \frac{d^2R}{dt^2} + \frac{3}{2} \left(\frac{dR}{dt}\right)^2 = \frac{p(R)-p(t)}{\rho} \qquad (2\text{-}3)$$

in which R = radius of cavity at time t, $p(R)$ = pressure at bubble boundary, $p(t)$ = ambient pressure field assumed to be a function of time during the life history of the bubble, ρ = density of the liquid. Considering only vapor pressure and surface tension forces, the pressure at the bubble boundary will be:

$$p(R) = p_v - \frac{2\gamma}{R} \qquad (2\text{-}4)$$

in which p_v = vapor pressure of the liquid, γ = surface tension. Substituting Eq. (2-4) into (2-3) produces an equation predicting bubble growth:

$$p_v - \frac{2\gamma}{R} - p(t) = \frac{3}{2}\rho\left(\frac{dR}{dt}\right)^2 + \rho R\frac{d^2R}{dt^2} \qquad (2\text{-}5)$$

Actual solution to the above equation is very difficult for the case of vortex cavitation found in sudden enlargements. The function $p(t)$ is a random variable dependent upon the turbulent characteristics of the shear layer downstream of the enlargement. Therefore, it is very difficult to estimate the pressure as a function of time during the life history of a cavity. In addition, the actual size distribution of the cavitation nuclei entering the enlargement cannot be measured. This fact complicates the selection of an initial condition for the variable R in Eq. (2-5). Finally, since vortex cavitation is involved the flow surrounding the cavity may not be irrotational. This will imply that Eq. (2-3) should be replaced with a more complicated equation, further compounding the problem.

Kermeen and Parkin [20] have studied incipient cavitation in the wake of a family of sharp-edged circular disks. Experimental studies indicated that vortex cavitation was present in the shear layer. The authors then used a semi-empirical procedure to calculate the pressure within the vortex cores. This is the only detailed study the present author could find concerning shear layer flows and vortex cavitation.

The cavitation damage to the wall of a sudden enlargement generally takes place when the cavitation intensity is moderate to heavy.

Therefore, actually there are many cavitation nuclei growing and collapsing within the flow. This presents the real prospects of a two-phase (gas-liquid) flow system which tends to complicate the analytical analysis. These events may cause further complications such as stabilization of vortices by cavitation cavities [68].

Another major problem facing an analytical solution is the calculation of the collapse position of the cavity; the distance between the collapse position and the conduit wall determines to a large extent what actual forces are exerted on the wall. However, the determination of collapse position would necessitate the prediction of cavity movement within the flow field and also calculations of the cavity radius during its growth and collapse cycles. These are major problems, but even if they were solved there would still remain the considerable problem of determining the interaction between resulting impact forces and the solid boundary. For example, it would be necessary to determine the bubble collapse model (spherical or high velocity jet) for various collapse situations. It is also difficult to describe how a particular solid will react to impulse loadings due to a cavitation attack. With present knowledge it is almost impossible to mathematically express a model to describe material removal.

Scaling laws for cavitation erosion - Appendix I presents some scaling equations for cavitation intensity, I_e:

$$I_e = \frac{\Delta y}{\Delta t} S_e \qquad (2\text{-}6)$$

in which Δy = mean depth of erosion, Δt = time interval, S_e = strain energy or erosion strength. The term $\Delta y/\Delta t$ is a measure of the volume removal of material per area per time. Therefore, the method presented

in Appendix I by Thiruvengadam can be applied in the damaging regime of cavitation, but is not useful in determining incipient cavitation damage. I_e represents the power absorbed per unit eroded area. Equation (2-6) indicates that if the values of I_e and S_e are known, then the volume removal of material per area per time $(\Delta y/\Delta t)$ can be calculated.

The cavitation intensity must somehow be related to the intensity of bubble collapse. Assuming shallow indentations formed from plastic deformation, Thiruvengadam related I_e to intensity of bubble collapse by Eq. (8-20) of Appendix I:

$$I_e \propto P_i \cdot R \cdot f$$

This relation indicates that intensity of bubble collapse is the product of three terms: (1) P_i, the impact pressure of the mechanism forming the indentation, (2) R, the size of the jet or shock, and (3) f, the frequency at which indentations are formed on the solid surface.

The next step in the analysis was to relate P_i, R, and f to hydrodynamic characteristics such as velocity, pressure, and size of the system. Thiruvengadam assumed that the impact pressure could be generated by three different methods: spherical cavity collapse and two types of high velocity jet damage. Rayleigh's analysis [42] was basically used to estimate P_i for spherical cavity collapse; while, the study of Plesset and Chapman [40] was used in the analysis of the jet type damage.

A procedure was then used to relate the size of the jet or shock to the cavity radius at beginning of collapse, R_o, through Eq. (8-32). This relation indicates that the size of the jet or shock depends upon the degree of cavitation and a characteristic length of the system.

In order to obtain this relation, Thiruvengadam assumed unseparated flow and used the minimum pressure coefficient to introduce the cavitation index at inception into the analysis.

Finally, the frequency at which indentations were formed upon the solid surface was estimated based upon the premise that the number of bubbles that collapse is related to the number that become unstable and grow. Using this idea along with an assumed size distribution for the cavitation nuclei and the incipient cavitation criteria due to Johnson [19], Thiruvengadam was able to estimate f.

The present study is concerned with cavitation damage in sudden enlargements. It would be useful if the scaling laws for cavitation erosion presented in Appendix I could be modified for damage analysis of sudden enlargements.

In order to apply the relation, $I_e \propto P_i \cdot R \cdot f$, the value of R must be estimated in terms of hydrodynamic variables, see Eq. (8-32) of Appendix I. In the derivation of this relation the flow was assumed to be unseparated; this is certainly not the case for orifice type flows. In the separated flow condition the minimum pressure, $\overline{p}_{min}$, will occur within the flow field. The minimum pressure coefficient in the flow field, $\overline{C}_{p,min}$, may be defined as:

$$\overline{C}_{p,min} = \frac{\overline{p}_{min} - p_o}{\frac{1}{2}\rho V_o^2} \tag{2-7}$$

in which p_o = free stream pressure and V_o = free stream velocity. However, the reference by Johnson mentioned in Appendix I indicates that

$$\sigma_i = \frac{p_o - p_v}{\frac{1}{2}\rho V_o^2} \text{ (at inception)} \approx -\overline{C}_{p,min} \tag{2-8}$$

For separated flow conditions, the same derivation for R_o may be followed as presented in Appendix I except p_{min} should be replaced by $\bar{p}_{min}$ and Eqs. (8-30) and (8-31) replaced by Eqs. (2-7) and (2-8) respectively. This analysis will again lead to Eq. (8-32), however the value of σ_i must be experimentally determined for the particular separated flow problem under consideration.

The impact pressure due to spherical cavity collapse is described by Eqs. (8-22) and (8-23) of Appendix I for a cavity containing a non-condensible gas obeying Boyles's law. However, in order to perform calculations the value of Q_o must be expressed in terms of hydrodynamic variables. Assuming a perfect gas, the partial pressure of the gas at beginning of collapse would be:

$$Q_o = K_1 \frac{1}{Vol_o} \qquad K_1 = \text{Constant} = Q_{ini}\ Vol_i$$

in which Q_{ini} = partial pressure of gas in cavity at beginning of growth cycle, Vol_i = volume of cavity at beginning of growth cycle, Vol_o = maximum volume of cavity at beginning of collapse. However, it is known that $Vol_o \propto R_o^3$. Therefore, the following expression is valid:

$$Q_o \propto \frac{1}{R_o^3}$$

but by substituting Eq. (8-32) of Appendix I into this expression it is found that

$$Q_o \propto \frac{1}{\ell^3(\sigma_i-\sigma)^{3/2}} \tag{2-9}$$

Now Eq. (2-9) can be combined with Eqs. (8-23) and (8-22) of Appendix I to produce

$$P_i \propto P_o \exp\left(\frac{2}{3} P_o \ell^3 (\sigma_i - \sigma)^{3/2}\right) \qquad (2\text{-}10)$$

Eq. (2-10) will be used in Chapter V to estimate impact pressures for spherical cavity collapse.

Chapter III

EXPERIMENTAL FACILITIES AND PROCEDURE

Laboratory

Experimental studies were conducted in the Hydro Machinery Laboratory of Colorado State University. The laboratory is housed in a 70 by 192 ft prestressed concrete building. The 3-ft thick concrete floor slab with anchors installed on 10-ft centers was designed to minimize vibrations in the slab and building during testing. Water is supplied to the facilities by the U.S. Bureau of Reclamation's Horsetooth Reservoir.

The static pressure in the laboratory varies between 85 and 115 psig due to seasonal variation of reservoir storage. However, a booster pump is available to deliver small discharges at pressures up to 250 psig. The maximum discharges are approximately 90 cfs in the 24-in. test line and 30 cfs in the 12-in. line. Water is passed through the laboratory into a downstream receiving lake.

The water used in the experimental studies was untreated and no measures were taken to control nuclei count, nuclei size, air content or temperature of the water. However, the air content has been found to be near air saturation and the water temperature only varied between 4.00 and 10.25 degrees centigrade during the tests. It is reasonable to assume high nuclei count under the given conditions, which should minimize scale effects due to nuclei.

Test Components

Geometrically similar circular concentric sharp-edged orifices were used to determine pressure (velocity) and size scale effects. A

description of the orifices used in the 3-, 6-, and 12-in. pipes is given in Table 1 and Fig. 1.

A 2-in. diameter low β ratio, long-radius flow nozzle was fabricated for testing in a 6-in. diameter line. Details of the nozzle are shown in Fig. 2.

Specially constructed test sections were used downstream of the test orifices and nozzle. Three different sizes of test sections were constructed; one for each of the pipe sizes--3-, 6-, and 12-inches. The purpose of the test section was to allow the insertion of a test specimen for measuring cavitation damage. The 6-in. test section is shown in Fig. 3; 3- and 12-in. test sections were geometrically similar to the 6-in. section. The 1100-0 aluminum test specimen was attached by two screws to the compression bar shown in Fig. 4. The compression bar served the purposes of holding the test specimen secure and sealing the pipe opening necessary for insertion of the aluminum test specimen. The seal was obtained by using an O-ring on the compression bar and applying pressure with the toggle clamps. Upon insertion, the bottom side of the 1100-0 aluminum test specimen fitted flush with the interior pipe wall. This system provided an efficient means of taking specimens in and out of the test section while maintaining a good seal during actual tests.

All aluminum specimens were highly polished and checked for surface irregularities before being placed in the test section.

The test section installed in the pipeline is shown in Fig. 5. Similar piping and control systems were used in the 3- and 12-in. tests. The upstream and downstream control valves were used to regulate the upstream and downstream pressures. Two isolation valves were needed

TABLE 1 DIMENSIONS OF TEST ORIFICES

Inside Diameter of Pipe (inches) D	Diameter of Orifice (inches) d_o	Orifice to Pipe Ratio d_o/D	Lip Thickness (inches) T	Thickness of Orifice Plate (inches) O_t
3.00	1.168	0.3893	0.04	0.187
3.00	1.333	0.4443	0.04	0.187
3.00	1.500	0.5000	0.04	0.187
3.00	2.000	0.6667	0.04	0.187
3.00	2.400	0.8000	0.04	0.187
6.00	2.315	0.3858	0.08	0.375
6.00	2.666	0.4443	0.08	0.375
6.00	2.991	0.4985	0.08	0.375
6.00	4.000	0.6667	0.08	0.375
6.00	4.785	0.7975	0.08	0.375
12.0	4.570	0.3808	0.16	0.750
12.0	7.980	0.6650	0.16	0.750
12.0	9.600	0.8000	0.16	0.750

See Fig. 1 for definition of terms.

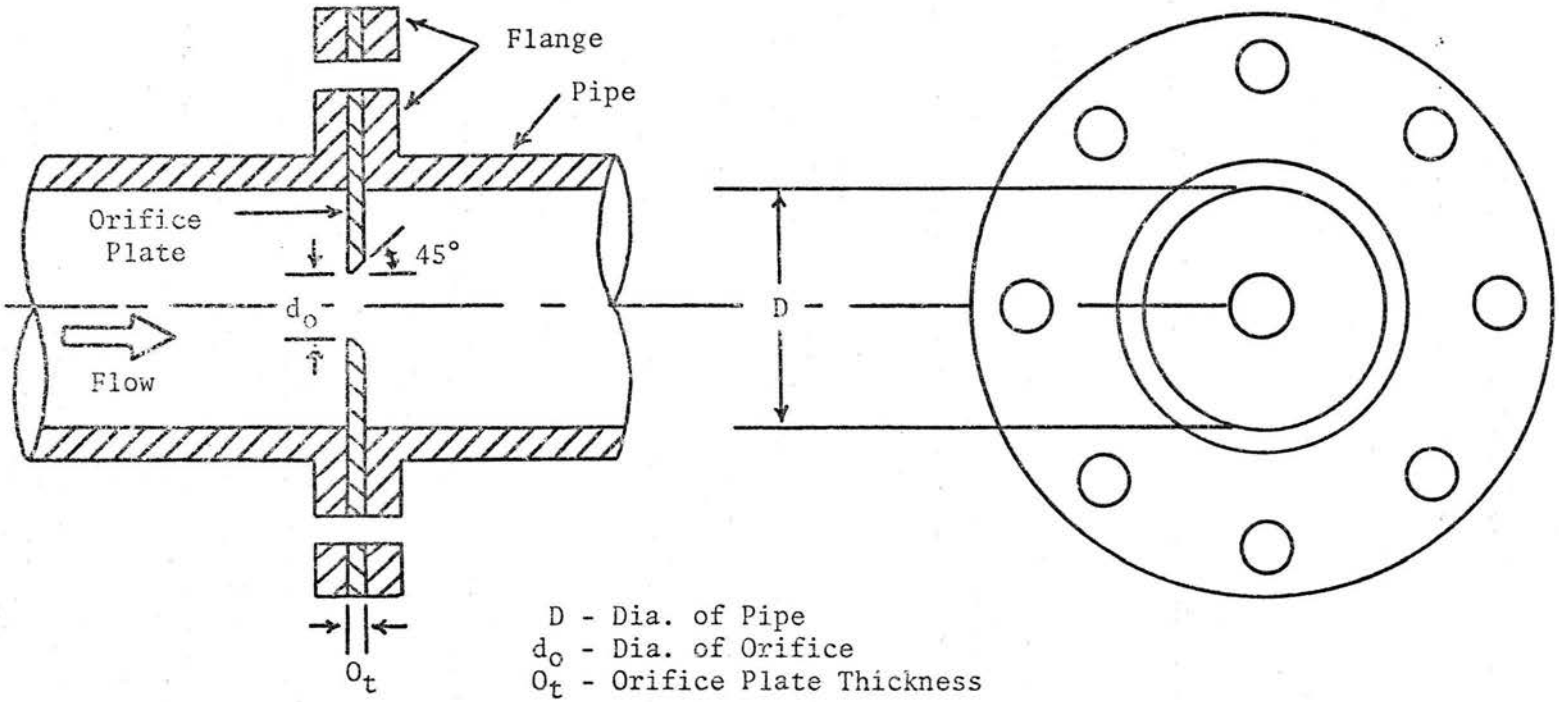

Fig. 1 Test Orifice

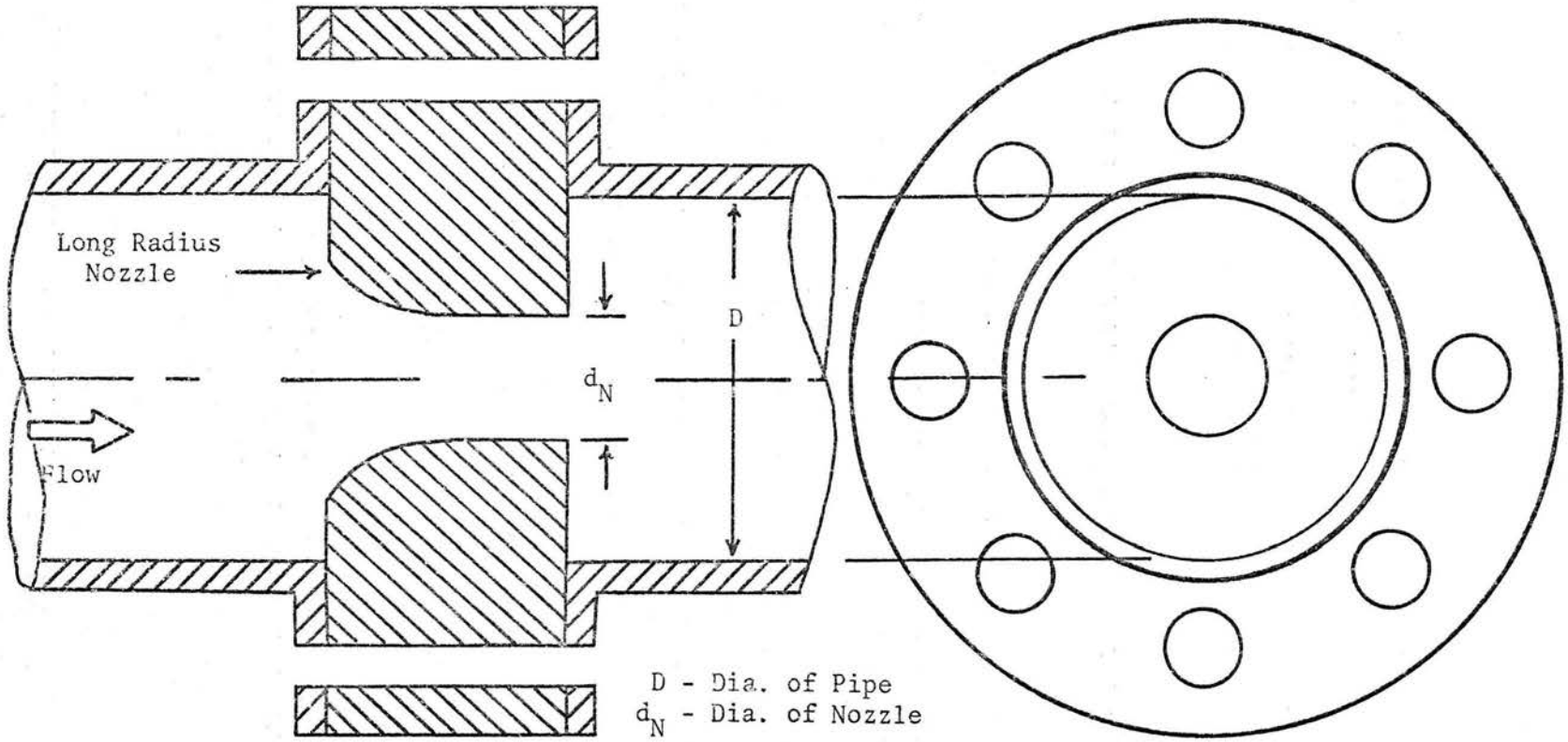

Fig. 2 Long Radius Nozzle

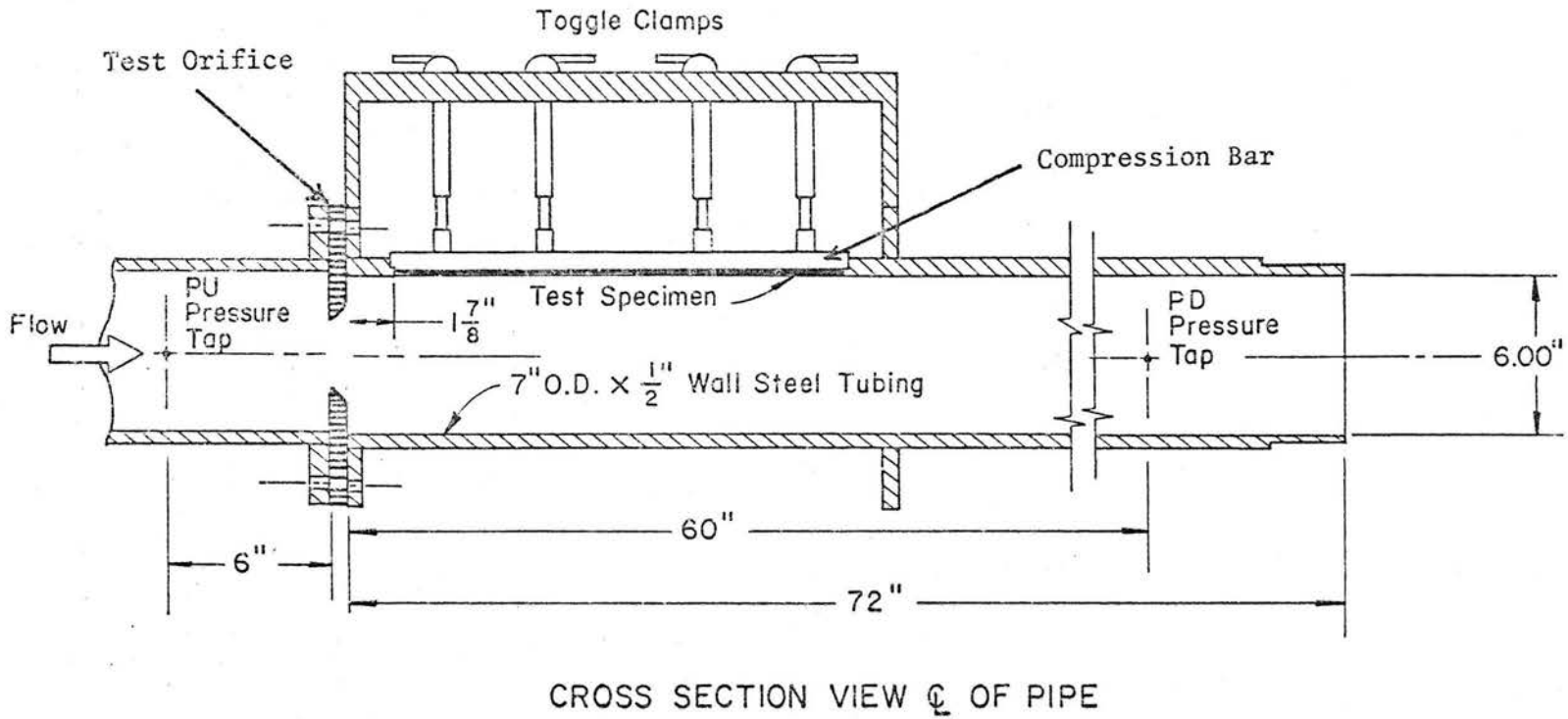

Fig. 3 Cavitation Damage Test Section
(D = 6.0-inches)

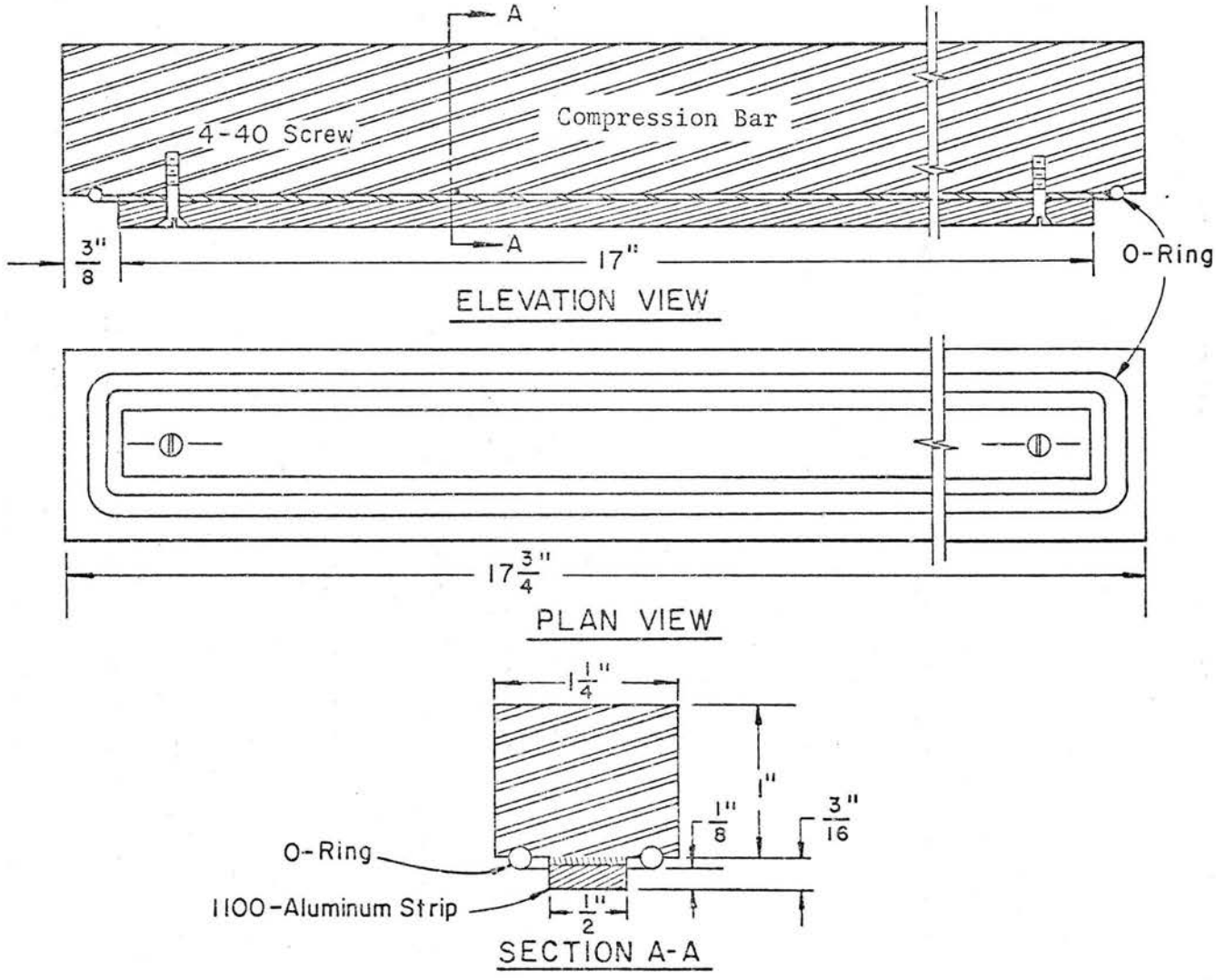

Fig. 4 Compression Bar and Aluminum Specimen

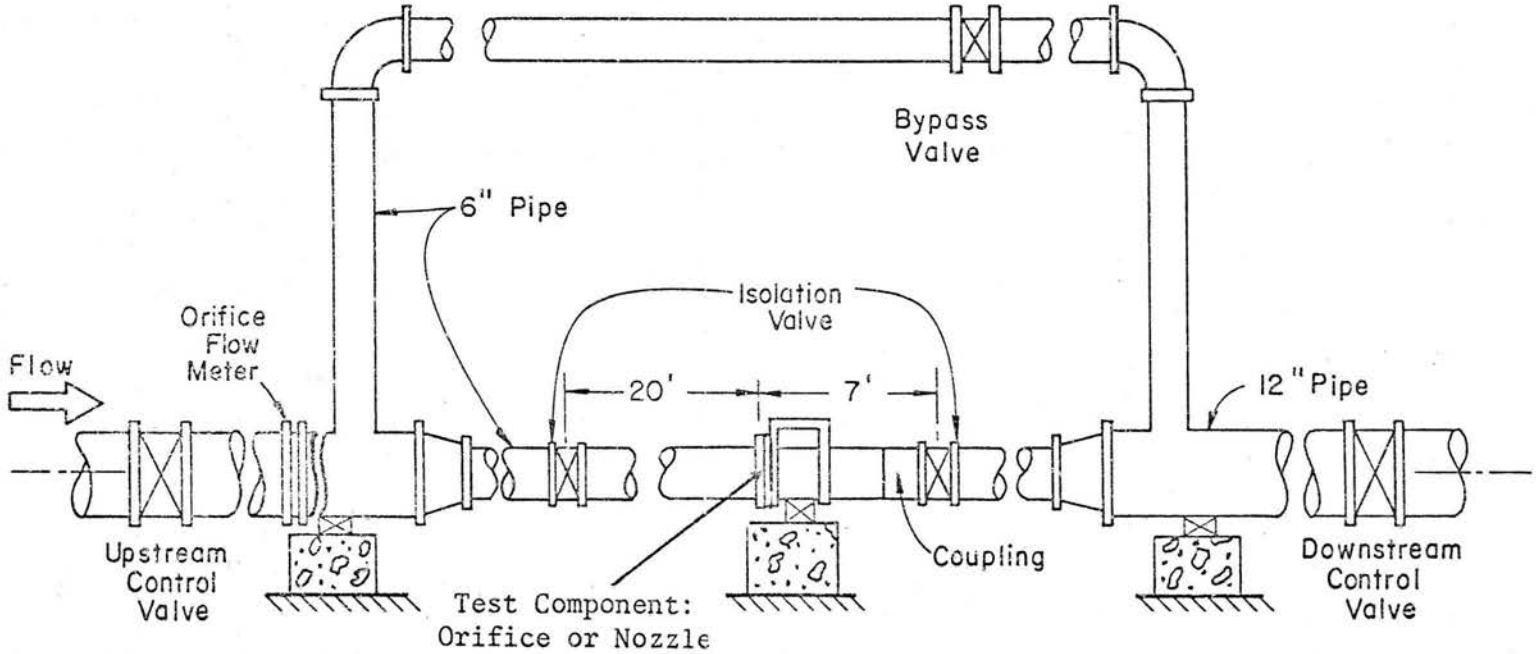

ELEVATION VIEW

Fig. 5 Piping and Control System

to divert flow and relieve pressure in the test section so aluminum test specimens could be removed or replaced. During replacement or removal of test specimens, the flow was diverted through the upper line by opening the bypass valve. For regular damage tests the isolation valves were open and the bypass valve closed.

Procedure for Cavitation Damage Study

The sequence for typical cavitation damage testing will now be explained. The procedure consisted of basically six steps:

1. A "dummy" steel specimen was attached to the compression bar in the test section. The isolation valves were completely opened and all other valves partially opened to allow water to pass through the system. After a period of time the downstream control valve was closed bringing the system to static pressure. At this time residual air was released from the test lines.

2. The bypass valve was closed and the upstream and downstream control valves set to obtain the desired degree of cavitation in the test section.

3. The bypass valve was opened and isolation valves closed thereby diverting the flow and relieving pressure in the test section. Toggle clamps were released; the compression bar removed and the "dummy" specimen replaced by a polished 1100-O aluminum specimen. The compression bar was replaced in the test section and the toggle clamps set to securely seal the test section. Isolation valves were opened allowing part of the total flow to pass through the test section. Residual air was removed at this time.

4. The bypass valve was closed causing total flow to pass through the test section and establishing the desired degree of cavitation at the orifice or nozzle.

5. After an appropriate time interval, the bypass valve was opened relieving cavitation in the test section. Step 3 was repeated except the aluminum test specimen was removed and replaced by the "dummy" specimen.

6. Step 2 was repeated to set the next set of cavitating conditions and the process repeated.

A number of parameters were measured during the cavitation damage tests:

1. The temperature of the water, using laboratory type mercury thermometers.

2. The atmospheric pressure, using a precision microbarograph.

3. Mean pressures; P_u at one pipe diameter upstream, P_d at 10 diameters downstream. A precise, calibrated dial gage was used to measure mean pressures.

4. The discharge, using a suitable flow measuring pipe orifice located upstream of the test section. Pressure drop across the flow measuring orifice was measured using a mercury filled or Meriam filled differential manometer.

5. Sound intensity of the cavitation observed qualitatively by ear.

6. Vibration, using a piezoelectric-type sensing element and a vibration meter (General Radio, type 1553-A).

7. The time the aluminum test specimen was subjected to cavitation damage, using a stopwatch.

Data Processing

After testing, the 1100-O aluminum test specimens were analyzed for cavitation damage. This analysis was divided into two separate stages. First, a grid was placed over the specimens and the number of pits in each grid section were counted using a 3 1/2 power magnification. Even pits with small diameter and depth of penetration could be observed by reflecting light off the specimen at different angles. The local cavitation pitting rate (pits/square inch/minute) was found in each grid section by dividing the number of pits in the section by the section area and time of the test run. Using this analysis the distribution of local cavitation pitting rate could be determined downstream of the orifices and nozzle.

The number of pits per area per time is not enough information to completely describe the cavitation damage. The volume of the pits was also taken into consideration. This was accomplished by scanning selected test specimens with a Nikon metallurgical microscope. The diameter of the pits was measured using a calibrated scale in the microscope eye-piece and a magnification of 50. Depth of the pits was determined by using the fine focusing adjustment at a 200 magnification. The microscope was focused on the bottom of the pit and then on the surface of the specimen at the periphery of the pit. The elevation difference in microns could be estimated by subtracting the readings on the fine focusing adjustment at the two positions.

Chapter IV

EXPERIMENTAL RESULTS

The experimental results will be presented under four different topics; the first three areas are concerned with the character and distribution of the damage and the fourth with correlating orifice and nozzle damage results.

First, consider flow through pipeline orifices when the system size and upstream pressure are held constant. As the velocity is increased, cavitation will eventually begin. Further increases of velocity will create more intense cavitation conditions, finally leading to damage on the conduit walls and the 1100-O aluminum specimens. Increasing the flow will cause more intense damage to occur on the specimens and conduit wall. Damage under these conditions will be discussed in the first section of this chapter.

The next situation considered is submerged orifice flow with system size and cavitation index, sigma, held constant but increasing upstream pressure and therefore discharge. This situation has important implications when hydraulic model studies are conducted at reduced pressure to simulate prototype structures. It has often been found that pressure (velocity) scale effects may exist and holding sigma constant as the system pressure is increased will not produce similar cavitating conditions in model and prototype. Damage under these conditions is discussed in the second section.

The final section for orifices considers constant upstream pressure and cavitation index, but varying system size. Again this is a common situation occurring in hydraulic models of sudden enlargements. For

example, cavitating conditions of a model, reduced in physical size but tested at prototype pressure, may be extrapolated to prototype structures by maintaining a constant value of cavitation index in model and prototype. However, due to size scale effects the cavitation conditions are often different.

A number of sudden enlargements are constructed with nozzle type entrance conditions. Sweeney [55] used a momentum analysis and experimental data to propose a method for predicting incipient cavitation damage in nozzles. This method allows the prediction of nozzle cavitation damage using experimental data from orifice tests. Therefore, it was important in the present study to test the validity of Sweeney's ideas. This was achieved by testing for cavitation damage with a long-radius nozzle and comparing the results with orifice tests.

Cavitation Damage with Varying Sigma

One important aspect of this cavitation research was to determine the area of cavitation damage. Figure 6 shows the upstream and downstream limits plus the area of maximum pitting for various 3-in. orifices tested. The data points were not plotted in Fig. 6 for the upstream and maximum pitting limits for simplification. The upstream, maximum, and downstream pitting limits occurred farther from the orifice as the value of d_o/D decreased. The upstream boundary of the pitting zone extended from $x/d_o \approx 0.4$ for $d_o/D = 0.80$ to $x/d_o \approx 1.3$ for $d_o/D = 0.389$. The area of maximum pitting varied from $x/d_o \approx 0.9$ to $x/d_o \approx 5.0$ and the downstream boundary from $x/d_o \approx 1.6$ to 8.0 over the same d_o/D range. All the above measurements were made for cavitation index values greater than the choking cavitation index.

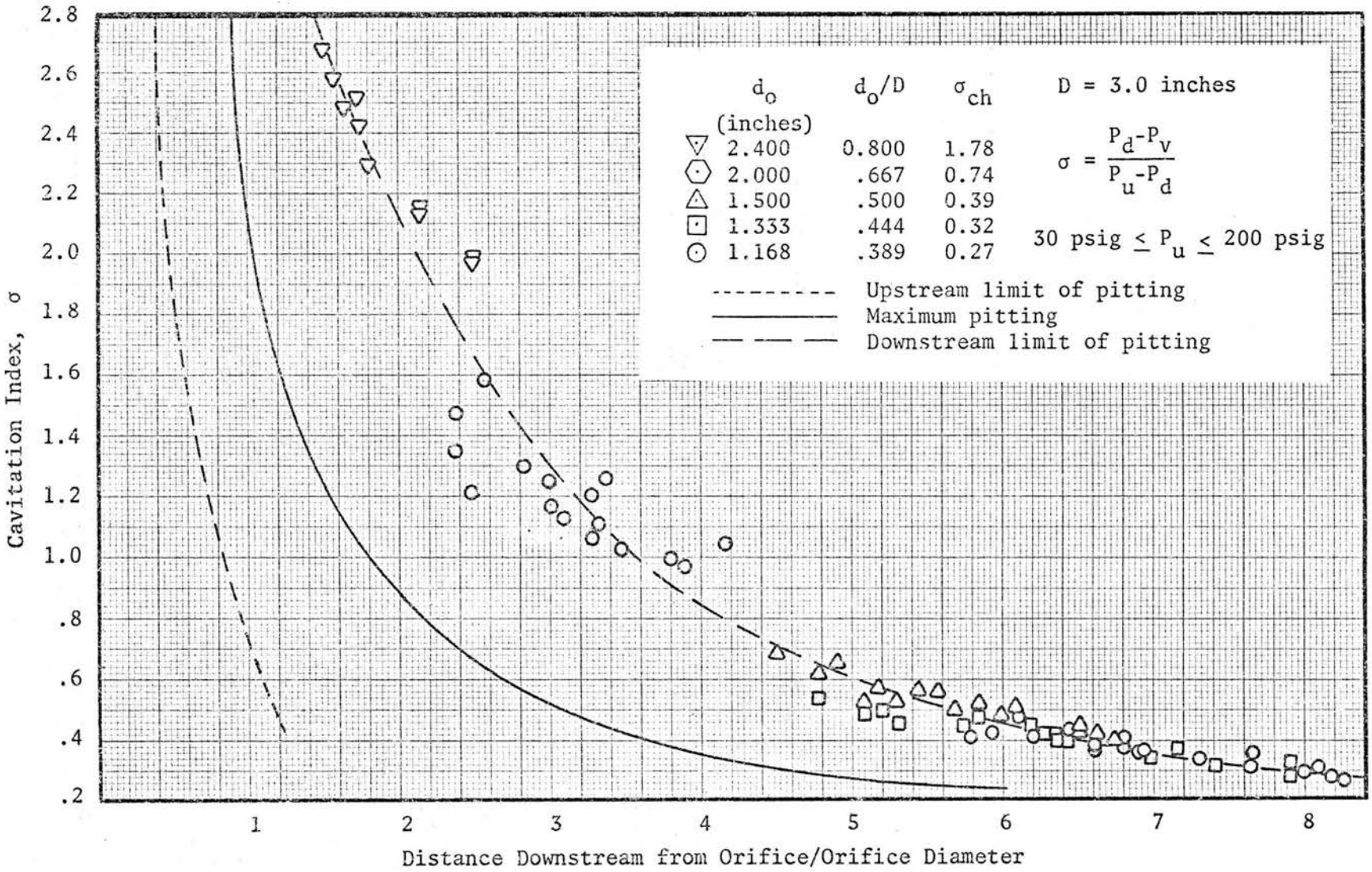

Fig. 6 Effect of Cavitation Index on Location of Pitting

Typical localized cavitation pitting rate distributions are shown in Fig. 7 for a 1.5-in. diameter orifice in a 3-in. I.D. pipe with P_u = 200 psig. The maximum localized cavitation pitting rate is defined as the pitting rate at the peak of the distribution curves. This is an important parameter and will be used to characterize damage in the subsequent analysis. The reattachment location shown in Fig. 7 by the arrow and symbol R_1 was obtained from the work by Teyssandier and Wilson [58]. It is interesting to note that the majority of the cavitation pitting is upstream from the reattachment point. This was found to be the case for all orifices tested.

A series of test runs was made to see if any relationship could be detected between the time of exposure and the maximum localized cavitation pitting rate (MPR). Tests were conducted using the 1.168-in. diameter orifice in the 3-in. I.D. pipe for the same cavitation conditions. The time of the tests was varied between 5 and 20 minutes. The results showed that MPR was independent of exposure time; this fact allowed the actual cavitation damage runs to be conducted to produce specimens with a convenient number of damage pits to analyze. It should be mentioned that the time independence of cavitation pitting rate on soft aluminum has also been verified in the work by Knapp [24,25].

If maximum localized cavitation pitting rate (MPR) is plotted against the mean pipe velocity for a given orifice at constant values of P_u, damage curves such as Fig. 8 result. As Sweeney [55] noted, these curves indicate that the MPR is related to pipe velocity by the equation:

$$MPR \propto 10^{mV} \quad \text{for} \quad P_u = \text{const.} \tag{4-1}$$

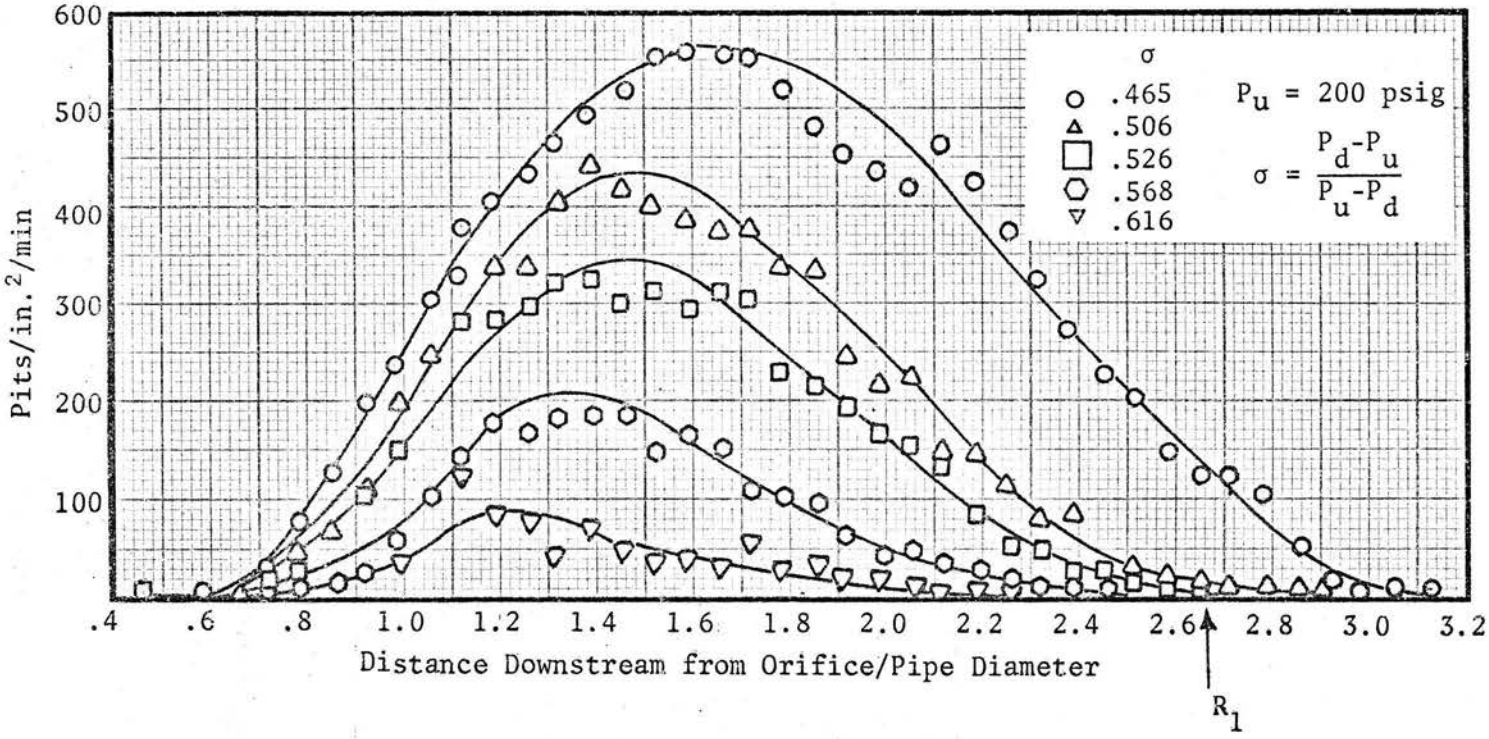

Fig. 7 Longitudinal Distribution of Cavitation Pitting, 1.5-inch, Orifice in 3-inch Pipe

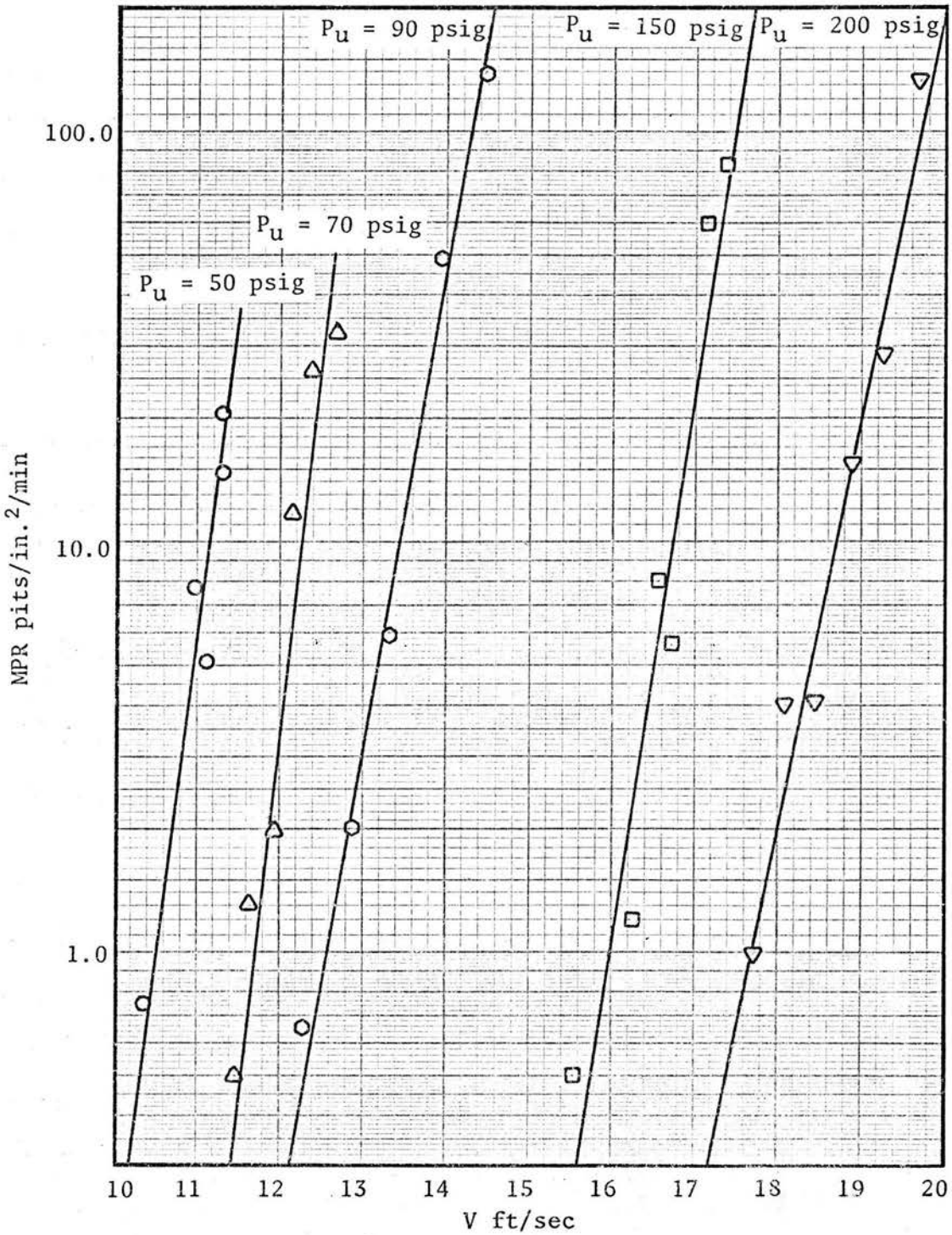

Fig. 8 Maximum Localized Cavitation Pitting Rate (MPR) vs Mean Pipe Velocity, 1.33-inch Orifice in 3-inch Pipe

in which m is the slope of the straight lines and V is the mean pipe velocity. Table 2 shows values of the constant m for orifice data in the 3-, 6-, and 12-in. pipes. The average value of m for the 3-in. data steadily decreases with increasing d_o/D values. This indicates that MPR increases more rapidly with average pipe velocity at smaller d_o/D values, see Appendix II. This is probably due to the fact that a higher level of cavitation is required, at small d_o/D, to produce damage to the pipe wall. Once damage begins, increasing the flow produces damage at a more rapid rate. From the results in Table 2, there seem to be no consistent trends for m to vary with system pressure, P_u, or pipe size for a given d_o/D value.

For all the orifices and pipe sizes tested it was found that the cavitation pitting was confined to within 3 pipe diameters of the orifice. Therefore, the conduit wall area for 3 pipe diameters downstream of the orifice is designated as the cavitation damage region. The parameter, R_a, is the average cavitation pitting rate over the cavitation damage region and has units of pits/in.^{2}/minute.

The 1100-O aluminum specimens were visually inspected to determine if the size of the cavitation pits changed with pipe velocity (or equivalently sigma) for P_u = const. Microscopic investigation revealed that the pit size generally increased as damage became worse although no dramatic changes of pit depth or diameter were observed.

The tests were conducted for time periods that produced a pitting density that was convenient for pit counting. This required that individual pits be separated; that is, specimens were not subjected to the cavitating flow long enough to produce "overlapping pit damage". Therefore, the aluminum specimens were always in the incubation period

TABLE 2 m VALUES FOR MAXIMUM LOCALIZED CAVITATION PITTING RATE EQUATION

d_o/D	P_u (psi)	m 3" line	m 6" line	m 12" line	Average m 3" line
0.389	50	2.42	1.44	----	2.46
	70	2.57	----	----	
	90	2.83	----	1.03	
	150	1.50	----	----	
	200	3.00	----	----	
0.444	30	1.91	2.84	----	1.46
	50	1.51	1.92	----	
	70	1.75	----	----	
	90	1.21	----	----	
	150	1.39	----	----	
	200	1.00	----	----	
0.500	50	1.64	1.27	----	1.20
	70	1.29	1.52	----	
	90	0.96	1.42	----	
	150	1.20	0.94	----	
	200	0.92	0.66	----	
0.667	30	0.59	0.70	0.58	0.50
	50	0.50	----	0.67	
	70	0.62	----	----	
	90	0.45	----	----	
	150	0.39	----	----	
	200	0.46	----	----	
0.800	30	0.32	0.49	----	0.34
	50	0.45	0.45	0.40	
	70	0.31	----	----	
	90	0.36	----	----	
	150	0.28	----	----	

of damage [60] and probably not subject to weight loss but merely isolated plastic deformation [11].

The cavitation pits possessed different types of geometry as shown in Figs. 9 and 10. Some pits were symmetrical, their volumes being similar to spherical segments with high diameter to depth ratios, Fig. 9a. It is suggested that such pits were formed by symmetrical forces or blows generated by symmetrical cavity collapse some distance from the solid boundary. Other symmetrical pits had cylindrical type volumes and again high diameter to depth ratios, see Figs, 9b and 10a. Still other pits were unsymmetrical and had relatively deep penetration at some particular area, see Figs. 9c and 10b. These pits could possibly be formed by a high velocity jet, or perhaps the "wave-guide" effect [26]. Since there were different type pits, it is difficult to precisely estimate what the damage mechanisms may be by mere visual inspection of the damage. However, it seems reasonable to postulate that both symmetrical shock waves and high velocity liquid jets along with perhaps other phenomenon produced the damage.

Cavitation Damage with Varying Upstream Pressure

Table 3 shows the variation of MPR for constant sigma and varying upstream pressure. The pitting rate is seen to increase rapidly with increasing velocity; this indicates pressure (velocity) scale effects are very significant. For example, for $d_o/D = 0.667$ and $\sigma \approx 1.20$, Table 3 shows that when the average pipe velocity is increased from 22.352 to 49.181 ft/sec (P_u = 30 to 200 psig) the MPR increased from 13.25 to 665.00 pits/in.^{2}/min. Therefore by approximately doubling the pipe velocity the MPR was increased by a factor of 50.

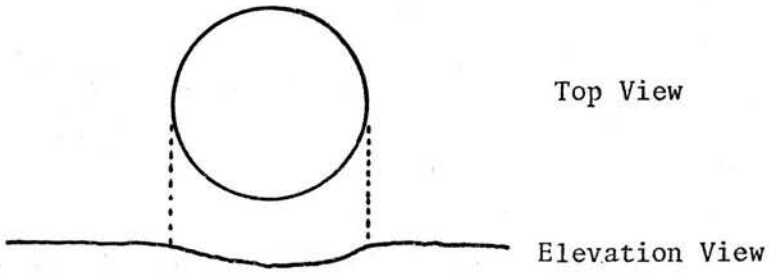

9a. Spherical Segment Pit

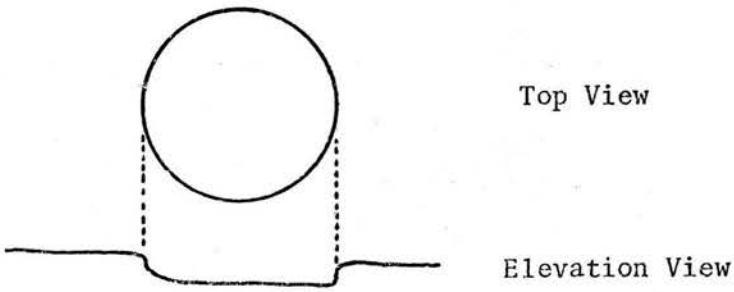

9b. Cylindrical Volume Pit

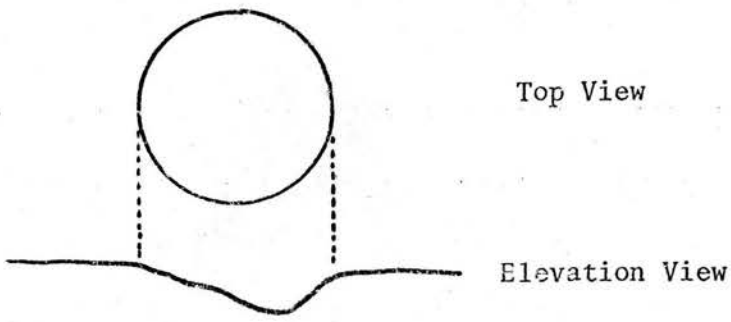

9c. Unsymmetrical Damage Pit

Fig. 9 Geometry of Cavitation Damage Pits in Soft Aluminum

A. Cavitation Pit, 12-inch Enlargement
$d_o/D = 0.667$, $\sigma = 0.998$, $P_u = 50$ psi

$$\sigma = \frac{P_d - P_v}{P_u - P_d}$$

B. Cavitation Pit, $d_o/D = 0.667$,
$\sigma = 1.142$, $P_u = 50$ psi

$$\sigma = \frac{P_d - P_v}{P_u - P_d}$$

Fig. 10 Views of Cavitation Pits in 12-inch Enlargement. Enlarged 48 Times.

TABLE 3 PRESSURE (VELOCITY) SCALE EFFECTS, 3-INCH ORIFICES

d_o/D	Upstream Pressure P_u (psi)	Velocity ft/sec	Cavitation Index	MPR pits/ $in.^2/min$	N See Eq. 4-2
0.3893	90	10.188	.486	0.33	7.6
	150	12.843	.490	1.67	
	200	14.719	.485	5.63	
	70	9.265	.450	1.33	4.3
	150	13.025	.450	5.67	
	50	8.373	.331	5.50	6.1
	90	10.786	.331	25.50	
0.4443	30	9.014	.404	3.83	6.9
	50	10.951	.403	7.60	
	70	12.623	.396	32.00	
	150	17.649	.408	330.00	
	30	8.757	.481	2.17	5.1
	200	19.634	.485	132.00	
0.5000	50	13.957	.566	4.67	6.2
	70	15.999	.563	21.75	
	150	22.421	.565	188.00	
	200	25.610	.568	192.00	
	50	14.140	.519	14.00	5.1
	70	16.254	.521	42.00	
	200	25.959	.526	342.00	
	30	10.826	.731	1.00	3.0
	200	24.058	.728	11.15	
0.6667	30	22.352	1.182	13.25	5.0
	150	43.504	1.185	360.00	
	200	49.181	1.214	665.00	
	70	29.316	1.487	2.00	5.2
	90	32.429	1.493	4.00	
	200	46.471	1.483	22.80	
0.8000	30	34.665	2.838	0.67	4.7
	150	68.261	2.809	16.70	
	70	47.543	2.951	4.17	4.5
	150	67.213	2.928	19.50	

$$\text{Cavitation index} = \sigma = \frac{P_d - P_v}{P_u - P_d}$$

Sweeney [55] and others found the MPR was related to velocity by:

$$MPR \propto V^N \quad \text{for} \quad \sigma = \text{const.} \tag{4-2}$$

in which V is average pipe velocity and N was found to be in the range from 4 to 7. The data in Table 3 indicate that for the present study N varied from 3.0 to 7.6 with an average value of 5.3; there seems to be no consistent variation of N with d_o/D or σ.

In addition to the MPR analysis just described, it is important to also estimate the influence of pressure (velocity) on the depth and diameter of the cavitation damage pits. Therefore certain test specimens were scanned with a microscope and Table 4 prepared. A certain percentage (col. 5) of the deeper and larger diameter pits on each specimen were chosen for comparison purposes. The data for each d_o/D are for $\sigma \approx$ constant. Due to the limited amount of data involved, it is difficult to make precise statements about the trends presented in Table 4. However, the first and last sets of data, $d_o/D = 0.44$, 0.667, show significant increases in both depth and diameter of larger pits. Part of this might be attributed to deaeration of the water for tests at $P_u = 30$ psi. Some suppression of damage was encountered during certain tests at low pressures when the pressure downstream from the orifice was negative. However, other studies have verified the fact that pressure (velocity) scale effects exist for both MPR and pit size. For example, Knapp [24,25] studied cavitation damage on 1100-O aluminum for a fixed cavity. He found, similar to the results just mentioned, that the cavitation pitting rate was proportional to the velocity raised to a power. Also, the percentage of large pits increased as velocity was increased for a constant value of sigma.

TABLE 4 PRESSURE (VELOCITY) SCALE EFFECTS ON PIT DEPTH AND DIAMETER

d_o/D	Pressure Upstream P_u (psig)	Velocity, V (ft/sec)	Cavitation Index	X - % of Pits Considered	Average Depth of Deepest X% of Pits (inch x 10^4)	Average Diameter of X% of Largest Diameter Pits (inch x 10^3)
(1)	(2)	(3)	(4)	(5)	(6)	(7)
.444	30	9.014	.404	0.50	1.5748	3.2880
	150	17.649	.408	0.50	4.3963	7.2838
.500	30	10.968	.635	5.90	0.9843	4.9320
	50	13.616	.640	5.90	1.9094	4.8224
	70	15.738	.639	5.90	1.4026	4.8635
	90	17.579	.641	5.90	1.9948	4.3657
.667	30	22.352	1.182	1.88	2.1872	3.1358
	200	49.181	1.214	1.88	5.2107	6.2375

$$\text{Cavitation index} = \sigma = \frac{P_d - P_v}{P_u - P_d}$$

Cavitation Damage with Varying Pipe Size

As the system size was varied from 3- to 12-in. in diameter, no significant changes in the geometrical location or distribution of the cavitation pitting were observed. Also for a given d_o/D ratio, upstream pressure and mean pipe velocity, the maximum localized cavitation pitting rate did not vary significantly with system size. This fact is shown in Fig. 11. For constant P_u and d_o/D the data for the 3-, 6-, and 12-in. orifices all plot on the same line. Plots of average cavitation pitting rate, R_a, over the cavitation damage region, and mean pipe velocity produced results similar to Fig. 11. The value of R_a was linearly related to mean pipe velocity on the semi-log plots for a given d_o/D and upstream pressure. Again, as in Fig. 11, the data for the 3-, 6-, and 12-in. orifices produced similar results indicating the relation between R_a and mean pipe velocity for given P_u and d_o/D was independent of system size.

The most significant observations related to the influence of the pipe size on damage was the fact that the pit depth and diameter increased as the system size increased. A microscope was used to estimate the depth and diameter of the deeper and larger diameter pits on selected specimens. These results are shown in Table 5. Considering the results as a whole, the average depth of the deeper pits on the specimens increased by an average value of 1.7 when the size of the pipe was increased from 3-in. I.D. to 12-in. I.D. Likewise, the average diameter of the larger diameter pits on the specimens increased by an average value of 1.8 with the same pipe size increase. Even though the pitting rate is constant, the increased pit depth and diameter implies an increasing cavitation intensity with pipe size.

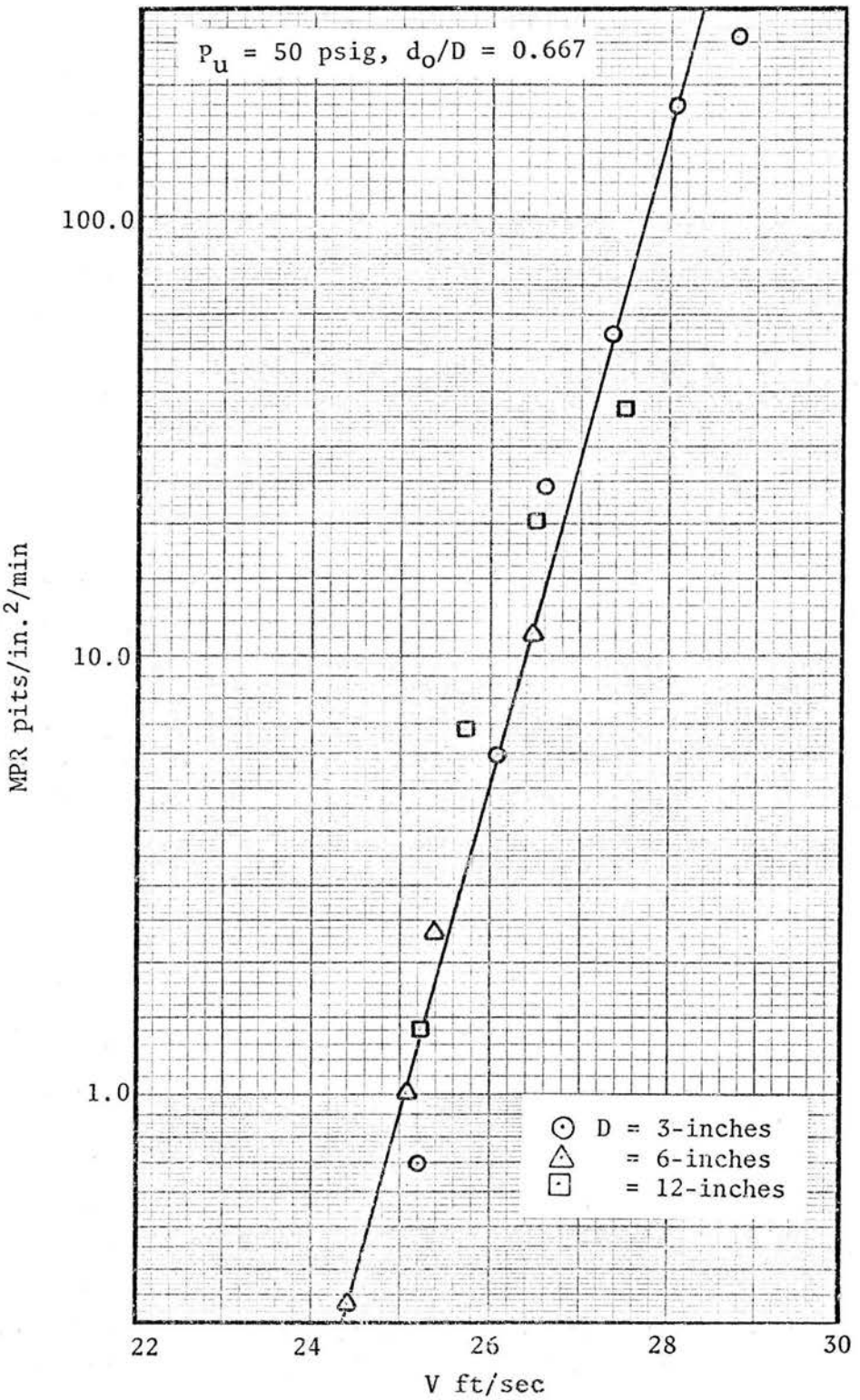

Fig. 11 Variation of MPR with Pipe Size

TABLE 5 CHANGE OF PIT CHARACTERISTICS WITH PIPE SIZE

d_o/D	Upstream Pressure P_u (psig)	D (inches)	$\sigma = \frac{P_d - P_v}{P_u - P_d}$	X - % of Pits Considered	Average Depth of Deepest X% of Pits (inch x 10^4)	Average Diameter of X% of Largest Diameter Pits (inch x 10^3)
(1)	(2)	(3)	(4)	(5)	(6)	(7)
.667	50	12	1.302	5.99	3.299	4.960
.667	50	6	1.232	5.99	2.122	3.490
.667	50	3	1.350	5.99	2.205	3.069
.667	50	12	0.998	1.59	4.964	8.340
.667	50	3	1.003	1.59	3.123	5.480
.667	50	12	1.142	2.44	4.552	9.360
.667	50	3	1.134	2.44	2.907	4.550
.800	50	12	2.47	2.70	2.672	5.250
.800	50	6	2.51	2.70	2.093	3.820
.800	50	3	2.44	2.70	2.582	3.560
.800	50	12	2.67	6.41	2.861	4.060
.800	50	3	2.78	6.41	1.378	2.470
.381	90	12	0.406	6.36	2.975	5.980
.381	90	3	0.492	6.36	1.260	2.630

Nozzle Results

Semi-log plots of MPR versus mean pipe velocity for a 2 x 6-in. nozzle tested at upstream pressures between 50 and 200 psig produced linear relations, similar to orifice data in Fig. 8. Visual observations revealed no significant change in pit size compared with the damage produced during the 6-in. orifice tests.

Fifteen damage tests were conducted to determine the location of pitting downstream from the 2-in. diameter long radius nozzle. The tests included variations of upstream pressure (50-200 psig) and various degrees of cavitation damage at each upstream pressure. This caused the boundary of the cavitation damage area to vary. The upstream boundary of the pitting for the nozzle varied between $x/d_N = 1.94$ to 3.79 with an average value of $x/d_N = 2.76$. The area of maximum pitting varied between $x/d_N = 4.69$ to 6.39 with an average of $x/d_N = 5.35$. Finally, the average downstream limit of pitting was $x/d_N = 7.56$ with maximum deviations of $x/d_N = 6.29$ and 8.49. The pitting rate distributions were very similar to the ones shown in Fig. 7.

Chapter V

DISCUSSION AND ANALYSIS OF EXPERIMENTAL RESULTS

This chapter analyzes the basic results presented in Chapter IV. The discussion and analysis presented in this chapter is divided into three topic areas.

First, an incipient cavitation damage design criteria based upon maximum localized cavitation pitting rate, MPR, on soft aluminum is established. Pressure (velocity) and size scale effects for the incipient damage condition in sudden enlargements are evaluated. Empirical equations are introduced for scaling incipient cavitation damage to different pressures and sizes.

The second section of this chapter provides information to estimate the trends and variation in the average energy of pit formation at the incipient damage condition. It is found that even though the MPR may be maintained constant in two situations, the volume or size (and therefore energy of pit formation) may vary greatly. Therefore the second section presents a more refined analysis of the incipient damage condition by considering both MPR and a measure for the energy of formation of the pits.

The final section discusses the severity of the cavitation attack when the system is operated beyond the incipient damage point. The analysis of the damaging regime of cavitation is conducted by using the cavitation intensity, I_{exp}, as a measure of the intensity of cavitation attack. The variation of I_{exp} is studied under three different conditions: (1) varying cavitation index, sigma, (2) varying upstream pressure (velocity), and (3) varying pipe size. The scaling laws for

cavitation erosion mentioned in Chapter II and shown in Appendix I will also be used along with experimentally measured flow field data to predict damage under the above three conditions.

Incipient Damage Based on Pitting Rate

Definition and Uses of Incipient Damage Condition

As mentioned in Chapter II [67], cavitation design data have been experimentally identified for three of the four cavitation limits defined for sudden enlargements. Experimental data useful for practical design exist for incipient, critical, and choking cavitation; only the incipient damage condition has not been studied in detail. It would be helpful in the design of sudden enlargement energy dissipators to provide a practical method of predicting incipient damage.

Considering the experimental results discussed in the last chapter, Fig. 8 indicates that the cavitation damage (measured in terms of MPR) increases very rapidly with mean pipe velocity for a given P_u, system size, and d_o/D ratio. These straight line relations on semi-log plots are convenient for interpolating or extrapolating the experimental data. Graphs such as Fig. 8 were used to define a mean pipe velocity at incipient damage, V_{id}, for a given upstream pressure, system size, and d_o/D ratio. However, V_{id}, should be carefully and conservatively selected since slight error in the pipe velocity may cause large increases in cavitation damage.

For the present study, V_{id} was defined for a particular orifice at a given upstream pressure by selecting the velocity corresponding to an MPR of 1 pit/in.^{2}/min. Although this definition of V_{id} is somewhat arbitrary, there are facts that indicate this is a reasonable criteria

for selection. Considering application of results to other materials, Knapp [24] noted that 1100-O aluminum is soft enough for immediate permanent deformations to result from cavitation blows that would cause ultimate failure of harder structural materials. Sweeney [55] also showed that for the same cavitating conditions, the pitting rate on cold rolled steel with a Brinell hardness of 145 was about 1/100 that of 1100-O aluminum. Therefore, a pitting rate of 1 pit/in.^{2}/min on soft aluminum does produce damage on common, harder structural materials but at a much slower rate.

Table 6 shows the value of V_{id} and σ_{id} for orifices tested in 3-, 6-, and 12-in. pipes. Table 7 indicates V_{id} and σ_{id} for the 2-in. dia nozzle tested in a 6-in. dia line. The corrected downstream pressure, P_d, at incipient damage for a given upstream pressure, P_u, was calculated (it was not experimentally measured) using the definition of C_d and the value of V_{id}. Once P_d was known at incipient damage, a measured value of P_v along with the given P_u were used to calculate σ_{id}.

There are several important facts that should be mentioned concerning Table 6. First, for a given d_o/D ratio and pipe size the value of the σ_{id} increases as P_u is increased. This fact has important implications concerning pressure (velocity) scale effects for the incipient damage condition; if there are no pressure (velocity) scale effects the value of σ_{id} should remain constant as P_u is increased.

TABLE 6 HYDRAULIC CHARACTERISTICS RELATED TO INCIPIENT CAVITATION DAMAGE IN SUDDEN ENLARGEMENTS OF 3-, 6- AND 12-INCHES

Pipe Size in.	Orifice Size in.	d_o/D	β	β'	C_d	P_u psi	P_d psi	V_{id} fps	σ_{id}
3.00	1.168	0.389	6.60	11.06	0.100	50	6.2	8.1	0.421
						70	12.3	9.3	.425
						90	19.3	10.3	.446
						150	42.4	12.7	.507
						200	63.6	14.3	.556
	1.333	0.444	5.07	8.33	0.133	30	1.68	8.7	.490
						50	8.8	10.5	.510
						70	18.8	11.7	.605
						90	28.7	12.8	.667
						150	55.4	15.9	.715
						200	82.8	17.7	.811
	1.500	0.500	4.00	6.53	0.179	50	12.4	13.6	.654
						70	23.0	15.2	.749
						90	33.9	16.6	.822
						150	65.3	20.4	.915
						200	90.5	23.2	.938
	2.000	0.667	2.25	3.49	0.385	30	12.9	21.0	1.468
						50	25.8	25.0	1.570
						70	38.6	28.5	1.618
						90	52.6	31.1	1.733
						150	93.2	38.3	1.856
						200	127.5	43.2	1.927
	2.400	0.800	1.56	1.97	0.648	30	18.9	34.6	2.802
						50	34.8	40.4	3.092
						70	49.6	46.8	3.029
						90	65.6	51.2	3.189
						150	113.5	62.6	3.444
6.00	2.315	.386	6.72	11.27	.098	50	6.66	7.9	.435
	2.666	.444	5.07	8.38	.135	30	1.9	8.8	.502
						50	9.99	10.5	.555
	2.991	.499	4.02	6.58	.180	30	5.66	11.0	.734
						50	14.42	13.3	.748
						70	23.53	15.2	.769
						90	33.90	16.7	.822
						150	65.47	20.5	.919
						200	92.67	23.1	.977
	4.000	.667	2.25	3.48	.381	50	25.00	25.1	1.488
	4.785	.798	1.57	2.25	.642	30	19.22	33.5	2.915
						50	34.63	40.0	3.047
12.00	4.570	.381	6.89	11.57	.097	--	--	--	--
						70	11.44	9.1	.400
						90	17.66	10.1	.413
	7.980	.665	2.26	3.49	.377	50	24.37	25.1	1.427
						70	37.87	28.1	1.558
	9.600	.800	1.56	2.21	.643	50	34.54	40.2	3.023

$$\sigma = \frac{P_d - P_v}{P_u - P_d} \qquad \beta = \frac{\text{Pipe Area}}{\text{Orifice Area}} \qquad \beta' = \frac{\text{Pipe Area}}{\text{Jet Area}}$$

TABLE 7 TEST DATA RESULTS 2-IN. NOZZLE
(D = 6.0 inches)

d_N (in.)	β'	C_d	P_u (psig)	P_d (psig)	P_{min} (psig)	V_{id} (ft/sec)	σ_{id}
2.000	9.00	0.123	50	6.80	-4.56	9.90	0.440
			70	15.74	1.15	11.03	.515
			150	46.28	17.93	15.35	.564
			200	68.27	32.25	17.27	.611

$$\sigma = \frac{P_d - P_v}{P_u - P_d} \qquad \beta' = \frac{\text{Pipe Area}}{\text{Jet Area}}$$

Table 8 was constructed to show the variation of σ_{id} with pipe size. For a given upstream pressure, P_u, and d_o/D ratio, the experimental results for σ_{id} in Table 8 show no strong or consistent trend to vary with pipe size. Although the orifices used in these studies were carefully machined to hopefully produce geometrically similar orifices, there was some variation of d_o/D with pipe size. Small variations of d_o/D and geometry could be the reason for orifices of approximately the same d_o/D value having slightly different C_d values in the three pipe sizes. These facts along with unavoidable experimental errors could produce variations in σ_{id} of the magnitude shown in Table 8. For these reasons the author considers the value of σ_{id} not to vary significantly with pipe size for a constant P_u and d_o/D.

Table 9 shows the relation of σ_{id} to the cavitation indices at inception, critical, and choking levels of cavitation. All values of d_o/D for D = 3.0 in. dia show that $\sigma_{ch} < \sigma_{id} < \sigma_c < \sigma_i$. Column (8)

TABLE 8 INCIPIENT CAVITATION DAMAGE SIZE SCALE EFFECTS FOR ORIFICES

d_o/D	P_u (psig)	V_{id} (ft/sec)			$\sigma_{id} = \frac{P_u - P_v}{\rho V_{id}^2}$			$\sigma_{id} = \frac{P_d - P_v}{P_u - P_d}$		
		D = 3"	D = 6"	D = 12"	D = 3"	D = 6"	D = 12"	D = 3"	D = 6"	D = 12"
0.38	50	8.1	7.9	---	70.42	73.56	---	.421	.435	---
	70	9.3	---	9.1	70.56	---	73.68	.425	---	.400
	90	10.3	---	10.1	71.57	---	74.37	.446	---	.413
0.44	30	8.7	8.8	---	41.33	40.52	---	.490	.502	---
	50	10.5	10.5	---	41.90	42.12	---	.510	.555	---
0.50	50	13.6	13.3	---	24.91	26.17	---	.654	.748	---
	70	15.2	15.2	---	26.35	26.44	---	.749	.769	---
	90	16.6	16.7	---	27.50	27.30	---	.822	.822	---
	150	20.4	20.5	---	28.94	28.65	---	.915	.919	---
	200	23.2	23.1	---	29.23	29.60	---	.938	.977	---
0.67	50	25.0	25.1	25.1	7.387	7.341	7.270	1.570	1.488	1.427
	70	28.5	---	28.1	7.517	---	7.635	1.618	---	1.558
0.80	30	34.6	33.5	---	2.621	2.811	---	2.802	2.915	---
	50	40.4	40.0	40.2	2.822	2.890	2.857	3.092	3.047	3.023

TABLE 9 FOUR LEVELS OF ORIFICE CAVITATION
(D = 3.0")

d_o/D (1)	P_u (psig) (2)	σ_i (3)	σ_c (4)	σ_{id} (5)	σ_{ch} (6)	CD_{id} (7)	Q_{id}/Q_i (8)
0.389	50	1.09	0.93	0.421	0.264	0.810	1.29
	70			.425		.805	1.29
	90			.446		.780	1.28
	150			.507		.706	1.25
	200			.556		.647	1.23
0.500	50	1.53	1.15	.654	0.381	0.762	1.34
	70			.749		.680	1.30
	90			.822		.616	1.27
	150			.915		.535	1.24
	200			.938		.515	1.23
0.667	30	2.87	1.96	1.468	0.665	0.636	1.40
	50			1.570		.590	1.37
	70			1.618		.568	1.36
	90			1.733		.516	1.33
	150			1.856		.460	1.30
	200			1.927		.428	1.28
0.800	30	6.10	3.68	2.802	1.65	0.741	1.49
	50			3.092		.676	1.43
	70			3.029		.690	1.42
	90			3.189		.654	1.41
	150			3.444		.597	1.37

of Table 9 indicates the relation between the discharge at cavitation inception and the discharge at incipient damage for given d_o/D ratio and P_u. As P_u is increased for a given d_o/D ratio, the value of Q_{id}/Q_i decreases by a small amount: for $d_o/D = 0.667$, changing P_u from 30 to 200 psig will change Q_{id}/Q_i from 1.40 to 1.28. In addition, for constant P_u the value of Q_{id}/Q_i increases as d_o/D increases. For example, if $P_u = 50$ psig, increasing d_o/D from 0.389 to 0.800 increases Q_{id}/Q_i from 1.29 to 1.43.

The fact that Q_{id}/Q_i decreases as P_u is increased for a given d_o/D can be explained by considering pressure (velocity) scale effects. As mentioned before, there are no pressure scale effects for cavitation inception in orifices. However, there is a pressure scale effect for the incipient damage condition. This pressure scale effect is non-conservative since damage happens at a lower flow than would be indicated by sigma values calculated at lower pressures. Therefore, at higher pressures incipient damage occurs closer to incipient cavitation.

Increasing Q_{id}/Q_i with increasing d_o/D for constant P_u can be explained by inspecting the variation of V_i and V_{id} with d_o/D for a given P_u. Letting $P_u = 50$ psig and using the data in Table 9 produces the results:

$$V_{id} \propto (d_o/D)^{2.21}$$

$$V_i \propto (d_o/D)^{2.12}$$

Using these relations it can be shown that

$$\frac{Q_{id}}{Q_i} \propto \frac{V_{id}}{V_i} \propto (d_o/D)^{0.09}$$

Therefore both V_{id} and V_i increase with increasing d_o/D; however, V_{id} increases more rapidly thereby producing a small increase in Q_{id}/Q_i with d_o/D.

It is also interesting to consider the variation of cavitation degree with d_o/D for a given system size. The cavitation degree at a certain value of σ is defined as

$$CD = \frac{\sigma_i - \sigma}{\sigma_i - \sigma_{ch}} \qquad \sigma_{ch} \leq \sigma \leq \sigma_i \tag{5-1}$$

in which CD = cavitation degree at cavitation index σ, σ_i = incipient cavitation index, σ_{ch} = choking cavitation index. Notice that at cavitation inception CD = 0.0 and at the choking condition, CD = 1.0. Therefore, CD ranges from a value of 0.0 to 1.0 as the level of cavitation goes from the lightest possible level, σ_i, to the most severe level, σ_{ch}. Table 9, col. 7, shows the cavitation degree at the incipient damage condition, $\sigma = \sigma_{id}$ in Eq. (5-1). For a given d_o/D ratio the value of CD_{id} steadily decreases with increasing P_u. Considering the first three d_o/D ratios, for a given value of P_u the value of CD_{id} steadily decreases as d_o/D increases. For example, letting P_u = 50 psig, CD_{id} changes from 0.810 to 0.590 as d_o/D is changes from 0.389 to 0.667.

Noise can also be used to measure the cavitation degree. During the experiments noise level was estimated by ear. It was very evident that noise increased at the incipient damage condition with decreasing d_o/D for a constant P_u. Assuming noise is a measure of cavitation level, this would indicate a corresponding increase in cavitation level.

The above analysis concerning CD and observations of noise during the experiments both indicate that the cavitation field is at a more advanced stage at incipient damage as d_o/D is decreased. These facts can be explained by noting that as d_o/D decreases the shear layer is displaced from the pipe wall. Therefore, higher levels of cavitation will be required at lower d_o/D values in order to transport the cavities to the wall region. Once damage begins on the pipe wall, the MPR increases more rapidly for lower d_o/D values, see Table 2, Chapter IV and Appendix II. This fact indicates more cavitation cavities in the near wall region at incipient damage and therefore higher levels of cavitation at lower d_o/D values for a given P_u.

The data for cavitation degree concerning $d_o/D = 0.800$ in Table 9 did not follow the trend of data found for the first three d_o/D values. Later calculations concerning incipient damage also indicate that the $d_o/D = 0.800$ data differs from the trends established in the smaller d_o/D value orifices. The data taken for $d_o/D = 0.800$ was obtained by using a 2.400-in. dia orifice in a 3.00-in. I.D. line. This is a very large orifice for the 3-in. line causing the shear layer downstream from the orifice to be in close proximity to the pipe wall. As the d_o/D values decrease for the other orifices the shear layer will be moved farther from the pipe wall. For this reason the author suspects that geometry of the pipe wall and shear layer caused the deviations of the $d_o/D = 0.800$ data from the other results.

The flow field for orifices with small d_o/D may be characterized by a constricted type of flow. That is the fully established upstream velocity profile is drastically changed into a liquid jet situation and

associated jet dissipation downstream from the orifice. However for large d_o/D values, this flow situation will be modified. Now instead of changing the upstream flow field drastically, the orifice may act more as a surface roughness submerged in a fully developed boundary layer. Both situations produce a shear layer where vortex type cavitation is initiated; but there are sizable variations in geometry and nature of the flow field. It is not unexpected that trends for cavitation inception and incipient damage established with small and moderate values of d_o/D will not apply to the large d_o/D ratios (surface roughness type situations).

Pressure (Velocity) Scale Effects

The past section presented values of σ_{id} and V_{id} for experimental tests conducted at various pressures and orifice sizes. The following sections will use these basic data to quantify the scale effects and develop empirical equations to predict σ_{id} or V_{id} for different orifices operating at other conditions.

As mentioned in Chapters I and II, scale effects cause deviations from the elementary similarity relations linking the cavitation index, σ, to geometric and kinematic conditions. Viscosity, gravity, surface tension, thermodynamic properties, and turbulence effects as well as contaminations in the liquid can give rise to scale effects. In the present study, it is important to define any scale effects that may exist for the incipient damage condition.

Pressure scale effects for cavitation damage are usually evaluated by maintaining the cavitation index constant and increasing the velocity of flow. If the cavitation damage remains constant with velocity at

the given cavitation index there are no pressure scale effects. Table 3 verifies the existence of pressure scale effects for incipient cavitation damage in orifice flow. Considering the 2.400-in. dia orifice, a velocity of $V = 34.6$ ft/sec at $\sigma \approx 2.8$ produces an MPR of approximately 1.00 pits/in.^{2}/min which is the incipient damage criteria. Table 3 indicates that if σ is kept at 2.8 and the velocity is increased to 68.3 ft/sec the MPR becomes 16.70 pits/in.^{2}/min. Therefore, there is a definite pressure scale effect for the incipient damage condition. In fact, Chapter IV mentions that $MPR \propto V^N$, with N varying from 3.0 to 7.6 for σ = const. This relation indicates a rapidly increasing MPR with increasing pipe velocity.

Pressure scale effects can also be considered from another viewpoint. If the MPR is maintained at 1.00 pit/in.^{2}/min for a given pipe size and d_o/D ratio; the value of the cavitation index at MPR = 1.00 pit/in.^{2}/min, σ_{id}, should remain constant as P_u is increased. However, Table 6 shows that σ_{id} increases as the upstream pressure is increased.

Figure 12 was developed to show the variation of σ_{id} with P_u. The log-log plot gives straight line relationships between σ_{id} and $P_u - P_v$ indicating the relation is independent of pipe size. The slope of the linear plots was 0.24, which indicates a relation of

$$\sigma_{id} = \text{const.} \ (P_u - P_v)^{0.24} \qquad (5\text{-}2)$$

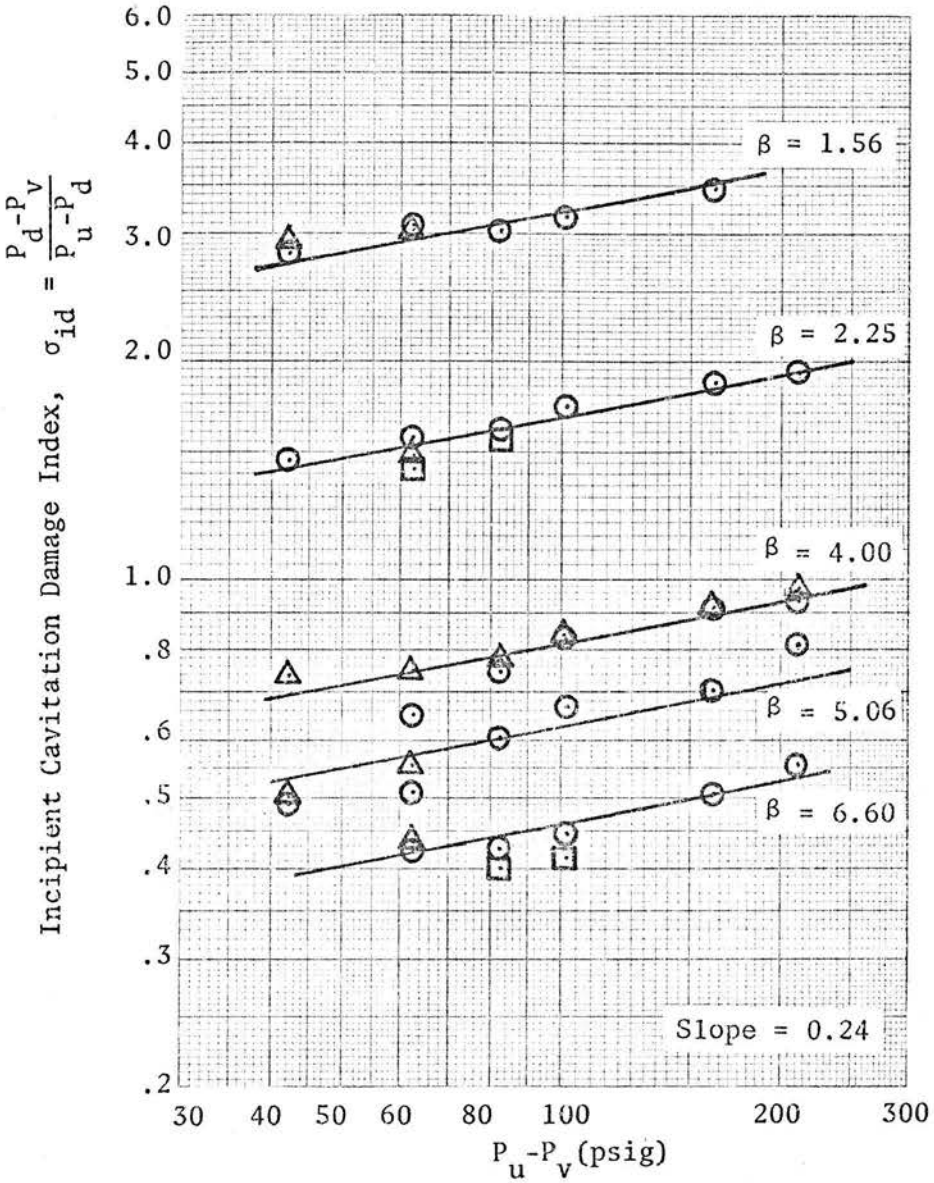

Fig. 12 Pressure Scale Effects Indicated by σ_{id} vs $P_u - P_v$

in which σ is defined as $(P_d-P_v)/(P_u-P_d)$. If the constant is evaluated in terms of the reference data given in Table 6, Eq. (5-2) becomes:

$$\sigma_{id} = \sigma_{idr}\left(\frac{P_u-P_v}{P_{ur}-P_{vr}}\right)^{0.24} \qquad d_o/D = \text{const.} \tag{5-3}$$

in which σ_{idr}, P_{ur}, and P_{vr} are reference data from Table 6 for the given d_o/D ratio. A similar equation can be developed using P_d and P_{dr} instead of P_u and P_{ur}.

Another method of determining scaling equations for pressure (velocity) scale effects has been introduced by Tullis and Govindarajan [67]. One form of the cavitation index is:

$$\sigma = \frac{P_u - P_v}{\frac{1}{2}\rho V^2} \tag{5-4}$$

When σ is evaluated at the incipient damage condition, this definition of sigma can be used to solve for V_{id}:

$$V_{id} = C_1(P_u-P_v)^{0.5} \tag{5-5}$$

in which $C_1 = (2/\rho\sigma_{id})^{0.5}$. This equation indicates that if σ_{id} = const. the mean pipe velocity at incipient damage, V_{id}, should be proportional to $(P_u-P_v)^{0.5}$. Some typical experimental data shown in Table 6 are plotted in Fig. 13; all the data show a pressure scale effect defined by:

$$V_{id} = C_1(P_u-P_v)^{0.45} \tag{5-6}$$

Since the exponent is different from 0.5, the experimental data indicates a pressure scale effect for the incipient damage condition. Figure 13

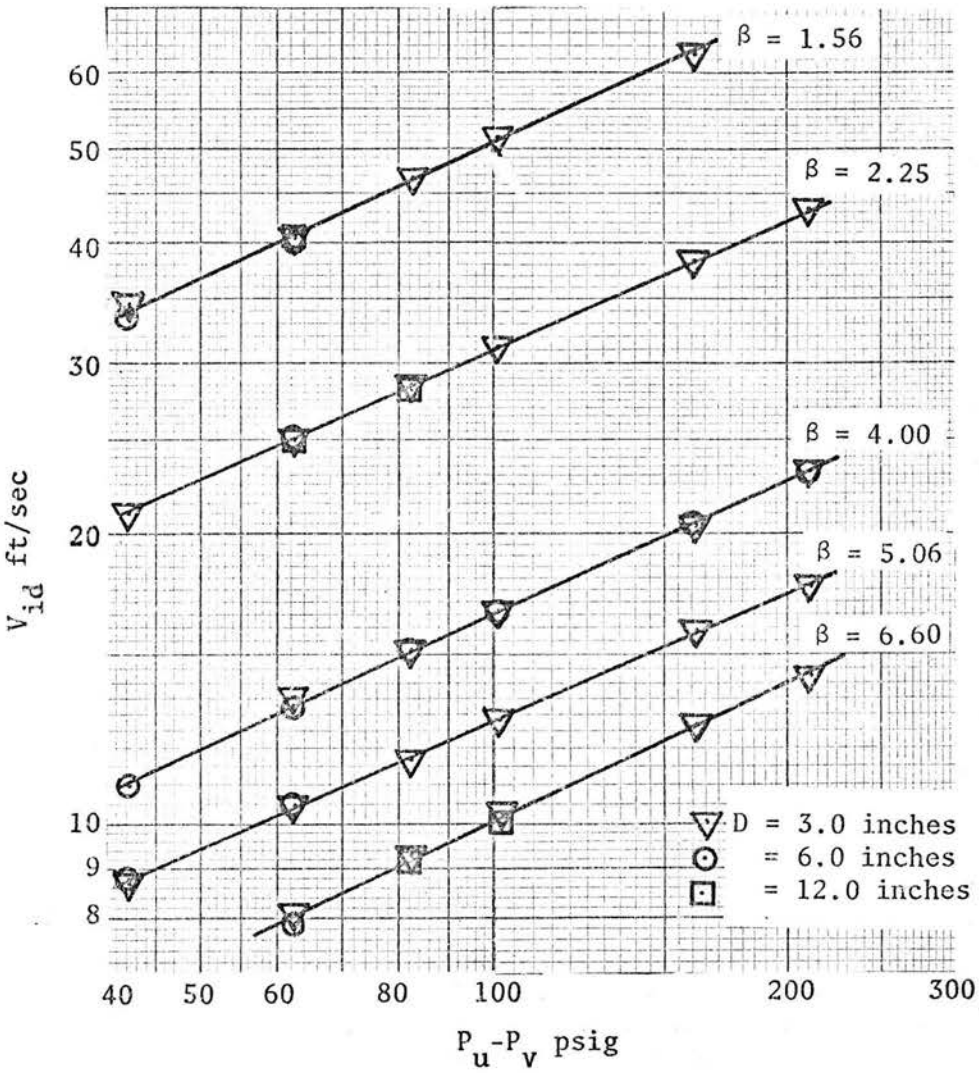

Fig. 13 Pressure Scale Effects Indicated by V_{id} vs P_u-P_v

also indicates that the pressure scale effect is independent of pipe size for a given d_o/D ratio. Using the reference data in Table 6 to evaluate C_1, Eq. (5-6) becomes

$$V_{id} = V_{idr} \left(\frac{P_u - P_v}{P_{ur} - P_{vr}} \right)^{0.45} \tag{5-7}$$

Equation (5-7) was tested to see how closely it would predict the experimental data in Table 6. This was done by selecting an orifice and upstream pressure and therefore V_{id} from Table 6. These values were used as reference data in Eq. (5-7) to predict V_{id} for the selected orifice at other upstream pressures and to predict V_{id} for other orifices with the same value of d_o/D. This process was completed for all the orifices in Table 6. The error analysis produced the following results:

Average value of absolute error, $\overline{|Err|} = 1.4\%$

Standard deviation of absolute error, $S = 1.3\%$

Absolute value of largest error, $|Err|_{max} = 7.6\%$

where absolute error refers to the magnitude of the error without regard to whether the error is positive or negative.

The 2-in. dia nozzle data were also plotted on log-log paper, V_{id} vs $P_u - P_v$. A least squares fit was placed through the data and the slope of the straight line was found to be 0.46. This value compares well with 0.45 found above for orifices. Therefore it seems that nozzles have the same pressure scale effects as orifices.

It is important to realize and appreciate the value of scaling model data according to Eq. (5-7) instead of traditional methods of maintaining constant sigma values in model and prototype. For example,

suppose it is necessary to scale the incipient damage condition in a sudden enlargement, $d_o/D = 0.800$ in a 3-in. dia line, from $P_u = 30$ psig to $P_u = 150$ psig. If a model test is conducted at $P_u = 30$ psig, Table 3 shows that the value of V_{id} will be approximately 34.7 ft/sec or a sigma value of 2.8. Table 3 also indicates that if the incipient damage condition is scaled by maintaining sigma ≈ 2.8 in the prototype, the maximum pitting rate at the higher pressure would be approximately 17 times greater than desired. This problem can be eliminated by scaling the reference data with Eq. (5-7), for example using reference values: $P_{ur} = 30$ psig, $V_{idr} = 34.7$ ft/sec. Assuming $P_v = P_{vr} = -12.20$ psig, Eq. (5-7) will predict a value of $V_{id} = 63.6$ ft/sec at 150 psig. This value is only 1.6% from the actual velocity of incipient damage found in experiments, $V_{id} = 62.6$ ft/sec, see Table 6. This procedure insures that the system will be operating near 1 pit/in.^{2}/min at the higher pressure.

Variation of V_{id} with System Size

It is very important to establish the variation of V_{id} and σ_{id} with changing pipe size for a given upstream pressure and d_o/D ratio. Govindarajan [10] and Tullis and Govindarajan [67] tested a series of geometrically similar orifices in pipes of 1-, 3-, 6-, 12-, and 24-inches in diameter. They found that both the incipient and critical levels of cavitation were subject to size scale effects for a given d_o/D ratio and upstream pressure. The value of σ_i and σ_c steadily increased as pipe size increased; or alternately the magnitudes of V_i and V_c at constant P_u both decreased as pipe size increased. As shown earlier in Table 8, the present tests revealed no systematic

change of σ_{id} with pipe size for a given d_o/D ratio and upstream pressure.

Considering the 3-in. data for V_{id} as base values, the percentage change in V_{id} between the 3-in. and the 6- or 12-in. data may be calculated. The average percent change in V_{id} between the 3-, 6-, and 12-in. data for a given d_o/D and P_u was only 1.1%. The maximum percentage change in V_{id} was 3.47%. Both of these errors are within the experimental accuracy of the tests and probably should be considered as "experimental scatter" of the results.

It should be mentioned again that this present analysis concerning size scale effects is based upon cavitation pitting rate only. No attention is given to the volume or size of the cavitation damage pits. Further study mentioned in a coming section of this chapter demonstrates that size scale effects do exist for the incipient damage condition if pit size is included in the analysis.

Scaling Equations for Orifices

In this section empirical scaling equations are developed from the data in Table 6 to predict V_{id} for orifices with various upstream pressures, d_o/D ratios, and different pipe diameters. The previous section has shown that V_{id} based on cavitation pitting rate is not a function of pipe size. In addition the pressure scaling can be conducted with Eq. (5-7) using reference data in Table 6. However, the variation of V_{id} with d_o/D ratio must still be determined.

Sweeney [55] used dimensional analysis to show that

$$V_{id} = V_{idr} \left(\frac{P_u - P_v}{P_{ur} - P_{vr}} \right)^{0.45} \frac{f_2(C_d)}{f_2(C_{dr})} \qquad (5\text{-}8)$$

or since C_d is directly related to β

$$V_{id} = V_{idr} \left(\frac{P_u - P_v}{P_{ur} - P_{vr}} \right)^{0.45} \frac{f_3(\beta)}{f_3(\beta_r)} \tag{5-9}$$

In addition, Sweeney related β to β' and proposed the equation:

$$V_{id} = V_{idr} \left(\frac{P_u - P_v}{P_{ur} - P_{vr}} \right)^{0.45} \frac{f_4(\beta')}{f_4(\beta_r')} \tag{5-10}$$

The variable β' was introduced so the incipient damage condition for sudden enlargements with nozzle type entrances could be predicted using experimental data concerning orifices. The above equations are extensions of Eq. (5-7) and include the variation of V_{id} with d_o/D; d_o/D is directly related to C_d, β, and β'. The function f_2 can be determined by maintaining P_u constant and plotting the data in Table 6 to produce Fig. 14. Similar plots can be established for Eqs. (5-9) and (5-10). Eqs. (5-8) to (5-10) become:

$$V_{id} = V_{idr} \left(\frac{P_u - P_v}{P_{ur} - P_{vr}} \right)^{0.45} \left(\frac{C_d}{C_{dr}} \right)^{0.83} \tag{5-11}$$

$$0.097 \leq C_d \leq 0.648$$

$$V_{id} = V_{idr} \left(\frac{P_u - P_v}{P_{ur} - P_{vr}} \right)^{0.45} \left(\frac{\beta}{\beta_r} \right)^{-1.07} \tag{5-12}$$

$$1.56 \leq \beta \leq 6.89$$

$$V_{id} = V_{idr} \left(\frac{P_u - P_v}{P_{ur} - P_{vr}} \right)^{0.45} \left(\frac{\beta'}{\beta_r'} \right)^{-0.98} \tag{5-13}$$

$$1.97 \leq \beta' \leq 11.57$$

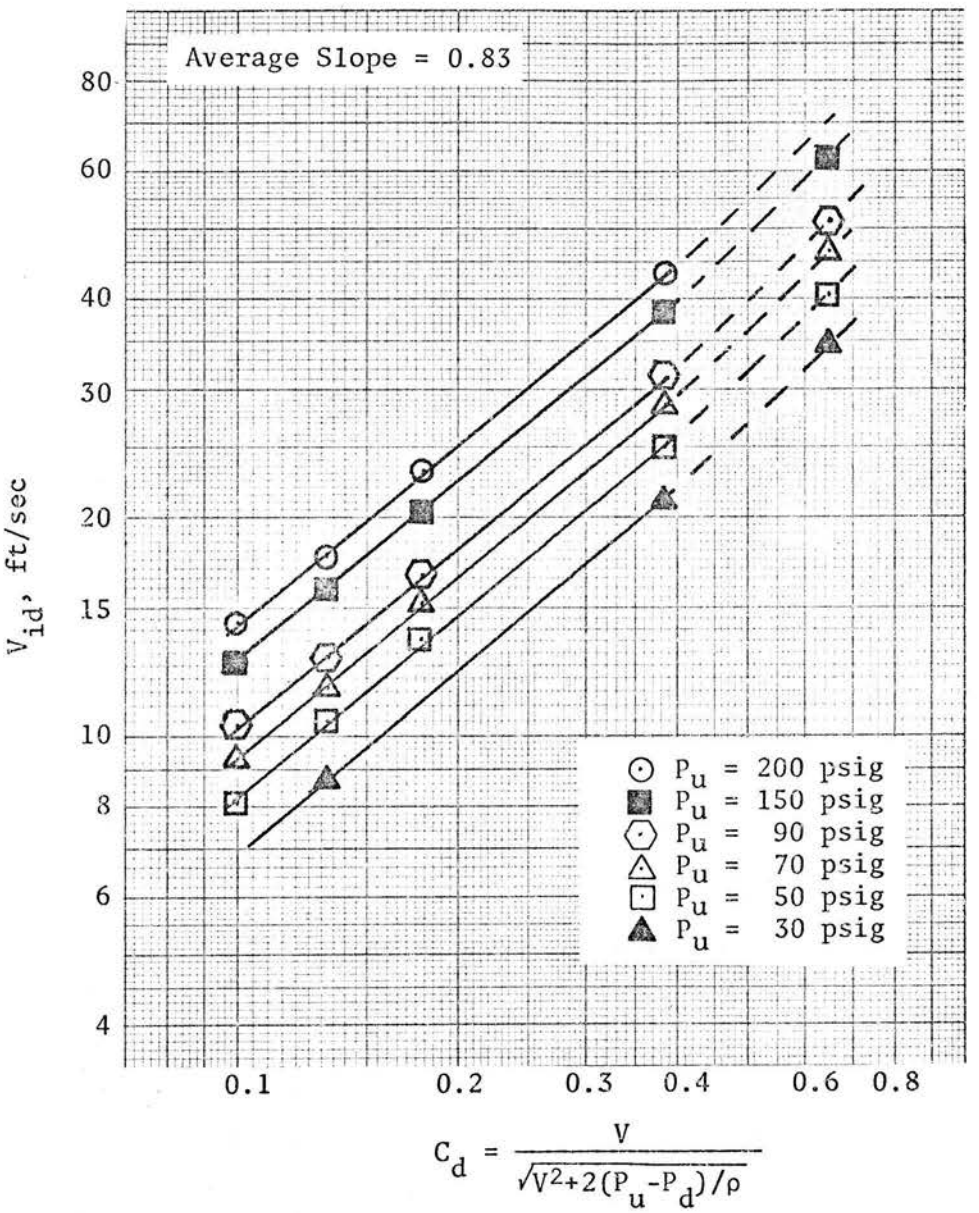

Fig. 14 Geometric Effects: V_{id} vs C_d (see Sweeney [55])

Equations (5-11) to (5-13) represent the final scaling equations for V_{id}. The limits below each equation represent the range of C_d, β, and β' tested in the present experiments. Although the experiments were conducted to upper limits of P_u = 200 psig and D = 12.0-inches, the consistency of the experimental data indicates the equations may be used to extrapolate results to higher pressures and larger diameters. The reference values, P_{ur}, V_{idr}, C_{dr}, β_r, and β_r', can be chosen from the orifices with $d_o/D \leq 0.667$ and listed in Table 6. When these values are substituted into Eqs. (5-11) to (5-13), they will accurately predict the orifices satisfying $d_o/D \leq 0.667$ and conservatively estimate V_{id} (predict a V_{id} value less than experimental value) for $d_o/D \geq 0.800$.

An error analysis was conducted to determine the accuracy of Eqs. (5-11) to (5-13) for predicting the orifice damage data in Table 6. Each orifice shown in Table 10 was used along with its various upstream pressures and V_{id} values for reference data in Eqs. (5-11) to (5-13) to predict V_{id} values for all other orifices with $d_o/D \leq 0.667$. The results show that the experimental data could be more closely predicted by Eq. (5-11) followed by Eq. (5-13) and finally Eq. (5-12). When the 2.666-in. diameter orifice along with its P_u and V_{id} values were used as reference data in Eq. (5-11), the average value of the absolute error in prediction of V_{id} for the other orifice data was only 0.9%.

Prediction of Incipient Nozzle Damage

Many sudden enlargements are constructed with nozzle type entrances. Sweeney [55] used a momentum analysis and experimental data to propose a method for predicting incipient cavitation damage in nozzles. This method allows the prediction of nozzle damage using

TABLE 10 ERRORS IN SCALING EQUATIONS (ORIFICES)

Reference Orifice d_o inches	Equation (5-11)			Equation (5-12)			Equation (5-13)		
	$\overline{\lvert Err \rvert}$-%	S-%	$\lvert Err \rvert_{max}$-%	$\overline{\lvert Err \rvert}$-%	S-%	$\lvert Err \rvert_{max}$-%	$\overline{\lvert Err \rvert}$-%	S-%	$\lvert Err \rvert_{max}$-%
1.168	1.1	0.8	4.8	4.1	1.7	7.6	2.4	1.5	5.9
1.333	1.3	1.0	5.5	2.7	2.6	11.8	2.2	1.5	7.0
1.500	1.3	1.0	4.3	2.3	2.4	10.8	1.6	1.2	5.4
2.000	1.0	0.9	4.6	2.0	2.1	9.5	1.6	1.3	5.4
2.315	1.8	1.1	5.4	3.0	1.4	7.1	1.9	1.5	5.7
2.666	0.9	0.9	4.1	2.0	2.1	9.1	1.6	1.0	4.2
2.991	1.1	1.0	5.5	2.3	2.4	11.3	1.5	1.0	5.5
4.000	1.2	0.8	3.0	2.0	2.0	8.8	2.0	1.2	4.8
4.570	2.3	1.5	5.9	7.8	2.8	13.3	2.8	1.8	7.5
7.980	1.9	1.0	4.2	2.3	1.8	8.8	2.0	1.3	5.4

experimental data from orifice tests. The basic parameter needed for this method is β', which must be defined for each orifice. Once β' is defined, the jet area can be calculated. The assumption is then made that a nozzle with a given P_u and jet area will have the same V_{id} as an orifice operating at the same P_u and producing the same jet area at the vena contracta as the nozzle. If this assumption is true, Eq. (5-13) could be used to predict V_{id} for nozzle flow using orifice reference data from Table 6.

In order to test this method, the orifices in Table 6 which had $\beta' \geq 3.45$ were used as reference values in Eq. (5-13) to predict V_{id} for comparison with the nozzle data in Table 7 ($\beta' = 9.00$). The errors in V_{id} were as follows:

$$\overline{|Err|} = 1.6\%$$
$$S = 1.1\%$$
$$|Err|_{max} = 5.6\%$$

The assumption that equal values of C_d for an orifice and nozzle indicate equal jet areas, allows the use of reference orifice data in Eq. (5-11) to predict incipient damage in nozzles. The value of C_d for the nozzle in Table 7 was found experimentally to be 0.123. The orifices in Table 6 which had $C_d \leq 0.385$ were used as reference data in Eq. (5-11) to predict V_{id} for a nozzle with $C_d = 0.123$. These calculated velocities were compared with the experimental results of Table 7. The errors in V_{id} were as follows:

$$\overline{|Err|} = 1.8\%$$
$$S = 1.1\%$$
$$|Err|_{max} = 4.2\%$$

These two tests indicate that Eqs. (5-11) and (5-13) can be used with orifice reference data in Table 6 to predict incipient cavitation damage in sudden enlargements with nozzle entrances.

Variation of Average Energy of Pit Formation at V_{id}

The preceding analysis was concerned with establishing and predicting an incipient cavitation damage condition. The criteria for incipient damage was MPR = 1 pit/in.^{2}/min on 1100-O aluminum. This is a restricted definition of incipient damage; a more general definition would consider the pitting rate plus a measure of the energy expended by the cavitation in forming the pits [24,25]. This section will investigate the average energy of pit formation at the incipient damage condition, MPR = 1.0 pit/in.^{2}/min.

Knapp [26] developed a method to estimate the energy for pit formation in 1100-O aluminum by measuring the pit dimensions. Several basic assumptions were necessary. First, the work done on the surface by the collapsing cavity in producing a given volume of plastic flow was assumed to be the same as the work done in a hardness test producing the same volume of plastic flow. Therefore, the volume of plastic flow was considered to be independent of the rate of loading. Next, Knapp assumed, as a first approximation, that the geometry of the pits could be approximated by spherical segments so that the volume could be approximated by measuring the depth and diameter of the pit. The energy for formation was estimated by multiplying the pit volume by the amount of energy per volume of plastic flow, determined from hardness tests.

This procedure was used to estimate energy of pit formation in the present study. A static hardness test was conducted on the test

specimens and it was found that 36,550 in.-lbs of energy were needed per cubic inch of plastic flow. The damage pits were assumed to be spherical segments so pit volumes could be conveniently estimated. Therefore, the following equation was used:

$$E_p = 36{,}550 \frac{\text{in.-lbs}}{\text{in.}^3} \times \text{Vol}_p \ (\text{in.}^3) \qquad (5\text{-}14)$$

in which E_p = energy of pit formation and Vol_p = pit volume.

As previously mentioned, the damage specimens were scanned with a microscope and the depth and diameter of the larger pits were measured. Therefore, in the following analysis the measure of energy expended by the cavitation in forming pits is estimated by an average energy of pit formation for a certain percentage of the largest pits on the specimen. The symbol $\overline{E}_p\text{-}X\%$ indicates the average energy of pit formation for the largest pits which represents $X\%$ of the total pits.

The cavitation intensity parameter, I_{exp}, is determined by multiplying the cavitation pitting rate $(R_a\text{-}X\%)$ by the energy of pit formation $(\overline{E}_p\text{-}X\%)$. The units of I_{exp} are (in.-lb/sec/in.^{2}). Actually this parameter represents the energy expended by the cavitation in plastic formation of pits for a given surface area over a given time interval. $I_{exp}\text{-}X\%$ represents the amount of energy per area per time or power per area directed by the cavitation on a solid surface in plastic formation of the largest X percent of pits on the aluminum. Therefore

$$I_{exp}\text{-}X\% = \overline{E}_p\text{-}X\% \ \frac{\text{in.-lb}}{\text{pit}} \times R_a\text{-}X\% \ \frac{\text{pits}}{\text{in.}^2\text{-sec}} \qquad (5\text{-}15)$$

in which $R_a\text{-}X\%$ = cavitation pitting rate over cavitation damage region for largest $X\%$ of pits.

Upstream Pressure as a Variable

Equation (5-7) is a pressure scale effects equation that insures an MPR of approximately 1 pit/in.^{2}/min. This equation should be studied further to assure that the average energy of pit formation, and thus average pit volume, does not vary when Eq. (5-7) is applied. Table 11 was constructed for this purpose; it is noted that the value of $\overline{E}_p$-12% did not vary significantly as the pressure, P_u, was increased from 30-200 psig (V = 10.97-23.34 ft/sec). This agreed well with simple visual inspections, since the "naked eye" revealed no observable change in pit size with P_u.

This limited analysis seems to indicate that E_p at an MPR = 1.0 pit/in.^{2}/min will not vary when Eq. (5-7) is used to scale from one pressure to another. Since MPR and E_p are approximately constant, this would mean I_{exp} would not vary significantly when Eq. (5-7) is used for scaling.

Pipe Size as a Variable

Size scale effects for E_p at the incipient damage point should also be investigated. Table 12 lists experimental data taken in 3- and 12-inch diameter pipes. The two sets of data concerning the 3-inch dia system for d_o/D = 0.667 were linearly interpolated to find $\overline{E}_p$-10.2% = 0.34 x 10^{-5} in.-lb at MPR = 1.40 pits/in.^{2}/min. Using this interpolated value and the corresponding average energy of pit formation for the largest 10.2% of the pits in the 12-in. line (5.16 x 10^{-5} in.-lbs), it can be shown that as the pipe size is increased from 3 to 12 inches the value of $\overline{E}_p$-10.2% increases by a factor of 15.4. Similarly for d_o/D = 0.380, the value of $\overline{E}_p$-6.4% increases by a

TABLE 11 VARIATION OF $\overline{E}_p$ WITH UPSTREAM PRESSURE, MPR ≈ 1.33 Pits/in.^{2}/min (D = 6.0 inches, d_o/D = 0.50)

P_u (psig)	V (ft/sec)	Total Pits on Specimen	Number of Pits Analyzed	MPR Pits/in.^{2}/min	$\overline{E}_p$-12% (in-lb)x10^5
30	10.97	41	7	1.33	2.03
50	13.23	33	8	1.33	1.31
70	15.24	51	8	1.67	2.55
90	16.86	51	6	1.33	0.83
200	23.34	48	7	1.67	2.61

TABLE 12 VARIATION OF $\overline{E}_p$ WITH PIPE SIZE, MPR ≈ 1.50 Pits/in.^{2}/min

D (in.)	d_o/D	σ	P_u (psig)	V ft/sec	MPR Pits in.^{2}/min	X% Pits Considered	$\overline{E}_p$-X% (in-lb)x10^5
3	.667	1.501	50	25.33	0.67	10.2	0.04
					1.40*		0.34*
		1.350		26.07	5.83		2.14
12		1.375		25.29	1.40		5.16
3	.380	0.492	90	10.11	1.80	6.4	1.15
12		.406		10.15	1.67		38.50

*Interpolated value $\sigma = \frac{P_d - P_v}{P_u - P_d}$

TABLE 13 VARIATION OF $\overline{E}_p$ WITH ORIFICE DIAMETER, MPR ≈ 1.33 Pits/in.^{2}/min (D = 6.0 inches)

P_u (psig)	d_o/D	MPR Pits/in.^{2}/min	$\overline{E}_p$-2% (in-lb)x10^5
50	0.39	1.67	9.66
	0.50	1.33	3.33
	0.67	1.00	0.85
30	0.44	1.33	8.50
	0.50	1.33	3.39

factor of 33.5 when the pipe size is increased. These results demonstrate the magnitude of the increase in $\overline{E}_p$ at the incipient damage condition as system size is increased.

It is important to realize the significance of the above findings. Earlier in this chapter it was demonstrated that the velocity at incipient damage, V_{id}, (based upon a maximum localized cavitation pitting rate of 1 pit/in.^{2}/min) did not vary with pipe size. However, the present findings concerning the average energy of pit formation for a certain percentage of the larger pits indicate that the average energy of pit formation at the incipient damage condition (MPR = 1.0 pit/in.^{2}/min) increases rapidly with pipe size. Therefore, if the incipient damage criteria is based upon maintaining a constant value of cavitation intensity (I_{exp}-X%) instead of a constant pitting rate, there will be a definite size scale effect for incipient damage.

Orifice Dia./Pipe Dia. as a Variable

In Chapter IV (see Table 2 and Appendix II) it was shown that as the orifice diameter decreased for a given pipe size the rate of change of pitting rate with velocity at V_{id} increased. Also, earlier in this chapter results were presented to show that cavitation degree defined by Eq. (5-1) increased at the incipient damage condition (MPR = 1 pit/in.^{2}/min) as d_o/D ratio decreased.

Now additional information will be presented concerning the variation of the cavitation damage characteristics with orifice diameter at the incipient damage condition. The results of Table 13 indicate that for a given upstream pressure the average energy of pit formation increases with decreasing d_o/D ratio at incipient damage. For example, for P_u = 30 psig, d_o/D = 0.50, D = 6.0 inches the

MPR = 1.33 pits/in.^{2}/min and $\overline{E}_p$-2% = 3.39 x 10^{-5} in.-lbs. However, at the same conditions except d_o/D = 0.44 the $\overline{E}_p$-2% increased to 8.50 x 10^{-5} in.-lbs, or an increase by a factor of 2.51.

Even though MPR = 1 pit/in.^{2}/min for orifices of different diameters at incipient damage, it seems that the actual physical condition of cavitation becomes more severe at the incipient damage condition as d_o/D decreases. This is largely due to more advanced stages of cavitation, larger values of E_p, and larger d(MPR)/dV values at incipient damage as orifice diameter decreases.

Cavitation Damage Regime

The previous sections of this chapter analyzed conditions at the incipient damage point. The following analysis is concerned with determining the variation of average energy of pit formation, cavitation pitting rate, and cavitation intensity (I_{exp}) when the maximum pitting rate is beyond incipient damage. Such information is important for practical applications, since it is sometimes economical to operate certain devices in the cavitation damage regime. It is necessary to predict cavitation erosion rates in such situations.

The cavitation damage regime study will be investigated under three different situations: (1) varying sigma, (2) varying upstream pressure, and (3) varying pipe size. Cavitation damage in sudden enlargements under these three situations will be a function of both cavitation pitting rate (number of impact blows causing plastic indentations/area/time) and the intensity or strength of the impact blows. The parameter I_{exp} - X% will be used to estimate cavitation

damage since it is a function of both cavitation pitting rate (R_a-X%) and intensity of impact blows ($\overline{E}_p$-X%). However, in each situation the cavitation pitting rate and intensity of impact will both be investigated to determine the influence of each variable on the cavitation damage.

The scaling laws for cavitation erosion presented in Appendix I and further discussed in Chapter II will be used along with experimentally measured flow field data to predict the variation of cavitation pitting rate and intensity of impact blows. The results of these computations will be compared with the results found by inspection of the soft aluminum damage specimens. For example, the variable f found by the scaling laws for cavitation erosion should be comparable to the experimental values of R_a and MPR. In addition, the energy of pit formation (E_p) should be a function of both P_i (impact pressure) and R (size of damage mechanism) found with the scaling equations of Appendix I.

Cavitation Damage with Varying Sigma

Equation (8-36) of Appendix I can be used to predict n^* which represents a measure of the number of nuclei that become unstable and grow. Thiruvengadam assumed that the number of bubbles that collapse was related to n^*, and in addition that the frequency of indentations on a solid surface due to cavitation attack, f, was proportional to n^*. With these assumptions Eq. (8-36) can be used to estimate f. The variables V_o, W, σ_i, and σ were experimentally measured during the cavitation damage experiments for sudden enlargements. The characteristic velocity, V_o, was chosen to be the average

velocity of flow through the pipe orifice, V_{jet}. The characteristic pressure was chosen as the minimum mean pressure at the pipe wall downstream from the orifice, P_{min}, (see Govindarajan [10]). The value of σ_i was calculated from experimental data by Govindarajan [10]. Thiruvengadam [60] indicates that the value of $\bar{d}$ may range between 10^{-5} and 10^{-2} feet. Calculations were conducted for $\bar{d} = 10^{-5}$ and 10^{-3} feet, but it was found that the variation of $\bar{d}$ had a minor influence on the calculated values of n^* and therefore f.

Table 14 shows the results of the calculations for f under conditions of varying sigma. The values of f given in columns (4) and (5) are normalized with respect to the incipient damage condition. The last two columns of Table 14 show the results for cavitation pitting rate, MPR and R_a, found by visual inspection of soft aluminum test specimens. The results indicate that Eq. (8-36) for $\bar{d} = 10^{-3}$ or 10^{-5} feet does not adequately predict the increase in cavitation pitting rate found by experiment. For example, letting $D = 3$ inches, $d_o/D = 0.67$, $\bar{d} = 10^{-5}$ ft and decreasing the cavitation index from the incipient damage condition ($\sigma = 0.854$) to 0.168 will increase f by a factor of 1.225 according to Eq. (8-36). However, actual pit counting on the soft aluminum showed that MPR increased by a factor of 178 and R_a by a factor of 349.

The preceding analysis demonstrates the difficulty in analytically estimating the frequency at which indentations will form on the downstream conduit walls. Thiruvengadam assumed that the number of bubbles that collapse is related to the number of bubbles that become unstable and grow. Of course, this is a very reasonable assumption within itself, but the present author feels that this idea

TABLE 14 VARIATION OF f WITH VARYING SIGMA
P_u = const.

D (inches)	dc/D	σ	f/f_{id} Eq. (8-36) $\bar{d} = 10^{-3}$ ft	$\bar{d} = 10^{-5}$ ft	Experimental Results $\frac{MPR}{MPR_{id}}$	$\frac{R_a}{R_{a_{id}}}$
(1)	(2)	(3)	(4)	(5)	(6)	(7)
3.0	0.67	0.854	1.000	1.000	1.000	1.000
		.562	1.043	1.085	5.830	4.758
		.310	1.098	1.177	53.500	93.407
		.168	1.128	1.225	178.000	349.236
12.0	0.67	0.686	1.000	1.000	1.000	1.000
		.590	1.017	1.024	6.800	4.327
		.413	1.052	1.071	21.000	26.621
		.230	1.092	1.124	37.000	69.903
3.0	0.80	0.938	1.000	1.000	1.000	1.000
		.737	1.049	1.109	4.500	6.209
		.565	1.096	1.202	66.470	64.737
12.0	0.80	0.786	1.000	1.000	1.000	1.000
		.594	1.044	1.063	6.500	6.217
		.490	1.070	1.099	37.333	36.578

$$\sigma = \frac{P_{min} - P_v}{1/2\ \rho\ V_{jet}^2}$$

does not address the main objective. The objective should be to estimate the number of cavities that collapse close to the wall and cause indentations on the surface not merely the total number of bubbles that collapse. Also, the number of cavities that collapse in the near wall region will not only be related to the number of nuclei that become unstable and grow in the shear layer, but also very dependent on the hydrodynamic characteristics of the flow field between the shear layer and the conduit wall. Or equivalently, the percentage of the cavities, originated in the shear layer, that reach the conduit wall

and cause damage is very dependent on the transport mechanism transferring the cavities.

Table 15 shows some results concerning variation of impact pressure, size of damaging mechanism, average energy of pit formation, and cavitation intensity for orifices of constant size and upstream pressure but varying values of sigma. The variables in columns (4) to (6) were calculated using the cavitation damage scaling equations and experimentally measured flow field data. R was calculated with Eq. (8-32) of Appendix I using a characteristic length, ℓ, of $(D - d_o)/2$. The jet impact pressure, column (5), was calculated using Eq. (8-24) of Appendix I; column (6) calculations were made using Eq. (2-10). All results are normalized with respect to the incipient damage condition.

The cavitation damage scaling equations indicate that the size of the damaging mechanism increases with decreasing sigma while the impact pressure for both spherical and jet impact decrease. These two actions would have a counterbalancing effect on the intensity of impact blows. The experimental data shown in column (9) verify this fact since the intensity of impact, measured by $\overline{E}_p$ - X%, does not greatly vary over the tests conducted.

The rapidly increasing cavitation pitting rate, see columns (3) and (8), and not increases in intensity of impact, column (9), seem to be the major reason for increasing cavitation damage with decreasing sigma. The increased cavitation pitting rate with decreasing sigma can be attributed to the following physical action. As the downstream pressure is decreased and the velocity through the orifice increased the intensity of the vortices in the shear layer is increased. This

TABLE 15 VARIATION OF P_i, R, $\overline{E}_p$-X%, AND I_{exp}-X% WITH SIGMA, CONSTANT PIPE SIZE AND P_u = 50 psig

D (in.) (1)	d_o/D (2)	MPR (pits/in.^{2}/min) (3)	R/R_{id} Eq. 8-32 (4)	Jet $P_i/P_{i_{id}}$ Eq. 8-24 (5)	Spherical $P_i/P_{i_{id}}$ Eq. 2-10 (6)	X-% (7)	R_a-X% (pits/in.^{2}/min) (8)	$\overline{E}_p$-X% (in-lbs x 10^5) (9)	I_{exp}-X% (in-lbs/in.^{2}/min) x 10^5 (10)	$\frac{V-V_{id}}{V_{ch}-V_{id}}$ (11)	σ (12)
3.00	0.67	178.0	1.149	0.255	0.200	4.4	1.89	4.79	9.05	0.387	1.003
		53.5	1.120	.441	.380		0.51	4.65	2.37	.297	1.134
		5.8	1.067	.717	.680		0.03	2.99	0.09	.130	1.350
3.00	0.80	66.5	1.132	0.723	0.725	6.3	0.43	2.29	0.98	0.398	2.440
		4.5	1.073	.864	.868		.04	1.07	.04	.204	2.776
12.00	0.80	37.3	1.052	0.716	0.361	2.7	0.10	14.57	1.51	0.287	2.470
		6.5	1.034	.825	.150		.02	19.74	.35	.179	2.670
12.00	0.67	37.0	1.059	0.405	1.9×10^{-12}	1.5	0.13	90.15	11.63	0.289	0.998
		21.0	1.036	.669	1.6×10^{-6}		.05	188.21	9.24	.164	1.142
		6.8	1.013	.891	2.1×10^{-2}		.01	54.81	0.44	.055	1.302

$$\sigma = \frac{P_d - P_v}{P_u - P_d}$$

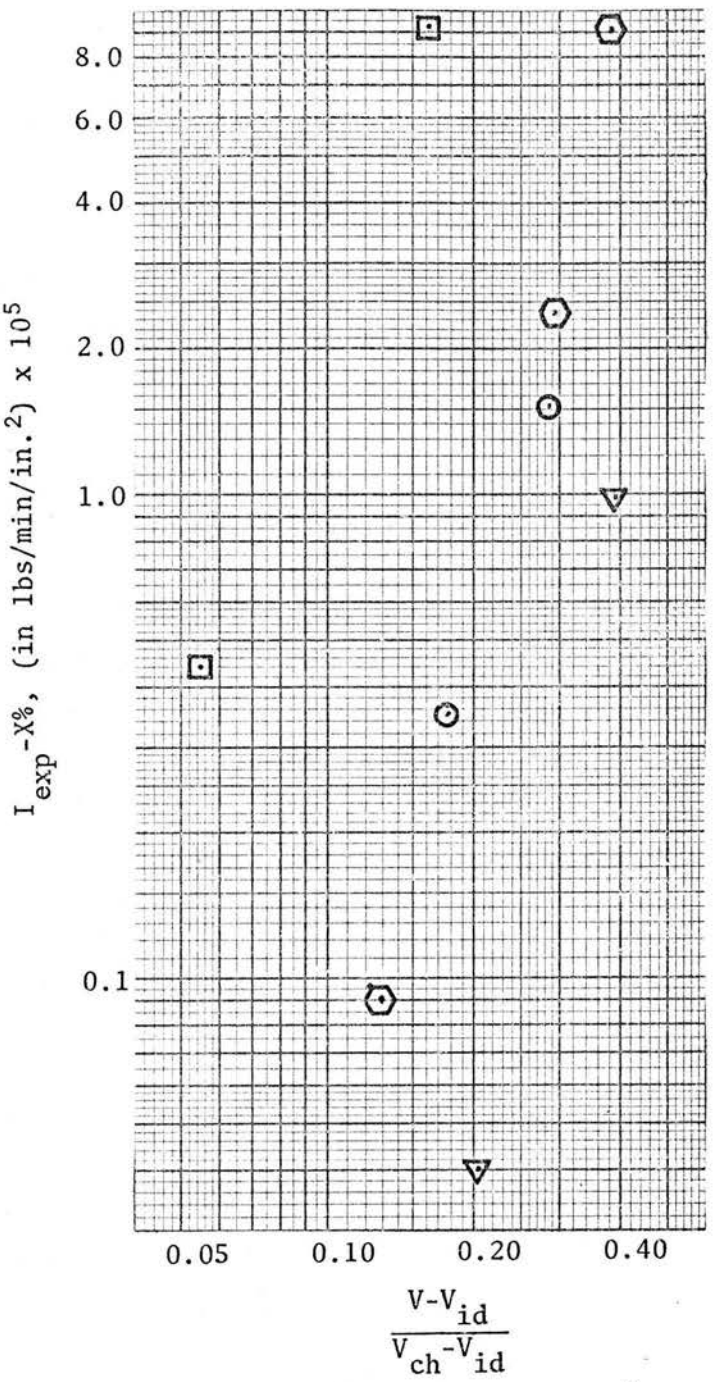

	D (inches)	d_o/D	Slope
▽	3.0	0.80	4.79
⊙	12.0	0.80	3.10
⬡	3.0	0.67	4.16
⊡	12.0	0.67	2.79*

*Omitting point (0.289, 11.63)

Fig. 15 Variation of I_{exp}-X% with Sigma, Constant Pipe Size and P_u

Cavitation Damage with Varying Upstream Pressure

Equation (8-36) of Appendix I was used to predict the frequency of indentations on the solid surface downstream from the sudden enlargement for conditions of varying upstream pressure. The results, normalized with respect to the P_u = 30 psig data, are shown in Table 16; again as in the case of varying sigma (Table 14), the damage scaling equation seriously underestimates the rate of increase of cavitation pitting rate found by inspection of soft aluminum specimens. As previously mentioned, this error is probably due to the fact that Eq. (8-36) does not consider the frequency of indentations to be a function of the flow field.

Table 17 shows some results concerning the variation of impact pressure, size of damaging mechanism, average energy of pit formation and cavitation intensity for orifices of constant size and sigma but varying upstream pressure. The variables in columns (4) to (6) were calculated in the same manner as discussed in the previous section concerning varying sigma. The cavitation damage scaling equations indicate that the size of the damaging mechanism, column (7), remains constant as the upstream pressure is increased. However, the impact pressure due to both high velocity jet and spherical collapse increase as P_u is increased. The combination of constant size of damaging mechanism and increasing impact pressure indicates that the intensity of impact blows should increase with increasing pressure. This fact was experimentally verified by the results concerning $\overline{E}_p$ - X% in column (12). $\overline{E}_p$ - X%, an experimental measure of intensity of impact blows, consistently increases with increasing upstream pressure except for the D = 6.0-inch data at P_u = 90 psig.

TABLE 16 VARIATION OF f WITH VARYING PRESSURE (VELOCITY), D = const.

D (in.) (1)	d_o/D (2)	P_u (psig) (3)	V_{jet} (ft/sec) (4)	σ (5)	Frequency of Impacts: $f/f_{30\ psig}$ Eq. (8-36) $\bar{d} = 10^{-3}$ ft (6)	Frequency of Impacts: $f/f_{30\ psig}$ Eq. (8-36) $\bar{d} = 10^{-5}$ ft (7)	Experimental Results: $\frac{MPR}{MPR_{30\ psig}}$ (8)	Experimental Results: $\frac{R_a}{R_{a\ 30\ psig}}$ (9)
6.0	0.50	30	45.21	0.400	1.000	1.000	1.000	1.000
		50	54.79		1.213	1.313	3.750	4.316
		70	63.33		1.403	1.586	7.502	9.838
		90	70.74		1.567	1.817	15.370	18.835
3.0	0.67	30	50.29	0.400	1.000	1.000	1.000	1.000
		200	110.66		2.204	2.598	50.189	39.153
3.0	0.44	30	45.66	0.291	1.000	1.000	1.000	1.000
		150	89.80		1.970	2.324	86.162	145.630

$$\sigma = \frac{P_{min} - P_v}{\frac{1}{2}\rho V_{jet}^2}$$

TABLE 17 VARIATION OF P_i, R, $\overline{E}_p$-X%, AND I_{exp}-X% WITH UPSTREAM PRESSURE, CONSTANT PIPE SIZE AND SIGMA

D (in.) (1)	d_o/D (2)	P_u (psig) (3)	V (ft/sec) (4)	σ (5)	MPR (pits in.^{2}/min) (6)	R/$R_{30\ psig}$ Eq. (8-32) (7)	Jet $P_i/P_{i_{30\ psig}}$ Eq. (8-24) (8)	Spherical $P/P_{i_{30\ psig}}$ Eq. (2-10) (9)	X-% (10)	R_a-X% (pits/in.^{2}/min) (11)	$\overline{E}_p$-X% (in-lb x 10^5) (12)	I_{exp}-X% (in-lb/in.^{2}/min) x 10^5 (13)
3.00	0.67	30	22.35	1.182	13.25	1.000	1.000	1.000	1.9	0.049	3.48	0.17
		200	49.18	1.214	665.00	0.987	5.734	13.364		1.908	38.65	73.74
6.00	0.50	30	10.97	0.635	1.33	1.000	1.000	1.00	5.9	0.009	2.78	0.03
		50	13.62	.640	5.00	.998	1.493	16.76		0.039	6.10	0.24
		70	15.74	.639	10.00	1.004	1.838	135.09		0.089	16.79	1.49
		90	17.58	.641	20.50	1.005	2.257	1414.9		0.169	7.55	1.28
3.00	0.44	30	9.01	0.404	3.83	1.000	1.000	1.00	0.5	0.004	2.06	0.01
		150	17.65	.408	330.00	1.001	3.693	25.64		0.553	41.53	22.97

$$\sigma = \frac{P_d - P_v}{P_u - P_d}$$

The most important fact concerning Table 17 is the indication of a very large increase in I_{exp} - X% with increasing pressure or velocity. For example, increasing the value of P_u from 30 to 150 psig (V = 9.01 to 17.65 ft/sec) while maintaining $\sigma \approx 0.405$ for D = 3.0-inches and $d_o/D = 0.444$ increases the value of I_{exp} - X% by a factor of 2297. Similar results are seen for the data concerning D = 3.00-inches, $d_o/D = 0.67$ where I_{exp} - X% increases by a factor of 434. Both these increases in cavitation intensity are a result of large increases in R_a - X% and $\overline{E}_p$ - X%, columns (11) and (12). In conclusion, Table 17 indicates that cavitation intensity rapidly increases with upstream pressure due to the combined effect of increasing cavitation pitting rate plus increasing intensity of cavitation blows.

Several factors dictate that the results of Table 17 be accepted with some reservations. First, Sweeney [55] noted that air being diffused out of solution downstream from the orifice may have influenced the damage for the orifices with $d_o/D = 0.389$, 0.444, and 0.500 tested at P_u = 30 psig. This fact might have influenced the last set of data ($d_o/D = 0.44$) presented in Table 17; however, the $d_o/D = 0.667$ data shows large increases in I_{exp} - X% where the air problem should not exist according to Sweeney [55]. Again there are several variables involved that could possibly influence the pressure scale effects and a completely generalized conclusion should not be drawn with the limited data in Table 17. However, these results do indicate the order of magnitude of the pressure scale effect on cavitation intensity.

Pressure scale effects on cavitation intensity can also be considered from somewhat of a different viewpoint. Consider the value

of cavitation intensity in the region of maximum localized cavitation pitting, $(I_{exp})_{MPR\ region}$. It is known in this area that $MPR \propto V^N$ where the N value may vary from 3.0 to 7.6. Therefore the relation

$$(I_{exp})_{MPR\ region} = (\bar{E}_p)_{MPR\ region} \times MPR$$

in which $(\bar{E}_p)_{MPR\ region}$ = average energy of pit formation for cavitation pits in the maximum pitting region, will imply that in this region

$$(I_{exp})_{MPR\ region} \propto (\bar{E}_p)_{MPR\ region} \times V^N$$

If it is assumed that $(\bar{E}_p)_{MPR\ region}$ will have a trend to increase with increasing upstream pressure (see damage scaling equation results in Table 17), then the cavitation intensity in the region of maximum localized pitting will increase at least as rapidly as V^N.

Cavitation Damage With Varying Pipe Size

Earlier observations in Chapter IV indicate that the value of MPR and R_a do not vary with pipe size for a given upstream pressure, mean pipe velocity, and approximately similar d_o/D and C_d values. This indicates that R_a - X% is a constant when Eq. (5-15) is used to calculate variations of I_{exp}-X% with pipe size for given d_o/D value, sigma, and P_u. Therefore, it is only necessary to determine the variation of average energy of pit formation with pipe size in order to define size scale effects for cavitation intensity.

Table 18 shows the results concerning the variation of impact pressure, size of damaging mechanism, and average energy of pit formation for orifices of given d_o/D ratios operated at P_u = 50 psig and approximately constant sigma values. The cavitation damage scaling

equations predict the size of the damage mechanism to increase with increasing pipe size. Also the spherical cavity collapse impact pressure, given by Eq. (2-10), was predicted to increase very rapidly with pipe diameter. For example, results for $d_o/D = 0.67$ and $\sigma \approx 1.29$ indicate that the impact pressure due to spherical cavity collapse increases by a factor of 1.1×10^{20} as pipe diameter increases from 3 to 12 inches. It would seem that increases of such magnitude would be very unlikely in actual physical situations. The impact pressure due to jet impact showed no consistent variation with pipe size. Therefore, the intensity of impact blows should increase with increasing pipe size due to increases in size of damaging mechanism and possibly spherical cavity impact pressures. This idea is experimentally verified in column (11) where $\overline{E}_p\text{-}X\%$ is shown to increase as pipe size is increased.

Figure 16 shows a semi-log plot of pipe diameter in inches and $\overline{E}_p\text{-}X\%$ from the data in Table 18. A table is also shown in the figure indicating the slopes of the least squares fit straight lines to the data. It should be noted that the value of the slope agrees fairly well except for one set of data, $\sigma \approx 2.48$. Omitting this data, the average of the other four slopes is 0.107. Therefore the following relation indicates the data trends

$$\overline{E}_p\text{-}X\% \propto 10^{0.107D} \qquad (5\text{-}16)$$

in which D = inside pipe diameter in inches.

The above relation between average energy of pit formation and pipe diameter is based on a limited amount of data. Only two of the five sets have more than two data points, therefore it is difficult to

TABLE 18 VARIATION OF P_i, R, AND $\overline{E}_p$-X% WITH PIPE SIZE, P_u = 50 psig

D (in.) (1)	P_d (psig) (2)	V (ft/sec) (3)	C_d (4)	d_o/D (5)	σ (6)	$R/R_{3''}$ Eq. (8-32) (7)	Jet $P_i/P_{i_{3''}}$ Eq. (8-24) (8)	Spherical $P_i/P_{i_{3''}}$ Eq. (2-10) (9)	X-% (10)	$\overline{E}_p$-X% (in-lb x 10^5) (11)
12	22.83	25.64	0.377	0.67	1.302	5.065	1.026	1.1×10^{20}	5.5	19.41
6	22.12	26.51	.381		1.232	2.352	0.632	7.845		5.55
3	23.53	26.07	.385		1.350	1.000	1.000	1.000		2.89
12	18.87	27.51	0.377	0.67	0.998	4.917	1.308	3.3×10^{10}	1.5	90.15
3	18.85	28.17	.385		1.003	1.000	1.000	1.000		12.00
12	20.97	26.51	0.377	0.67	1.142	4.937	1.249	1.5×10^{16}	2.4	121.74
3	20.91	27.43	.385		1.134	1.000	1.000	1.000		8.06
12	31.87	43.01	0.643	0.80	2.47	5.394	0.822	1.8×10^{3}	2.7	14.57
6	32.16	42.82	.642		2.51	2.720	0.603	1.171		5.75
3	32.05	44.22	.648		2.44	1.000	1.000	1.000		4.54
12	32.88	41.95	0.643	0.80	2.67	5.594	0.792	3.7×10^{3}	6.4	10.16
3	33.49	42.35	.648		2.78	1.000	1.000	1.000		1.07

$$\sigma = \frac{P_d - P_v}{P_u - P_d}$$

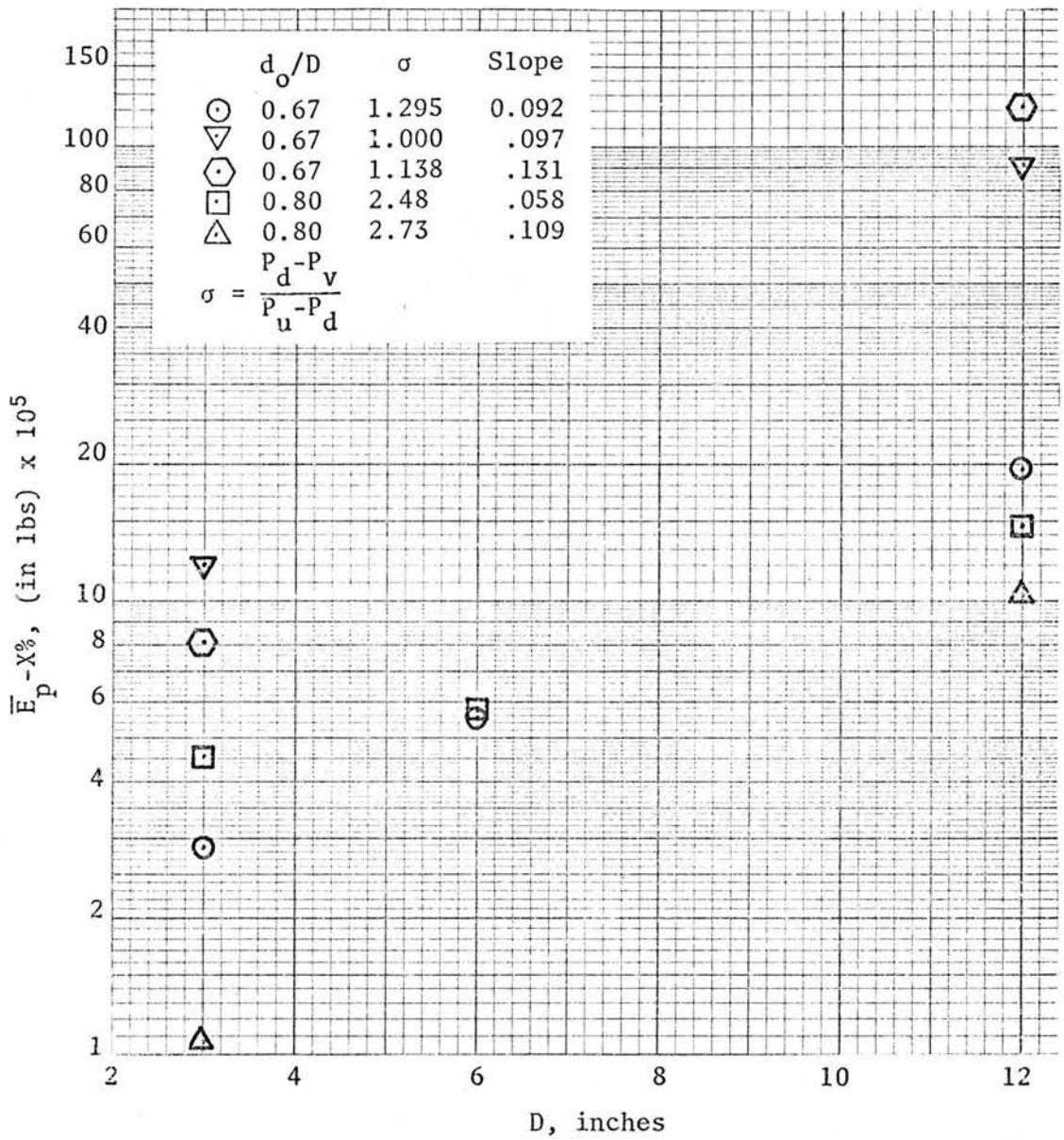

Fig. 16 Variation of $\bar{E}_p$-X% with Pipe Diameter

state a functional relationship between the two variables. Furthermore, this relationship would predict a very rapid increase in $\overline{E}_p$-X% with pipe diameter. It would be unwise to extrapolate the present experimental results concerning average energy of pit formation and pipe diameter to large pipe sizes (for example, $D \geq 3$ feet). Further study is needed to firmly establish a functional relationship; however, it is clear from the present results that average energy of pit formation increases quite rapidly with pipe size.

Now the value of cavitation intensity, I_{exp}-X%, can be estimated for each set of data in Table 18 by using Eq. (5-15). Table 19 shows the results; the values of P_d, V, C_d, and for the 3-, 6-, and 12-inch data have been averaged to give one value for each parameter. Since R_a-X% is a constant for a given set of data, the trend of the results for I_{exp}-X% are similar to those found for $\overline{E}_p$-X%.

Model-Prototype Cavitation Loading Relations

The major problem associated with the cavitation damage regime is to predict the cavitation erosion of a prototype structure given certain flow conditions. One possible procedure for approaching this problem would be to construct a hydraulic model of the device where laboratory studies could be performed [60]. The damaging region of the model would be constructed of a less resistant material and the erosion of the prototype would be predicted from model results. Two questions are associated with this procedure: (1) What is the relation between weight removal of the less resistant material and the prototype material under a given cavitation attack (see [60])? (2) What is the relation between the cavitation attack or loading system in the model and prototype?

TABLE 19 VARIATION OF I_{exp}-X% WITH PIPE SIZE

D (in.) (1)	P_u (psig) (2)	P_d (psig) (3)	V (ft/sec) (4)	C_d (5)	d_o/D (6)	σ (7)	X-% Pits Considered (8)	R_a-X% (9)	$\bar{E}_p$-X% (in-lb x 10^5) (10)	I_{exp}-X% (in-lb/min/in.^{2}) x 10^5 (11)
12	50	22.83	26.07	0.381	0.67	1.295	5.5	0.044	19.41	0.854
6									5.55	.244
3									2.89	.127
12	50	18.86	27.84	0.381	0.67	1.000	1.5	0.278	90.15	25.017
3									12.00	3.330
12	50	20.94	26.97	0.381	0.67	1.138	2.4	0.096	121.74	11.687
3									8.06	0.774
12	50	32.03	43.35	0.644	0.80	2.48	2.7	0.094	14.57	1.377
6									5.75	0.543
3									4.54	0.429
12	50	33.19	42.15	0.646	0.80	2.73	6.4	0.054	10.16	0.5462
3									1.07	0.0576

$$\sigma = \frac{P_d - P_v}{P_u - P_d}$$

The results of the present research can be used to investigate the second question mentioned above. Suppose there is a prototype orifice with $d_o/D = 0.67$ in a 2-foot diameter line. The operating conditions of the sudden enlargement are $P_u = 50$ psig and $\sigma = (P_d-P_v)/(P_u-P_d) = 1.295$. A laboratory study is to be conducted in order to predict material removal in the prototype structure. Assume the maximum pipe size available in the laboratory is $D = 3$ inches. Using previous experimental results the following questions will be investigated: (1) Can the same loading system in terms of number of impacts per area per time and intensity of the given impacts present in the prototype structure be simulated in the laboratory study? If not, what alternative method is available for simulating the loading system?

The following procedure can be used to estimate the cavitation conditions in the prototype. Previous experimental results indicate that both MPR and R_a are independent of system size for a given d_o/D ratio and flow condition (see Chapter IV, Fig. 11; semi-log plots of R_a vs V give similar results). This fact allows the prediction of prototype pitting rates from data obtained in 3-, 6-, and 12-inch diameter pipes. In addition, the linear plots on semi-log paper of $\overline{E}_p$-X% vs pipe diameter allow the extrapolation of the 3-, 6-, and 12-inch data to the 24-inch prototype (see Fig. 16). Using the above steps and experimental results previously obtained, the following conditions are predicted to exist in the prototype structure.

Prototype

Given: $P_u = 50$ psig

$d_o/D = 0.67$

$D = 2$ feet

$\sigma = (P_d - P_v)/(P_u - P_d) = 1.295$

$V = 26.14$ ft/sec

Cavitation loading results:

MPR = 6.5 pits/in.^{2}/min (see Fig. 11)

R_a = 0.85 pits/in.^{2}/min (from semi-log plots of R_a vs V)

R_a-4.4% = 0.037 pits/in.^{2}/min

$\overline{E}_p$-4.4% = 3.9×10^{-3} in-lbs (from plots similar to Fig. 16)

I_{exp}-4.4% = 1.46×10^{-4} in-lbs/in.^{2}/min (Eq. 5-15)

If the 3-inch model test is conducted at P_u = 50 psig and $\sigma = (P_d - P_v)/(P_u - P_d) = 1.295$, then the average pipe velocity in model and prototype will be equal. Since previous experimental results indicate that cavitation pitting rates are independent of pipe size, the values of MPR and R_a in the 3-inch model should be approximately equal to prototype values. Since $V = 26.14$ ft/sec in the model, the value of $(V - V_{id})/(V_{ch} - V_{id})$ is found to be 0.139. Figure 15 can then be used to determine that I_{exp}-4.4% = 1.1×10^{-6} in-lbs/in.^{2}/min. Equation (5-15) along with the model pitting rate, R_a = 0.037 pits/in.^{2}/min, and model intensity, I_{exp}-4.4% = 1.1×10^{-6} in-lbs/in.^{2}/min, can be used to show that $\overline{E}_p$-4.4% = 2.94×10^{-5} in-lbs in the model. This would indicate that the average energy of pit formation for the largest 4.4% of pits in the prototype is approximately 133 times the value in the model.

These results indicate that if the model test is conducted at the prototype upstream pressure and cavitation index, the cavitation pitting rates can be simulated but the intensity of impact blows can not. Therefore, the calculations show that the total loading system in terms

of both pitting rate and intensity of impact blows cannot be simulated in the 3-inch model.

A different procedure would be to conduct the model test at a higher upstream pressure, while maintaining the required pitting rates, MPR = 6.5 pits/in.^{2}/min and R_a = 0.85 pits/in.^{2}/min. Hopefully the average energy of pit formation would increase with the upstream pressure to the required value of $\overline{E}_p$-4.4% = 3.9 x 10^{-3} in-lbs. However, previous experimental studies concerning variation of $\overline{E}_p$-X% with upstream pressure at a given pitting rate showed almost no increase in average energy of pit formation, Table 11. Therefore, the present author is doubtful that this method could be used to generate the correct total loading system in the 3-inch model.

Finally, the previous experimental data indicate that it is impossible to simulate the same loading system in terms of number of impacts per area per time and intensity of the given impacts present in the prototype structure.

An alternative method of simulation would be to maintain the same value of I_{exp}-X% in the model and prototype. This approach would of course not be as preferable as simulating the total loading system but may be the only practical and realistic method of simulation.

For the problem under discussion, the value of cavitation intensity in the prototype (I_{exp}-4.4% = 1.46 x 10^{-4} in-lbs/in.^{2}/min) must be produced in the 3-inch model. Figure 15 contains the data necessary for the determination of flow conditions which will produce the required cavitation intensity. For P_u = 50 psig, D = 3.0 inches, d_o/D = 0.67 the experimental data show that $(V-V_{id})/(V_{ch}-V_{id})$ = 0.44 when I_{exp}-4.4% = 1.46 x 10^{-4} in-lbs/in.^{2}/min. Plugging in values of V_{id}

and V_{ch} shows that the model should be tested at a mean pipe velocity of 28.61 ft/sec to produce the given cavitation intensity. Using other experimental results the conditions in the model can be determined as:

Model

Given: $P_u = 50$ psig

$d_o/D = 0.67$

$D = 3$ inches

$\sigma = (P_d - P_v)/(P_u - P_d) = 0.916$

$V = 28.61$ ft/sec

Cavitation loading results:

MPR = 310 pits/in.^{2}/min (see Fig. 11)

$R_a = 71.0$ pits/in.^{2}/min (from semi-log plots of R_a vs V)

R_a-4.4% = 3.12 pits/in.^{2}/min

$\overline{E}_p$-4.4% = 4.67×10^{-5} in-lbs (Eq. 5-15)

I_{exp}-4.4% = 1.46×10^{-4} in-lbs/in.^{2}/min

It is important to discuss the relationship between the cavitation loading conditions in model and prototype when I_{exp}-X% is kept constant. Note that the value for average energy of pit formation in the prototype ($\overline{E}_p$-4.4% = 3.9×10^{-3} in-lbs) is about 84 times as large as the model value (4.67×10^{-5} in-lbs). However, the cavitation pitting rate in the model (R_a-4.4% = 3.12 pits/in.^{2}/min) is 84 times as large as the prototype. Therefore, the prototype loading system is composed of a number of impacts per area per time with fairly large intensity of impact which produces a given cavitation intensity, I_{exp}. The model loading system (which produces the same cavitation intensity) is composed of a larger number of impacts per area per time but the intensity of the impacts is much smaller in magnitude.

Chapter VI

SUMMARY AND CONCLUSIONS

This research study has been concerned with describing cavitation damage downstream from sudden enlargements. Sweeney [55] first defined an incipient damage point for cavitation damage in sudden enlargements. This incipient damage point was based upon maintaining a constant cavitation pitting rate (pits/in.^{2}/min) on soft aluminum specimens. Empirical equations were also developed for predicting the incipient damage point for orifices of various diameter operating at different upstream pressures in a 3-inch pipe.

The present research has extended the knowledge concerning the incipient damage design criteria defined above by conducting experiments in larger sized pipes and by inspecting not only the cavitation pitting rate but also the intensity of impacts. It was found that the empirical equations developed for the 3-inch diameter pipe could be used to accurately predict the incipient damage in larger sized pipes (6- and 12-inch diameter). For example, the pressure scale effects defined by Sweeney [55] were found to also apply for the larger sized pipes. Also for a given upstream pressure and orifice to pipe diameter ratio, the incipient damage point (based upon a maximum cavitation pitting rate of 1 pit/in.^{2}/min) was found to occur at the same mean pipe velocity. Therefore, no size scale effects were found for the incipient damage point based upon cavitation pitting rate.

The incipient damage point is based totally on analysis concerning the cavitation pitting rate; however, the severity of attack from cavitation is not only a function of pitting rate but also intensity of the

impact blows forming the pits. Therefore, the present study examined the variation of intensity of impact blows at the incipient damage level. The most important result of this study was the discovery that the intensity of impact blows (measured in terms of average energy of pit formation) increased significantly with pipe size at the incipient damage condition. Also, for a given pipe size and upstream pressure the intensity of impact blows increased at the incipient damage condition as the orifice to pipe diameter ratio decreased. For these same conditions, it was found that the rate of increase of cavitation pitting rate with pipe velocity at the incipient damage point increased as the orifice to pipe diameter ratio decreased. Finally, experimental results indicated that the intensity of impact blows remained constant at the incipient damage condition as the upstream pressure was increased for constant pipe size and orifice to pipe diameter ratio. This analysis concerning intensity of impact blows indicates that the incipient cavitation damage point (based upon pitting rate criteria) is not a unique point in terms of total cavitation loading conditions (pitting rate plus intensity of impact blows).

The cavitation damage regime (region where the maximum pitting rate is greater than 1 pit/in.^{2}/min) was also investigated. Since cavitation pitting rate and intensity of impact blows may vary independently in the cavitation damage regime, the severity of the cavitation attack was measured in terms of the cavitation intensity parameter. This parameter is the product of average cavitation pitting rate and average energy of pit formation (a measure of intensity of impact blows). Three different situations were studied to determine the variation of cavitation intensity in the damaging regime. First, sigma

was allowed to vary but the upstream pressure, pipe size, and orifice to pipe diameter were kept constant. Experimental studies of the soft aluminum specimens indicated the cavitation pitting rate increased rapidly as sigma was decreased. Cavitation damage scaling equations and experimental flow field data were used to predict the variation of intensity of cavitation impact blows. The size of the damaging mechanism (high velocity jet or spherical shock) increased with decreasing sigma. However, the impact pressure from both damaging mechanisms decreased with decreasing sigma. The intensity of cavitation blows are functions of both impact pressure and size of damaging mechanism. Therefore, these two variables exert counterbalancing actions on the growth of intensity of cavitation impact blows as sigma is decreased. Experimental results concerning average energy of pit formation (a measure of intensity of impact blows) verified that there was small change in magnitude of impact blows with decreasing sigma. Therefore, the increasing cavitation intensity with decreasing sigma is primarily due to increased cavitation pitting rate and not to increased intensity of cavitation impact blows.

The second situation studied concerned the variation of cavitation intensity under conditions of constant sigma, pipe size, and orifice to pipe diameter ratio but varying upstream pressure. This is the classical situation for determination of pressure scale effect on cavitation intensity. The experimental studies of aluminum test specimens indicated a rapidly increasing cavitation pitting rate with increased upstream pressure. The cavitation damage scaling equations predicted the size of the damaging mechanism to remain constant with increasing upstream pressure. However, the impact pressure due to both spherical

and high velocity jet were predicted to increase. The net result of the cavitation damage scaling equations was to predict an increased intensity of cavitation impact blows with increasing upstream pressure. This fact was again verified by measurements concerning average energy of pit formation. Therefore, the cavitation intensity increases rapidly with increasing upstream pressure due to the combined effect of increased pitting rate and increased intensity of impact blows.

Finally, variation of cavitation intensity was studied for conditions of varying pipe size with constant sigma, upstream pressure, and orifice to pipe diameter ratio. This type situation is appropriate for study of size scale effects on cavitation intensity. Experimental results concerning the soft aluminum specimens indicated that the cavitation pitting rate remained constant as pipe size increased. The cavitation damage scaling equations predicted the size of the damaging mechanism to increase with increasing pipe size. The impact pressure due to jet impact remained constant with increasing pipe size while the impact pressure due to spherical collapse showed trends to greatly increase. The net result of the cavitation damage scaling equations was to predict an increasing intensity of cavitation impact blows with increasing pipe size. This fact was verified by measurements concerning average energy of pit formation. Therefore, the cavitation intensity increases with pipe size due primarily to increased intensity of cavitation impact blows and not due to increased cavitation pitting rate.

The cavitation intensity parameter is important to consider when the cavitation loading system of a prototype structure is simulated in a hydraulic model. If the hydraulic model is reduced significantly in size, the present research indicates it will be impossible to simulate

the prototype loading system in the model in terms of both cavitation pitting rate and intensity of impact blows. An alternative modeling procedure is to maintain the same value of cavitation intensity in model and prototype.

The above paragraphs contain a summary of the results found in the present research study. Several important conclusions can be reached from this information.

Conclusion 1: Incipient damage scaling equations (based totally upon maintaining a constant cavitation pitting rate) were derived from experimental data and were used to accurately predict the incipient damage point for sudden enlargements with various upstream pressures, physical size, and orifice to pipe diameter ratio (see Eqs. (5-11) to (5-13)).

Conclusion 2: The damage condition, predicted by incipient damage scaling equations (based totally upon maintaining a constant cavitation pitting rate), is not a unique cavitation loading condition in terms of both cavitation pitting rate and intensity of cavitation impact blows forming the pits. This fact is due to variations in intensity of cavitation impact blows with orifice to pipe diameter ratio and pipe size (see Tables 12 and 13).

Conclusion 3: The total cavitation loading conditions in the damaging regime of cavitation is a function of both cavitation pitting rate and intensity of cavitation impact blows forming the pits. These two variables vary independently with cavitation index, upstream pressure, and system size; this fact causes difficulties in simulation of the total cavitation loading conditions in hydraulic models of reduced size.

Conclusion 4: The variation of cavitation pitting rate and intensity of impact blows for the cavitation damage regime can be summarized in the following statements. Decreasing the value of sigma for a given orifice to pipe diameter ratio, upstream pressure, and pipe size causes an increase in cavitation pitting rate with small changes in intensity of impact blows. Increasing the upstream pressure for a given orifice to pipe diameter ratio, sigma, and pipe size causes major increases in both cavitation pitting rate and intensity of impact blows.

Finally, increasing the pipe size for a given orifice to pipe diameter ratio, sigma, and upstream pressure increases the intensity of impact blows but does not influence the cavitation pitting rate.

Conclusion 5: A cavitation intensity parameter calculated as a product of cavitation pitting rate and a measure of intensity of impact blows (average energy of pit formation) is useful for characterizing the severity of a cavitation attack in the damaging regime.

BIBLIOGRAPHY

[1] Ball, J. W.: "Gate Valves and Globe Valves Used as Flow Regulators Under Heads up to 125 Feet," Transactions, ASME, August 1957.

[2] Ball, J. W.: "Sudden Enlargements in Pipelines," ASCE, Journal of the Power Division, December 1962.

[3] Ball, J. W. and Simmons, W. P.: "Progress Report on Hydraulic Characteristics of Pipeline Orifices and Sudden Enlargements Used for Energy Dissipation," U.S. Dept. of Interior, Bureau of Reclamation, Report No. Hyd-519, December 1963.

[4] Benjamin, T. B. and Ellis, A. T.: "The Collapse of Cavitation Bubbles and the Pressures Thereby Produced Against Solid Boundaries," Phil. Trans. Roy. Soc., London, Series A, Math. Phys. Sciences 206A, pp. 221-240, 1966.

[5] Chaturvedi, M. C.: "Flow Characteristics at Abrupt Axisymmetric Expansions," Ph.D. Dissertation, The State University of Iowa, August 1962.

[6] Daily, J. W. and Johnson, V. E., Jr.: "Turbulence and Boundary Layer Effects on Cavitation Inception from Gas Nuclei," Trans., ASME, 78, pp. 1695-1706, 1956.

[7] Ellis, A. T.: "Parameters Affecting Cavitation and Some New Methods for Their Study," Calif. Inst. of Tech. Hydrodyn. Lab. Report E-115.1, 1965.

[8] Gavranek, V. V., Bol 'shutkin, D. N., and Zel' dovich, V.I.: "Thermal and Mechanical Action of a Cavitation Zone on the Surface of a Metal," Fiz. metal. i Metalloved., 10, No. 2, pp. 262-268, 1960.

[9] Gilmore, F. R.: "The Growth and Collapse of a Spherical Bubble in a Viscous Compressible Liquid," Calif. Inst. of Tech. Hydrodyn. Lab. Report 26-4, 1952.

[10] Govindarajan, R.: "Cavitation Size Scale Effects," Ph.D. Dissertation, Colorado State University, Fort Collins, Colo., August, 1972.

[11] Hackworth, J. V. and Adler, W. F.: "Microscopic Investigations of Cavitation Erosion Damage in Metals," The Role of Cavitation in Mechanical Failures, NBS Special Publ. 394, pp. 54-61, 1973.

[12] Hammitt, F. G.: "Recent Theories of Cavitation Damage Including Non-symmetrical Bubble Collapse Effects," The Role of Cavitation in Mechanical Failures, NBS Special Publ. 394, pp. 31-35, 1973.

[13] Harvey, E. N.; Barnes, D. K.; McElroy, W. D.; Whiteley, A. H.; Pease, D. C.; and Cooper, K. W.: "Bubble Formation in Animals. I, Physical Factors," Jr. Cellular and Comp. Physiol., 24, No. 1, pp. 1-22, August 1944.

[14] Heymann, F. J.: "On the Time Dependence of the Rate of Erosion Due to Impingement on Cavitation," ASTM STP 408, pp. 70-110, 1967.

[15] Hickling, R. and Plesset, M. S.: "Collapse and Rebound of a Spherical Bubble in Water," Physics of Fluids, 7, pp. 7-14, 1964.

[16] Hogan, R. A.: "On the Measurement of the Air Content of Water," Report Concerning the Hydro Machinery Laboratory, Department of Civil Engineering, Colorado State University, Fort Collins, Colo., May 1967.

[17] Hooper, L. J.: "Experimental Investigation of Initiation of Cavitation Behind an Accelerated Circular Disk," Proc. 1962 IAHR Symp. on Cavitation and Hydraulic Machinery, Sendai, Japan, F. Numachi (ed.), pp. 125-141, 1963.

[18] Ivany, R. D.: "Collapse of a Cavitation Bubble in Viscous Compressible Liquid-Numerical and Experimental Analysis," Ph.D. Dissertation, The University of Michigan, Nuclear Engineering Department, 1965.

[19] Johnson, V. E., Jr.: "Cavitation Inception and Damage," Schiffstechnik, Bd. 13, pp. 19-26, Heft 65, 1966.

[20] Kermeen, R. W. and Parkin, B. R.: "Incipient Cavitation and Wake Flow Behind Sharp-Edged Disks," Calif. Inst. of Tech. Engr. Div. Report 85-4, 1957.

[21] Kirkwood, J. G. and Bethe, H. A.: "The Pressure Wave Produced by an Underwater Explosion," OSRD Report 588, 1942.

[22] Kling, C. L. and Hammit, F. G.: "A Photographic Study of Spark-Induced Cavitation Bubble Collapse," Trans. ASME, J. Basic Engr., 94, D, 4, pp. 825-833, 1972.

[23] Kling, C. L.; Hammitt, F. G.; Mitchell, T. M.; and Timm, E. E.: "Bubble Collpase Near A Wall in Flowing System," 16mm motion picture (silent) ASME Film Library, 1969.

[24] Knapp, R. T.: "Further Studies of the Mechanics and Damage Potential of Fixed Type Cavities," Proc. 1955 NPL Symp. on Cavitation in Hydrodynamics, Paper 19, HMSO, London, 1956.

[25] Knapp, R. T.: "Recent Investigations of Cavitation and Cavitation Damage," Trans. ASME, 77, pp. 1045-1054, 1955.

[26] Knapp, R. T.; Daily, J. W.; and Hammitt, F. G.: Cavitation, McGraw-Hill Book Company, pp. 346-351, 1970.

[27] Kohl, R. E.: "Experimental Studies to Establish Scaling Laws for Modeling Cavitation Damage," Hydronautics, Incorporated Technical Report 233-12, June 1968.

[28] Kornfeld, M. and Suvarov, L.: "On the Destructive Action of Cavitation," Jr. Appl. Phys., 15, pp. 495-503, 1944.

[29] Lamb, Horace: Hydrodynamics, Dover Publications, p. 122, 1945.

[30] Lienhard, J. H. and Goss, C. D.: "Influences of Size and Configuration on Cavitation in Submerged Orifice Flows," ASME, Fluids Engineering Conference, Pittsburgh, Pa., May 9-12, 1971.

[31] Mitchell, T. M. and Hammitt, F. G.: "Collapse of a Spherical Bubble in a Pressure Gradient," ASME Cavitation Forum, May 1970.

[32] Mousson, J. M.: "Pitting Resistance of Metals Under Cavitation Conditions," Trans. ASME, Vol. 59, pp. 399-408, 1937.

[33] Muller, A. and Gyr, A.: "An Explanation of the Pressure Minima Which Causes Cavitation by Means of a Vortex Model," ASME Cavitation Forum, May 1971.

[34] Naude, C. F. and Ellis, A. T.: "On the Mechanism of Cavitation Damage by Nonhemispherical Cavities Collapsing in Contact with A Solid Boundary," Trans. ASME, 83, Ser. D, J. Basic Engineering, pp. 648-656, 1961.

[35] Peterson, F. B.: "Physics Associated with Cavitation Induced Material Damage," The Role of Cavitation in Mechanical Failures, NBS Special Publ. 394, pp. 3-12, 1973.

[36] Plesset, M. S.: "Bubble Dynamics," in R. Davies (ed.), Cavitation in Real Fluids, Elsevier Publishing Company, Amsterdam, 1964.

[37] Plesset, M. S.: "The Dynamics of Cavitation Bubbles," Trans. ASME, J. Appl. Mech., 16, pp. 228-231, 1949.

[38] Plesset, M. S.: "The Pulsation Method for Generating Cavitation Damage," Trans. ASME, 85, Ser. D, J. Basic Engineering, pp. 360-364, 1963.

[39] Plesset, M. S. and Chapman, R. B.: "Collapse of a Vapor Cavity in the Neighborhood of a Solid Wall," Calif. Inst. of Tech., Div. of Engr. and Appl. Sci. Report 85-48, December 1969.

[40] Plesset, M. S. and Chapman, R. B.: "Collapse of An Initially Spherical Vapor Cavity in the Neighborhood of a Solid Boundary," Rep. 85-49, Calif. Inst. of Tech., Div. of Engr. and Appl. Sci., June 1970.

[41] Poritsky, H.: "The Collapse or Growth of a Spherical Bubble or Cavity in a Viscous Fluid," Proc. First U.S. Natl. Congr. Appl. Mech. (ASME), pp. 813-821, 1952.

[42] Rayleigh, Lord (Strutt, John William): "On the Pressure Developed in a Liquid During the Collapse of a Spherical Cavity," Phil. Mag., 34, pp. 94-98, August 1917.

[43] Ripken, J. F.: "Fundamentals of Cavitation," Control of Flow in Closed Conduits, Colorado State University, J. P. Tullis (ed.), pp. 353-377, 1970.

[44] Rouse, H.: "Cavitation in the Mixing Zone of a Submerged Jet," La Houille Blanche, pp. 9-19, January-February 1953.

[45] Rouse, H.: "Jet Diffusion and Cavitation," J. Boston Soc. Civil Engrs., 53, pp. 255-271, 1966.

[46] Rouse, H.: "On the Role of Eddies in Fluid Motion," American Scientist, Vol. 51, No. 3, September 1963.

[47] Rouse, H. and Hsu, Hsieh-ching: "On the Growth and Decay of A Vortex Filament," Proceedings First National Congress of Applied Mechanics, 1951.

[48] Rouse, H.; Hubbard, P. G.; and Spengo, A. C.: "Cavitation of Submerged Jets," Iowa Inst. of Hydr. Res., ONR Report, March 1950.

[49] Rouse, H. and Jezdinsky, V.: "Cavitation and Energy Dissipation in Conduit Expansions," 11th International Association for Hydraulic Research, Leningrad, pp. 1-4, 1965.

[50] Rouse, H. and Jezdinsky, V.: "Fluctuation of Pressure in Conduit Expansions," J. of the Hydraulics Division, ASCE, Proc. Paper No. 4815, Vol. 92, No. HY3, pp. 1-11, May 1966.

[51] Russell, S. O. and Ball, J. W.: "Sudden-Enlargement Energy Dissipator for Mica Dam," J. of the Hydraulics Division, ASCE, July 1967.

[52] Sami, S.: "Velocity and Pressure Fields of A Diffusing Jet," Ph.D. Dissertation, University of Iowa, August 1966.

[53] Sanford, C. L. and Appel, D. W.: "A Study of Flow Through Abrupt Two-Dimensional Expansions," University of Kansas, Studies in Engineering Mechanics, Report No. 7, June 1961.

[54] Shal'nev, K. K.: "Experimental Study of the Intensity of Erosion Due to Cavitation," Proc. Symp. on Cavitation in Hydrodynamics, (N.P.L. 1955), H.M.S.O., 1956.

[55] Sweeney, C. E.: "Cavitation Damage in Sudden Enlargements," Masters Thesis, Colorado State University, Fort Collins, Colo. May 1974.

[56] Syamala Rao, B. C.; Rao, N. S. L.; and Seetharamiah, K.: "Cavitation Erosion Studies with Venturi and Rotating Disk in Water," J. Basic Engineering, Trans., ASME, Series D, Vol. 92, pp. 563-579, 1970.

[57] Teyssandier, R.: "Internal Separated Flows Expansions, Nozzles, and Orifices," Ph.D. Dissertation, University of Rhode Island, 1973.

[58] Teyssandier, R. G. and Wilson, M. P.: "The Paradox of the Vena Contracta," ASME Paper No. 73-WA/FM-9, Presented at the Winter Annual Mtg., Detroit, Mich., Nov. 11-15, 1973, 5 p.

[59] Thiruvengadam, A.: "Effect of Hydrodynamic Parameters on Cavitation Erosion Intensity," Hydronautics, Inc. Technical Report 233-14, 1970.

[60] Thiruvengadam, A.: "Handbook of Cavitation Erosion," Hydronautics, Inc., Rep. No. T.R. 7301-1, January 1974.

[61] Thiruvengadam, A.: "Prediction of Cavitation Damage," Ph.D. Dissertation, Dept. of Hydraulic Engrg., Indian Institute of Science, Bangalore, India, 1961.

[62] Thiruvengadam, A. and Preiser, H.S.: "On Testing Materials for Cavitation Damage Resistance," J. Ship Research, Vol. 8, No. 3, pp. 39-56, December 1964.

[63] Thiruvengadam, A. and Waring, S.: "Mechanical Properties of Metals and Their Cavitation Damage Resistance," J. Ship Research, Vol. 10, No. 1, pp. 1-9, 1966.

[64] Timm, E. E. and Hammitt, F. G.: "Bubble Collapse Adjacent to A Rigid Wall, A Flexible Wall, and A Second Bubble," ASME Cavitation Forum, May 1971.

[65] Trilling, L.: "The Collpase and Rebound of A Gas Bubble," J. Appl. Phys., 23, pp. 14-17, 1952.

[66] Tulin, M. P.: "On the Creation of Ultra-Jets," L. I. Sedou 60th Anniversary Volume, Problems of Hydrodynamics and Continuum Mechanics, Moscow, 1969.

[67] Tullis, J. P. and Govindarajan, R.: "Cavitation and Size Scale Effects for Orifices," J. of the Hydraulics Division, ASCE, Vol. 99, No. HY3, Proc. Paper 9605, pp. 417-430, March 1973.

APPENDIX I

HYDRODYNAMIC MODELING OF EROSION INTENSITY

The following material is quoted directly from reference [60], pages 120-129. The method relates intensity of erosion, I_e, to fluid flow properties by analyzing the growth and collapse of vapor cavities. The derived equations provide a method for estimating cavitation intensity from measured fluid properties and flow parameters.

"Indentation and Rate of Erosion

If the stress caused by the collapse of the bubble exceeds the yield strength of the material, a permanent dent may be produced by a single impact. However, even if the collapse stress is less than the yield strength, a dent may still be produced after several collapses due to fatigue failure of the material. The actual fracture of a particle from the surface of the material may be produced from overlapping indentations caused by the collapse of many bubbles. For a single impact, the depth of indentation, $\Delta y'$, may be approximately related to the strength of the material, S_e, the impact pressure, P_i, and the size of the shock or jet, R, by the following relationship*

$$\Delta y' \cdot S_e \propto P_i \cdot R \qquad [8\text{-}19]$$

*The sign $\propto$ means "is proportional to". All the constants of proportionality are omitted in the following derivations since we are interested only in nondimensional ratios.

For a sufficiently shallow indentation of predominantly plastic character, the diameter of indentation, d, is proportional to $\sqrt{R \cdot \Delta y'}$. This result, when used with conventional relationships for hardness, will lead to relation [8-19]. Ideal plasticity is assumed. If the impact stress is much larger than the yield strength of the material, deep craters and associated plastic flow are produced on the surface of the material. This analysis is mainly applicable to materials that are neither too soft nor too strong, i.e., with yield strengths of the same order of magnitude as the impact stress.

If we use the simple analogy of a hardness test, the strength, S, corresponds to the appropriate hardness of the material (Figure 8-14). For the case of multiple impacts with a frequency of f, the rate of indentation may be approximated by

$$\frac{\Delta y}{\Delta t} \cdot S_e \propto P_i \cdot R \cdot f \qquad [8\text{-}20]$$

The left side of relation [8-20] represents the intensity of erosion, as given by relation [6-4], whereas the right side is the intensity of bubble collapse. The genesis of these ideas may be traced to References (61,99). The details of the derivations for relations [8-19] and [8-20], and the following result, including assumptions and limitations, are contained in Reference (174).

"The intensity of bubble collapse depends upon three parameters, namely the impact pressure, P_i, the size of the bubble or jet, and the frequency of impact. The approach is to relate these three parameters to hydrodynamic characteristics such as velocity, pressure, and size of the system. As shown in Figure 8-14, we can classify the bubble collapse mechanisms into three categories, spherical collapse, macrojet impact, and microjet impact. Rayleigh (7) and several other investigators considered the spherical collapse in detail. Plesset and Chapman (56) among others have considered the macrojet and microjet.

Spherical Collapse

"The collapse pressure due to spherical collapse, P_c, is given by

$$P_c \propto P_o \left(\frac{R_o}{R_c}\right)^3 \qquad [8\text{-}21]$$

where P_o and R_o correspond to initial pressure and radius and R_c is the final collapse radius. If the center of collapse is of the order of the initial radius, the impact pressure, P_i, is given by

$$P_i \propto P_o \left(\frac{R_o}{R_c}\right)^2 \qquad [8\text{-}22]$$

allowing for a (1/radius) attenuation (175). The relative radius, R_o/R_c, depends upon many factors including surface tension, noncondensible gas, heat transfer effects and compressibility of the liquid (176). For example, the influence of noncondensible gas obeying Boyle's law was given by Rayleigh (7) as

$$\frac{R_o}{R_c} \propto \exp\left(\frac{P_o}{Q_o}\right)^{1/3} \qquad [8\text{-}23]$$

where Q_o is the partial pressure of the gas at the beginning of the collapse. Similarly, other effects may also be evaluated (176).

Jet Impact

"The pressure caused by the jet may be classified into two categories: (1) the stagnation pressure developed by a long jet acting for a large duration, and (2) the water hammer pressure resulting from a short jet of small duration. According to Plesset and Chapman (56), velocity of the jet is proportional to $\sqrt{P_o}$. Then the stagnation pressure is proportional to P_o, whereas the water hammer pressure is proportional to $C\sqrt{\rho P_o}$; C is the sound speed and ρ is the density of the liquid;

$$P_i \propto P_o \quad \text{(for the case of stagnation pressure)} \qquad [8\text{-}24]$$

$$P_i \propto C\sqrt{\rho P_o} \quad \text{(for the case of water hammer pressure)} \qquad [8\text{-}25]$$

Growth of Bubbles

"The initial size of the bubble at the beginning of the collapse is related to the time available for growth and the pressure difference between the inside and the outside of the bubble (15), Figure 8-15. The growth time, τ_g, is directly proportional to the length of travel of the bubble and inversely proportional to the translational velocity of the bubble. The travel length is proportional to the cavity length which is proportional to the model length at a given cavitation number. Experimental observations by Ivany, Hammitt and Mitchell (177) show that the bubbles move at approximately the same speed as the liquid. The pressure causing growth is related to the difference between the vapor pressure, p_v, and the minimum pressure, p_{min}. The surface tension is neglected, but it is possible to account for it. These relationships may be written as follows:

$$R_o \propto \tau_g \sqrt{\frac{\Delta p}{\rho}} \qquad [8\text{-}26]$$

$$\tau_g \propto \frac{\ell}{V_o} \qquad [8\text{-}27]$$

$$\Delta p \propto p_v - p_{min} \qquad [8\text{-}28]$$

Combining these equations and using the relations for the cavitation number, σ, and the minimum pressure coefficient, $C_{p,min}$, given by Equation [2-12]:

$$\sigma = \frac{p_o - p_v}{\frac{1}{2}\rho V_o^2} \qquad [8\text{-}29]$$

and [2-9]:

$$C_{p,min} = \frac{p_{min} - p_o}{\frac{1}{2}\rho V_o^2} \qquad [8\text{-}30]$$

and assuming that σ_i, the cavitation inception number is

$$\sigma_i = - C_{p,min} \quad \text{[See Johnson (3)]} \qquad [8\text{-}31]$$

We get

$$R_o \propto \ell\ (\sigma_i - \sigma)^{1/2} \qquad [8\text{-}32]$$

Moreover, the radius of the jet, R_j, is assumed as:

$$R_j \propto R_o \qquad [8\text{-}33]$$

Frequency of Bubble Growth and Collapse

"As discussed earlier, the rate of erosion is related to the number of bubbles collapsing per unit time at a given location. The number of bubbles that collapse is related to the number of bubbles that become unstable and grow. Some of the parameters that affect the bubble instability are:

1. Nuclei size,
2. Surface tension,
3. Velocity,
4. Pressure, and
5. Size of the model.

"Johnson (3) considered these parameters and demonstrated that bubbles smaller than the critical size do not grow under a given set of flow conditions (Figure 2-5). For example, bubbles of the order of 10^{-4}-in. in diameter may not grow at speeds less than 60 fps whereas they may become critical at a speed of 120 fps, as shown in Figure 2-5.

"If n_o is the cumulative number of nuclei that pass a given point in a given time interval, then one can plot a distribution of sizes of these bubbles as shown in Figure 8-16. The relative nuclei size is $d/\bar{d}$ where $\bar{d}$ is the mean diameter and n is the cumulative number corresponding to the diameter d. As of now, there are no systematic measurements of such distributions in practical flow systems. However, if

we assume that the nuclei size is governed by a Weibull type of distribution, then

$$\frac{n}{n_o} = \exp\left[-\left(\frac{d}{\bar{d}}\right)^{\alpha}\right] \qquad [8\text{-}34]$$

where α is the Weibull shape parameter. It is easily recognized that the Weibull distribution gives the simple exponential distribution when $\alpha = 1$, the Rayleigh distribution when $\alpha = 2$, and approximates the normal distribution when $\alpha = 3.57$ (178).

"According to Johnson (3),

$$d^* = \frac{8\gamma}{3(p_v - p_{min})} \qquad [8\text{-}35]$$

where d^* = the critical diameter of the nucleus, and
γ = the surface tension of the liquid.

If n^* corresponds to d^*, and a simple exponential distribution is assumed for the nuclei size, one obtains (174):

$$n^* \propto \frac{V_o}{\bar{d}} \exp\left[\frac{-2.67}{W(\sigma_i - \sigma)}\right], \qquad [8\text{-}36]$$

where $W = \frac{1}{2}\rho V_o^2 \bar{d}/\gamma$ is the Weber number.

Scaling Laws for Cavitation Erosion

"So far, we have discussed the relationships governing the impact pressure, the size of the bubble or the jet, and the number of bubbles collapsing per unit time. We also showed in this section that the intensity of bubble collapse is the product of these parameters. For example, the jet impact case reduces to

$$I_e \propto P_i \cdot R_j \cdot f; \quad P_i \propto p_o$$

$$\propto p_o \ell(\sigma_i - \sigma)^{1/2} \frac{V_o}{\bar{d}} \exp\left[\frac{-2.67}{W(\sigma_i - \sigma)}\right] \qquad [8\text{-}37]$$

Again,

$$p_o - p_v = \sigma \frac{1}{2}\rho V_o^2$$

But

$$p_v << p_o \quad \text{for practical cases of erosion.}$$

Then

$$p_o \approx \sigma \frac{1}{2} \rho V_o^2$$

Hence

$$I_e \propto \frac{1}{2} \rho V_o^3 \frac{\ell}{\bar{d}} \sigma (\sigma_i - \sigma)^{1/2} \exp \left[\frac{-2.67}{W(\sigma_i - \sigma)} \right] \qquad [8\text{-}38]$$

Rearranging [8-43] in nondimensional groups, we obtain,

$$\textcircled{H} = \frac{\sigma}{\delta} (\Delta\sigma)^{1/2} \exp \left[- \frac{2.67}{W(\Delta\sigma)} \right] \qquad [8\text{-}39]$$

as an expression for the erosion number, $\textcircled{H}$, for the jet impact case; where

$$\textcircled{H} = \frac{I_e}{\frac{1}{2} \rho V_o^2} \quad - \text{ Erosion number} \qquad [8\text{-}40]$$

$$\delta = \frac{\bar{d}}{\ell} \quad - \text{ Relative nuclei size} \qquad [8\text{-}41]$$

$$W = \frac{\frac{1}{2} \rho V_o^2 \bar{d}}{\gamma} \quad - \text{ Weber number} \qquad [8\text{-}42]$$

$$\sigma = \frac{p_o - p_v}{\frac{1}{2} \rho V_o^2} \quad - \text{ Cavitation number} \qquad [8\text{-}43]$$

$$\sigma_i = \frac{p_i - p_v}{\frac{1}{2} \rho V_o^2} \quad - \text{ Cavitation inception number} \qquad [8\text{-}44]$$

$$\Delta\sigma = (\sigma_i - \sigma) \quad - \text{ Degree of cavitation} \qquad [8\text{-}45]$$

"Similar results for the water hammer pressure produced by microjets and for spherical shocks produced by spherical collapse are summarized in Table 8-2.

"If we examine the case of water hammer pressure, then

$$\textcircled{H} = \frac{\sigma}{\delta M} (\Delta\sigma)^{1/2} \exp \left[\frac{-2.67}{W(\Delta\sigma)} \right] \qquad [8\text{-}46]$$

where

$$M = V_o/C = \text{Mach number},$$

and

$$C = \text{the speed of sound in the liquid.}$$

For the case of spherical shock, we get

$$\textcircled{H} = \frac{\sigma}{\delta} (\Delta\sigma)^{1/2} \exp\left[\frac{2}{3}\left(\frac{p_o}{Q_o}\right) - \frac{2.67}{W(\Delta\sigma)}\right] \qquad [8\text{-}47]$$

where Q_o is the partial pressure of noncondensible gas in the bubble at the start of collapse."

APPENDIX II

VARIATION OF MPR AT V_{id} WITH d_o/D RATIO

As mentioned in Chapter V, the following relation holds for a given orifice at a given upstream pressure:

$$MPR = K\ 10^{mV} \qquad \text{for} \quad P_u = \text{const.} \tag{AII-1}$$

in which K is a constant. The constant K can be evaluated by the condition, MPR = 1.0 pit/in.^{2}/min at $V = V_{id}$, then

$$K = \frac{1}{10^{mV_{id}}} \tag{AII-2}$$

in which V_{id} = mean pipe velocity at incipient damage, see Chapter VI. Substituting Eq. (AII-2) into (AII-1) gives

$$MPR = \frac{1}{10^{mV_{id}}}\ 10^{mV} \qquad \text{for} \quad P_u = \text{const.} \tag{AII-3}$$

The rate of change of MPR with mean pipe velocity is given by:

$$\frac{d}{dV}(MPR) = \frac{1}{10^{mV_{id}}}\ m \cdot \ln 10 \cdot 10^{mV} \tag{AII-4}$$

Finally, the rate of change of MPR with mean pipe velocity at the incipient damage condition ($V = V_{id}$) will be given by:

$$\frac{d}{dV}(MPR)\Big|_{V_{id}} = m \cdot \ln 10 \tag{AII-5}$$

in which ln indicates natural logarithm.

If it is assumed for a given d_o/D ratio that m can be approximated by the average m value found in the 3-in. test line, Table 2,

then Table AII-1 results. This table shows that as the d_o/D ratio is decreased from 0.800 to 0.389, the change of MPR with mean pipe velocity at the incipient damage condition increases by a factor of 7.26.

TABLE AII-1. CHANGE OF MPR WITH MEAN PIPE VELOCITY (D = 3.0-in.)

d_o/D	m (average)	$\frac{d}{dV}(MPR)\Big\|_{V_{id}}$	χ
0.389	2.46	5.66	7.26
.444	1.46	3.36	4.31
.500	1.20	2.76	3.54
.667	0.50	1.15	1.47
.800	0.34	0.78	1.00

$$\chi = \frac{\frac{d}{dV}(MPR)\Big|_{V_{id}}}{\frac{d}{dV}(MPR)\Big|_{V_{id}} \quad \text{for} \quad d_o/D = 0.800}$$